KINETICS OF ELECTRON-TRANSFER QUENCHING OF EXCITED AROMATIC MOLECULES IN SOLUTION

A thesis submitted for the degree of

Doctor of Philosophy

by

Khalid Ali Abdullah

Department of Chemistry,

University of Warwick

March 1985

To my parents and family

ACKNOWLEDGEMENTS

I would like to express my deepest gratitude and appreciation to my supervisor Professor T.J. Kemp for his invaluable encouragement and suggestions given throughout the progress of this work.

I thank Mr. L. Chewter and Dr. S. Meech from the Royal Institution (London) for their assistance in respect of the fluorescence lifetime measurements cited in this thesis.

I am also grateful to the workshops of the Department of Chemistry for assistance in construction and maintenance of the laser assembly.

Mr. H. Beaton's assistance in the syntheses of many organotin compounds cited in this thesis is gratefully acknowledged.

I am indebted to the University of Mosul for study leave and the Iraqi Government for financial support to carry out this work.

ABSTRACT

The work described in this thesis is concerned with laser kinetic and spectroscopic investigations of two distinct types of charge-separation process following electronic excitation, namely, (i) the kinetics of quenching by intermolecular electron-transfer and (ii) the development of (intramolecular) excited state dipoles as evinced by solvatochromic effects on both fluorescence and triplet-triplet absorption spectra.

The kinetic studies refer to several systems, i.e. the fluorescence quenching of 9,10-dicyanoanthracene and 2-aminoanthracene in both polar and non-polar solvents and the triplet quenching of xanthone and thioxanthone, and also singlet thioxanthone, in MeCN/H_2O mixtures. Correlation of the logarithm of the quenching rate constant (k_{23}) with the free energy of the electron-transfer (ΔG^{o}_{23}) was attempted in terms of current models for electron transfer due to Marcus, Weller, Polanyi and others, sufficiently wider ranges in ΔG^{o}_{23} being utilised to effect reasonable discrimination.

In the case of 9,10-dicyanoanthracene, fluorescence quenching was effected both by donors (inorganic anions in MeOH/H_2O and alkylmetals in cyclohexane) and organic acceptors in MeOH (Chapter 3), while quenching of 2-aminoanthracene was by organic acceptors in MeOH (Chapter 4). In general the Polanyi treatment gave better agreement, although this could not always be distinguished from the Rehm-Weller model.

The quenching rates both of the singlet and triplet states of thioxanthone by inorganic anions were determined, enabling a comparison of their reactivity, as were the quenching rates of triplet

xanthone, all in MeCN-H_2O mixture (3:2 v/v), (Chapter 5). Triplet thioxanthone is quenched 10^2-fold more slowly by SCN^- and Br^- ions than singlet excited thioxanthone, which may be understood in terms of a higher value for ΔG°_{23} for the same acceptor in its singlet as compared with its triplet state. The triplet quenching rates were correlated more satisfactorily with ΔG°_{23} by the Polanyi treatment.

Solvatochromism was examined in two systems (Chapter 6) namely, the fluorescence of 2-aminoanthracene and N,N-dimethyl-2-aminoanthracene, comparison of which confirms (a) that the former is affected by solvent-donor hydrogen-bonding in hydroxylic solvents and (b) that Bilot-Kawski and related expressions provide a more specific analysis of solvatochromic affects than the Dimroth and related solvent parameters. The red-shift in the fluorescence maxima of these fluorophores with increasing solvent polarity was interpreted on the basis of increases in the dipole moment of the S_1 state over that of the S_o state.

While the fluorescence maxima of xanthone and thioxanthone show substantial red-shifts with increasing polarity, as measured by the polarisation function of Bilot and Kawski, indicating an increase in dipole moment on excitation, the triplet-triplet absorption transient spectra of xanthone, thioxanthone and N-methylacridone are strongly blue-shifted, indicating a decrease in dipole moment as estimated by the Suppan expression.

A great part of the work described in this thesis has reached the stage of publication, viz

(1) Electron-donor and -acceptor quenching of the fluorescence of 9,10-dicyanoanthracene in polar and non-polar solvent,
K.A. Abdullah and T.J. Kemp,
J. Photochem., 1985, 28, 61.

(2) Quenching of excited state xanthone and thioxanthone by inorganic anions,
K.A. Abdullah and T.J. Kemp,
J. Chem. Soc., Perkin Trans. 2, 1985, in press.

(3) Solvatochromic effects in the fluorescence of 2-aminoanthracene and N,N-dimethyl-2-aminoanthracene: a comparative study,
K.A. Abdullah and T.J. Kemp,
J. Photochem., 1985, in press.

ABBREVIATIONS

2-AA	2-aminoanthracene
ArH	aromatic hydrocarbon
Ar_2CO	aromatic ketone
CYH	cyclohexane
DCA	9,10-dicyanoanthracene
2-DMA	N,N-dimethyl-2-aminoanthracene
DMF	dimethylformamide
D	dipole moment unit (debye)
E.A.	electron affinity
ϵ	dielectric constant
ESA	excited state absorption
$E_T(30)$	Dimroth's solvent parameter
EtOH	ethanol
I.P.	ionisation potential
IC	internal conversion
ISC	intersystem crossing
MeCN	acetonitrile
MeOH	methanol
n	refractive index
NHE	normal hydrogen electrode
μ	dipole moment
PhCN	benzonitrile
PPh_3	triphenylphosphine
SCE	saturated calomel electrode
τ	lifetime
λ	wavelength
Z	Kosower's solvent parameter

PHYSICAL CONSTANTS

Physical constant	Symbol	Value in SI units
Elementary electronic charge	e	1.602×10^{-19} C
Avogadro's constant	N	6.022×10^{23} mol^{-1}
Faraday's constant	F	9.6485×10^{4} C mol^{-1}
Molar gas constant	R	8.314 J mol^{-1} K^{-1}
Planck's constant	h	6.626×10^{-34} J s
Boltzmann's constant	k	1.381×10^{-23}J K^{-1}
Speed of light in vacuum	c	2.998×10^{8} m s^{-1}
Mass of electron	m_e	9.1096×10^{-31} kg
Mass of proton	m_p	1.6726×10^{-27} kg
Absolute zero		-273.15^{o}C

Conversion Factors for Energy per Molecule or per Mole

	$J\ mol^{-1}$	$kcal\ mol^{-1}$	Electron Volts	$Centimetres^{-1}$
$1\ J\ mol^{-1}$	= 1	2.839×10^{-4}	1.036×10^{-5}	8.359×10^{-2}
$1\ kcal\ mol^{-1}$	= 4.184×10^{3}	1	4.336×10^{-2}	3.497×10^{2}
1 eV	= 9.649×10^{4}	23.060	1	8.065×10^{3}
$1\ cm^{-1}$	= 1.196×10	2.859×10^{-3}	1.240×10^{-4}	1

Conversion Factors

1 cm = 10^{8} Å = 10^{7} nm

1 sec = 10^{9} ns = 10^{6} μs

1 Debye = 3.336×10^{-30} C m

1 cal = 4.184 J

1 eV = 0.16022×10^{-18} J

CONTENTS

CHAPTER 1

INTRODUCTION

1.1 Formation and Decay of Excited States of Organic Molecules

Different systems of describing excited states are employed depending on which properties of the state are to be emphasized and on the amount of information available concerning the nature of the originating transition. Spectroscopists usually label electronic states according to the symmetry of the wavefunctions of these states, while for many photochemical discussions a molecular orbital notation, which classifies transitions according to the orbitals which the promoted electron leaves and enters, gives an adequate description.[1-5] The more important transitions given in order of increasing energy are $n \rightarrow \pi^*$, $\pi \rightarrow \pi^*$, $\sigma \rightarrow \pi^*$ and $\sigma \rightarrow \sigma^*$. The excited states formed by these promotions, due to absorption of a photon, which have the separated electrons with spins paired will be singlet states and they can be labelled as $^1(n, \pi^*)$ and $^1(\pi, \pi^*)$, while those states in which the separated electrons have parallel spins are labelled as $^3(n, \pi^*)$ and $^3(\pi, \pi^*)$ states.

Most organic molecules in their ground state have an even number of electrons arranged in pairs which occupy the lowest-energy molecular orbitals, giving a resultant ground singlet electronic state S_o. Higher excited singlet states are usually labelled S_1, S_2, etc., in order of increasing energy and the triplet states are correspondingly labelled as T_1, T_2, etc. as shown in the Jablonski diagram, Figure (1.1); a given triplet state always has a lower energy than the corresponding singlet state. The energy difference between corresponding $^1(n, \pi^*)$ and $^3(n, \pi^*)$ states is usually considerably smaller than that between corresponding $^1(\pi, \pi^*)$ and $^3(\pi, \pi^*)$ states. It follows that those molecules which have a lowest excited

singlet state which is a $^1(n, \pi^*)$ state do not necessarily have a $^3(n,\pi^*)$ state as their lowest triplet state.[2,3,5]

The absorption spectra of conjugated organic molecules are controlled by the selection rules (based on changes in spin and multiplicity) and the normal absorption is due to a singlet-singlet transition. The higher triplet states (T_2, T_3,...T_i) are formed when a molecule in its lowest triplet state (T_1) absorbs a new photon; the transition is called triplet-triplet absorption, which is spin-allowed, and it is shown in Figure (1.1).

Several processes may be involved in the relaxation, or intramolecular deactivation, of both singlet and triplet excited states. These include radiative and radiationless processes. In the former, an electronically excited molecule loses its excitation energy by emission of radiation, which is also known as luminescence.[1,3] There are two main kinds of radiative transition. The first is fluorescence, which is a spin-allowed process of emission between states of the same multiplicity and is usually $S_1 \rightarrow S_0$. In many aromatic compounds the potential energy surfaces of the ground and of the excited states appear to be very similar, and this often produced a mirror image relationship between the absorption and fluorescence spectra.[1,2,4] The second is phosphorescence, which is a spin-forbidden radiative transition between two states of different multiplicity, typically $T_1 \rightarrow S_0$. Since phosphorescence is spin-forbidden, the radiative lifetimes are very long, being typically 10^{-2} and 10 sec for $^3(n, \pi^*)$ and $^3(\pi, \pi^*)$ states respectively in the absence of heavy atoms in the molecule.[2,4] The triplet state T_1 is particularly sensitive to quenching processes and these account for the general lack of phosphorescence in fluid solution.

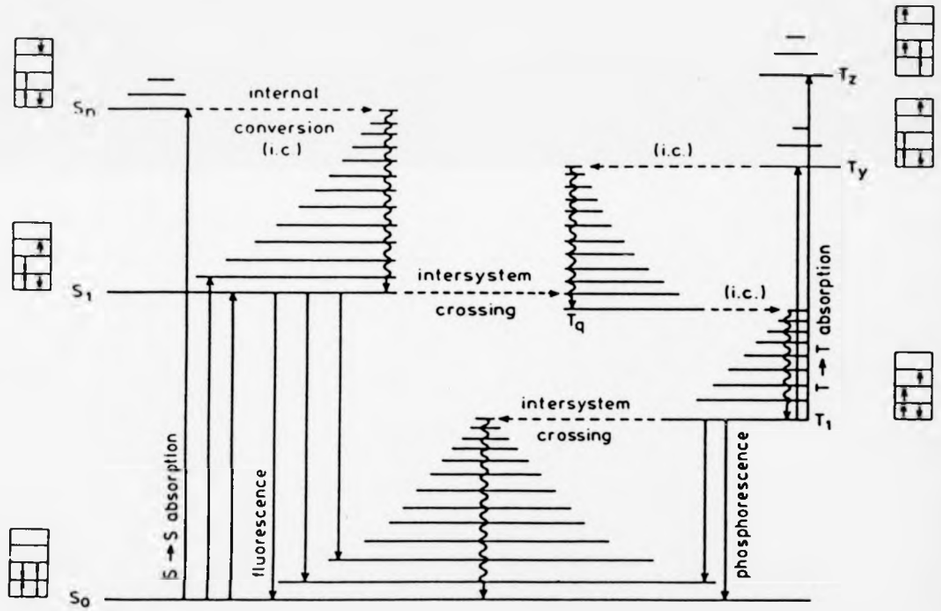

Figure (1.1) Jablonski diagram showing radiative and non-radiative transitions (continuous and wavy lines respectively) which occur between singlet and triplet states (from reference 4).

Since T_1 has a lower energy than S_1, the phosphorescence spectrum occurs at longer wavelengths than the fluorescence spectrum.

There are two types of photophysical radiationless transition, namely (i) non-radiative transitions between states of similar multiplicity, known as internal conversion, e.g. $S_2 \rightarrow S_1$, $T_2 \rightarrow T_1$, and (ii) those between states of different multiplicity, which are spin-forbidden, known as intersystem crossing, e.g. $S_1 \rightarrow T_1$, $T_1 \rightarrow S_0$. The very fast rate of internal conversion from upper singlet states makes photochemical events from the upper states unlikely and these occur mainly from the lowest excited singlet state. This process also accounts for the fact that the fluorescence yield is usually independent of the exciting wavelength and explains the extreme weakness of fluorescence from higher-singlet states. Although intersystem crossing from the state S_1 is spin-forbidden, and therefore much less probable than internal conversion, it often competes successfully with fluorescence from S_1. The intersystem crossing from S_1 is usually to a close-lying triplet state T_q, rather than directly to T_1, Figure (1.1).

Intersystem crossing from $T_1 \rightarrow S_0$ is less efficient than from $S_1 \rightarrow T_q$, so that sometimes the lifetime of T_1 may exceed one second. The major reason for this larger difference between T_1 and S_0 than between S_1 and T_q is that the large electronic energy gap gives a low Franck-Condon factor for this transition. The reverse intersystem crossing from $T_1 \rightarrow S_1$ has an activation energy equal to the energy difference between these two excited states and leads to the production of S_1 so long as T_1 is populated. This type of fluorescence, known as delayed fluorescence, has a lifetime comparable to that of the triplet state (phosphorescence) and it is not observed

at low temperature in glassy solution. It is sometimes known as E-type delayed fluorescence since it occurs in eosine and other dye molecules.[1,2,4-6]

A substance which accelerates the decay of an electronically excited state to the ground state or to lower electronically excited states by intermolecular deactivation processes is described as a quencher. Photophysical quenching promotes the radiationless deactivation of excited molecules, without any chemical change, while photochemical quenching leads to new ground state products, which forms the subject of synthetic photochemistry. Among the possible mechanisms for photophysical quenching are the heavy atom effect, energy transfer etc. while electron transfer is photochemical deactivation and the quenching processes are usually quantified by means of the well-known Stern-Volmer equation, (see section 2.5.1).

1.2 Excimer and Exciplex Formation

It was first noted by Förster and Kasper[7] in 1955 that increasing the concentration of pyrene not only quenches the normal pyrene fluorescence (self quenching), but also introduces a new fluorescence component. Because the absorption spectrum is not concentration-dependent, the fluorescence component must then be formed after electronic excitation and disappear on emission. Kinetic analysis shows that it is a 1:1 complex of an excited singlet state and the ground state of pyrene. The term excimer (excited dimer) used to describe this association was first introduced by Stevens and Hutton.[8] It has since been found that excimer formation is widespread among aromatic hydrocarbons.[9]

Excimer fluoresence differs from normal fluorescence because:[6,9]

(i) It lies in a region of longer wavelength since the (excited) state of the excimer complex generally lies below the fluorescence state.

(ii) It shows a broad, characteristic spectrum without vibrational structure because the ground state of the excimer is repulsive (unstable).

(iii) It is dependent on temperature, from which the enthalpy and entropy of dissociation can be evaluated. For pyrene, the enthalpy of dissociation is ~ 40 kJ mol^{-1} and the entropy of dissociation is ~ 80 J K^{-1}, showing that this excimer has a strongly bonded and rigid structure. Excimers derived from other hydrocarbons have smaller enthalpies, though the dissociation entropies are usually similar.[2]

In order to form an excimer for an excited aromatic molecule with its ground-state partner, the latter should approach the excited molecule within a distance of 3-4 Å during the lifetime of the excited state.[6] The possibility of excimer formation is dependent upon the spatial alignment of a pair of molecules, for example a parallel alignment for rigid planar aromatic rings in participating molecules. Excimers are formed in (relatively) concentrated solutions and in the solid state; in solution they may also result from diffusional collision between two triplet states which emits delayed fluorescence known as P-type (pyrene-type) delayed fluorescence.[5,6,9] Formation of this type of fluorescence shows a second-order dependence while that of E-type fluorescence has a first-order kinetic dependence.[2,5]

The term exciplex (excited complex) is used to describe atomic or molecular aggregates that are unstable in the ground state but are

stable under electronic excitation.[10,11] This definition is used to cover both excimer and heteroexcimer (electronically excited aggregates formed between dissimilar partners[12]). However most authors prefer to use the term exciplex as one equivalent to that of heteroexcimer; this type of species was first observed by Leonhardt and Weller[13] following the fluorescence quenching of perylene by N,N-dimethylaniline.

According to Rehm and Weller,[14] the energy of singlet exciplex formation $E_{(A^-D^+)}$ can be obtained by subtracting the dissociation enthalpy ΔH^* of the exciplex from the zero-zero spectroscopic energy ($\Delta^1 E_{o,o}$) of the component that is excited in the exciplex formation reaction, Figure (1.2). The value of ΔH^* for an exciplex exhibiting major charge-transfer character has been formulated in term of the oxidation potential (E_{D/D^+}) and the reduction potential ($E_{\bar{A}/A}$) of the donor and the acceptor respectively, equation (1.1), where C_1 is

$$\Delta H^* = \Delta^1 E_{o,o} - [E_{D/D^+} - E_{A^-/A}] + C_1 \qquad (1.1)$$

a constant related to the Coulombic interaction energy between the ions. The fluorescence energy ($h\nu_c^{max}$) of more than one hundred exciplexes of aromatic hydrocarbons in nonpolar solvents was found[14] to decrease as the ionisation potential (or E_{D/D^+}) of the donor decreases and the electron affinity (or $E_{A^-/A}$) of the acceptor increases; equation (1.2). The constant C_2 is related to the

$$h\nu_c^{max} = E_{D/D^+} - E_{A^-/A} + C_2 \qquad (1.2)$$

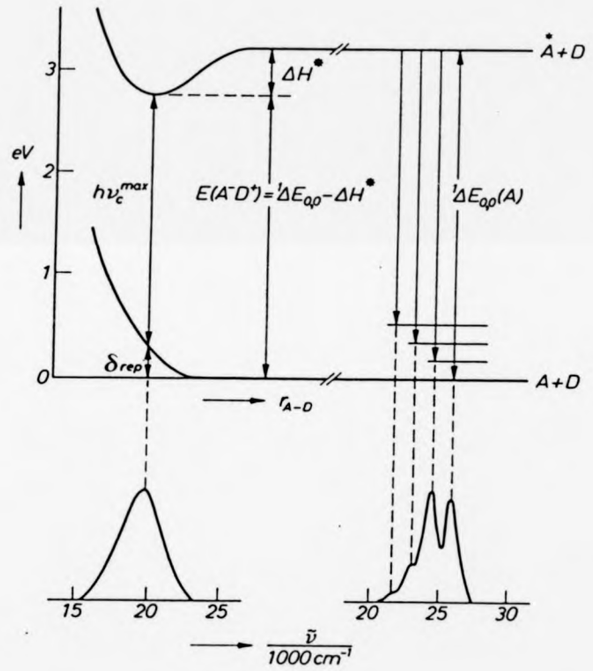

Figure (1.2) Potential energy curves showing singlet exciplex formation between singlet excited acceptor ($^1A^*$) and donor (D) which gives a broad structureless emission at lower frequencies than monomer fluorescence; see text. (From reference 14).

exciplex solvation energy. Hence, the energy of the singlet exciplex is given by equation (1.3), where $C_1 + C_2 = \delta_{rep.}$ in Figure (1.2)

$$E_{(A^-D^+)} = h\nu_c^{max} - (C_1 + C_2) \qquad (1.3)$$

has been found[14] to equal 0.28 ± 0.1 eV. The red shift in the exciplex fluorescence, as compared with monomer fluorescence, and its disappearance in polar solvents due to dissociation into radical ions led Rehm and Weller[14-16] to suggest the dipolar (charge separation) nature of the exciplexes. The formation of an exciplex as a consequence of fluorescence quenching of more than sixty donors and acceptors in acetonitrile was confirmed kinetically by the same workers.[15,16] Thus, the requirement for exciplex formation is that the standard free energy ΔG^o for the electron transfer process, given by equation (1.4), should be negative. Here $e^2/\varepsilon r$ is the Coulombic

$$\Delta G^o = E_{D/D^+} - E_{A^-/A} - \frac{e^2}{\varepsilon r} - \Delta^1 E_{o,o} \qquad (1.4)$$

interaction energy between the two radical ions at the encounter distance (r) in a solvent of dielectric constant (ε). Recently, the solvent effect on the singlet exciplex lifetime for the system pyrene/tertiary amines has been investigated by Weller[17,18] in more detail to reveal the role of the medium in the electron transfer process. The values of the rate constant ($k_{diss}^{exc.}$) of exciplex dissociation into solvated radical ion pair in polar solvents at room temperature range from 5×10^8 s^{-1} in acetonitrile to less than

than 10^6 s^{-1} in tetrahydrofuran and agree fairly well with value calculated from the empirical equation (1.5), where η is the solvent

$$k_{diss.}^{exc.} = \frac{2.3 \times 10^9}{\eta} \exp\left[\frac{-e^2}{\varepsilon k_B T}\left(\frac{1}{d} - \frac{1}{r}\right)\right] \qquad (1.5)$$

viscosity in cP, k_B is Boltzmann's constant, $d \simeq 3$ Å (interplanar separation within the exciplex) and $r \simeq 7$ Å (centre to centre distance within the encounter complex), while the other symbols have their usual meaning. The energy gained in such a spontaneous dissociation process for this system has been found[17] to be about 20 kJ mol^{-1} causing the lifetime of this exciplex to be short in polar solvents and clearly accounting for their higher stability (longer lifetime) in nonpolar solvents. Moreover, this confirmed a previous conclusion[19] that not only the ions, but also the triplet states of the fluorescing hydrocarbon function as intermediates in the quenching processes.[17,18] The existence of an exciplex (singlet or triplet) has been observed for many systems in nonpolar media on the basis of the appearance of a broad structureless luminescence band during fluorescence quenching for singlet exciplexes or transient absorption spectra during the quenching of triplet-triplet absorption for triplet exciplexes.[11] Triplet exciplexes have been studied in rather less detail, because few molecules phosphoresce with high quantum yield in solution, and their existence is usually determined by measurement of their absorption spectra by the laser flash photolysis method. In many cases the structure of the triplet exciplex has been found to be that of an ion pair and their wavefunction can be represented similarly to those of singlet exciplexes.[20]

An exciplex can be regarded as a molecular entity having its own properties just as a normal organic molecule, the only difference being that it has a repulsive ground state. Thus redox quenching rate constants of many singlet exciplexes have been used[21] to determine their redox potentials, as has their ability to give new emissions or even to form products (exciplex substitution).

The general wavefunction of excited complexes formed between two chromophores may be represented by the superposition of several configurations,[10,11] equation (1.6).

$$\psi \simeq C_1\phi(M_1^*M_2) + C_2\phi(M_1M_2^*) + C_3\phi(M_1^-M_2^+) + C_4\phi(M_1^+M_2^-) + C_5\phi(M_1M_2) \qquad (1.6)$$

Hence, the wavefunction of an exciplex can be represented by the linear combination of the wavefunctions of states with complete charge transfer and states of exciton resonance interaction by neglecting the fifth term of equation (1.6). This term plays an important role in excited charge-transfer complexes, formed by exciting ground-state molecular aggregates, which accounts for their stability in the ground state. In the case of excimers, $|C_1| = |C_2|$ and $|C_3| = |C_4|$. Exciton resonance interaction, i.e. the first two terms in equation (1.6), was assumed[10] in order to account for the stability of the excimer. Therefore, the excimer state may be expressed by equation (1.7)

$$\psi_{excimer} \simeq a[\phi(M_1^*M_2) \pm \phi(M_1M_2^*)] + b[\phi(M_1^-M_2^+) \pm \phi(M_1^+M_2^-)] \qquad (1.7)$$

Exciplex formation is not restricted to aromatic systems, and there is no requirement that exciplexes should necessarily luminesce.

If the sum of the rate constants for radiationless processes involved in relaxation of theexciplex is sufficiently high, the lifetime of the exciplex will be so short that its emission may be undetectable. The failure of the encounter complexes to give equilibrium exciplexes in some systems may be due[11] to either (i) the lack of binding energy (stability) or (ii) chemical reactivity (product formation). Recently, Davidson[11] reviewed the factors hindering the formation of equilibrium exciplexes which are:

(i) unfavourable steric interactions due to substituent groups present within the participating molecules.

(ii) The lack of conformational mobility in the linking chain of bichromophoric compounds hindered intramolecular excimer and exciplex formation. The relative orientation of the two groups is of far greater importance for the formation of an excimer than for an exciplex.

(iii) If a group has to undergo rehybridisation in the electron transfer reaction, this reorganisation may not be able to occur within the lifetime of the excited state. This factor has been used to explain the low quantum yield of exciplex formation between naphthalenes and aliphatic tertiary amines.[11]

Alternative routes leading to exciplexes formation are chemiluminescent or electrochemiluminescent processes, which involve radical-ion recombinations. This situation is well-established and has been reviewed extensively.[9,10,11]

1.3 Redox Properties of Photoexcited States

An electronically excited state induced in a molecule by absorption of light is virtually a new chemical species with its own chemical and physical properties different from those of the corresponding ground-state molecule. Excitation of an electron from a low-energy (bonding, HOMO) to a high-energy (antibonding, LUMO) orbital reduces the ionisation potential and increases the electron affinity of a molecule, as shown from the orbital scheme of Figure (1.3). Thus, an electronically excited state is expected to be both a better reductant and a better oxidant than the ground-state molecule.

In more rigorous spectroscopic terms, the relative situation of redox potential M/M^- and M^*/M^- (or M^+/M and M^+/M^*), where M is the ground-state molecule and M^* is the lowest excited state, is sketched in Figure (1.4). The situation is pictured to describe the oxidation of the molecule M. The electrochemical redox potentials of the couple M/M^+, $^3M^*/M^+$ and $^1M^*/M^+$ versus a reference couple Q/Q^- are related to the free energy change:

$$\Delta G = \Delta H - T\Delta S \qquad (1.8)$$

When the Stokes shift is small, (which is the shift between absorption and emission, caused by the change in size, shape and solvation of an excited state versus the ground state), the difference between the entropy of the excited and ground states may reasonably be neglected, ($\Delta S \simeq 0$ and $\Delta G = \Delta H$) so that:

$$\Delta G[M,M^+] - \Delta G[^3M^*,M^+] = \Delta H[M,M^+] - \Delta H[^3M^*,M^+] \qquad (1.9)$$

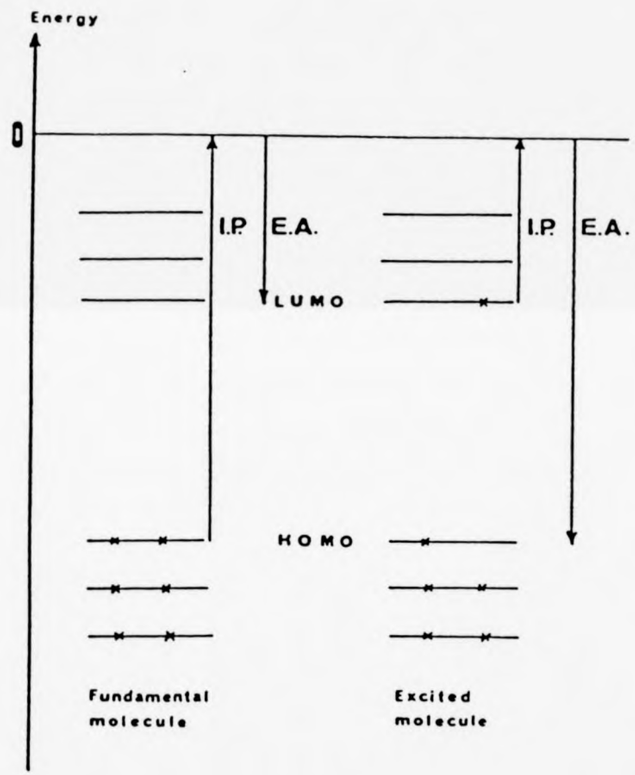

Figure (1.3) Schematic orbital diagram showing the decrease of the ionisation potential (I.P.) and the increase of the electron affinity (E.A.) upon excitation of a molecule. (From reference 24).

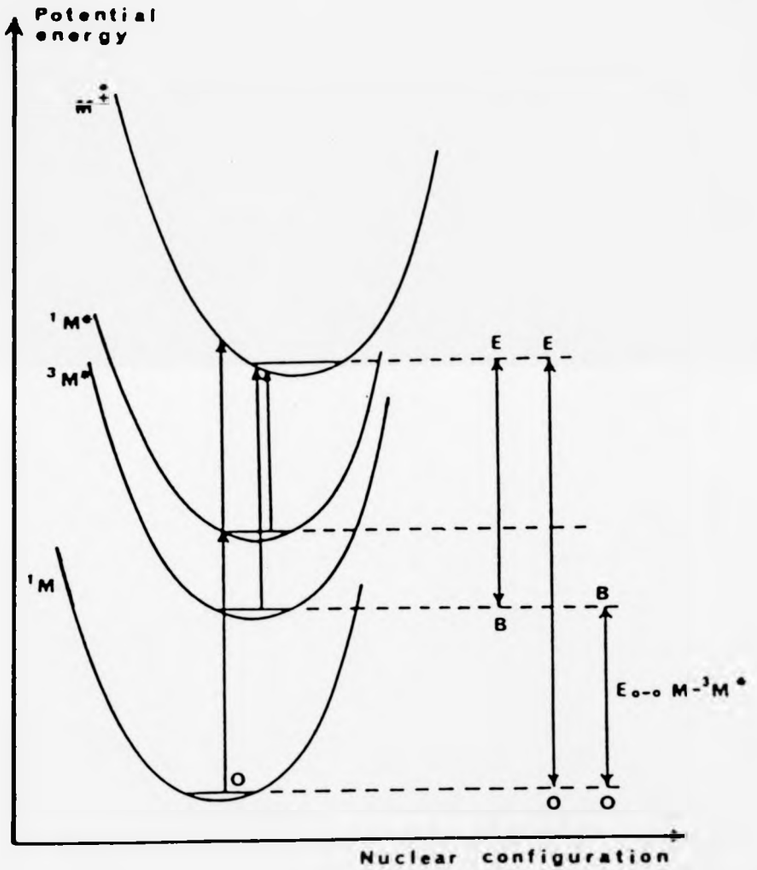

Figure (1.4) Potential energy curves featuring the excitation and ionisation processes of a molecule. ^1M is a ground-state organic molecule; $^1M^*$ is its lowest singlet excited state; $^3M^*$ is its lowest triplet excited state; $M^{+\cdot}$ is the cation radical.(From reference 24).

The right-hand side of equation (1.9) represent OE-BE = OB, where OE and BE are the equilibrium ionisation potentials of the ground and triplet states, respectively. If $E_{o,o}$ is the one-electron potential corresponding to the zero-zero spectroscopic energy of the excited state $^3M^*$, then $E^o(M^+/M)$ and $E^o(M^+/^3M^*)$ are the oxidation potentials of the ground and the lowest triplet states respectively. Since $\Delta G = \Delta H$ and $\Delta G = -nFE$ and

$$\Delta H[M \underset{OE}{\rightarrow} M^+] - \Delta H[^3M^* \underset{BE}{\rightarrow} M^+] = E_{o,o}(M \underset{OB}{\rightarrow} {}^3M^*) \qquad (1.10)$$

(here nF = 1) then

$$E^o(M^+,{}^3M^*) - E^o(M^+/M) = -E_{o,o}(M,{}^3M^*) \qquad (1.11)$$

The M^*/M^- redox couple can be approximated in the same way. So for any excited state:[22-26]

$$E^o(M^+/M^*) = E^o(M^+/M) - E_{o,o}(M \rightarrow M^*) \qquad (1.12)$$

$$E^o(M^*/M^-) = E^o(M/M^-) + E_{o,o}(M \rightarrow M^*) \qquad (1.13)$$

As the entropy corrections are very difficult to evaluate, equations (1.12) and (1.13) can be used to estimate redox potentials of photoexcited states from their ground state electrochemical redox potentials and their zero-zero spectroscopic transition energies. Equations (1.12) and (1.13) can be visualised in Figure (1.5) which shows the effect of photon absorption on the redox potential of ground state M.

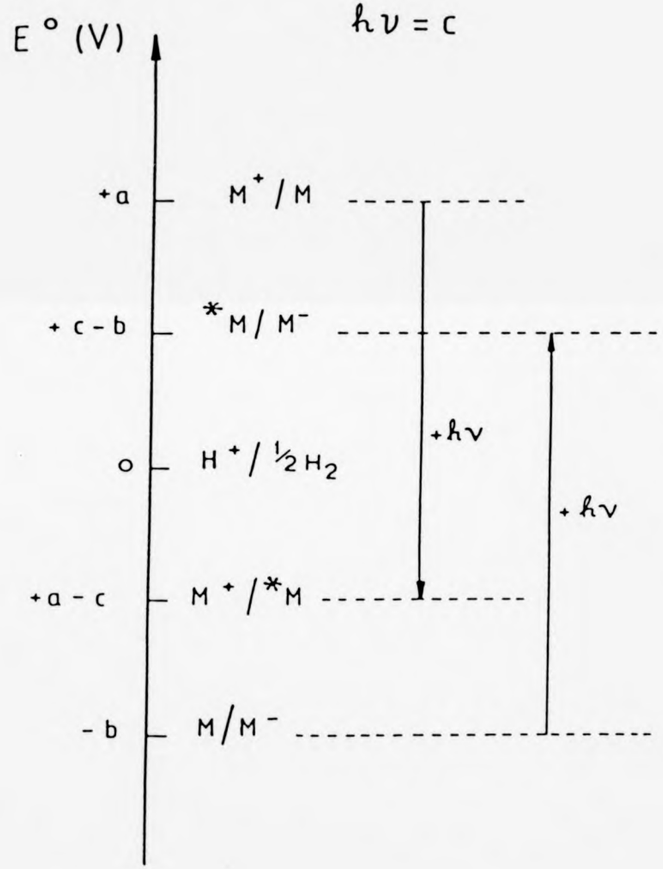

Figure (1.5) Schematic diagram showing the difference in redox properties of the ground and excited states of a molecule M according to equations (1.12) and (1.13); C is the one-electron potential corresponding to the zero-zero spectroscopic energy of the excited state. (From reference 22).

In organic molecules there is generally a large separation between oxidation states, so that an excited organic molecule can usually serve as either an electron donor or an electron acceptor but not both.[23,24] In transition-metal complexes the presence of redox sites on both metal and ligand offers additional possibilities unavailable to either the simple metal ion or the organic ligand molecules. The oxidation states are often closely spaced, so that it is often the case that an excited state can function as both electron donor and as electron acceptor.[23,24] As can be seen from Figure (1.5), when the oxidation and reduction potentials of a molecule are close enough, it is common to have light-driven crossing of the excited state potentials. Finally, in the case of organic molecules it must be emphasized that the excited singlet state is more oxidising than the corresponding triplet state; this follows from the energy difference between the two states that affect their redox potentials.[24]

There are three fundamental applications of redox reactions of photoexcited states:[25,26]

(i) For catalytic purposes; since the activation energy generally decreases with increasing exoergonicity, the reaction between one excited state species and another ground state chemical species may be much faster than that involving ground state reaction between the two chemical species.

(ii) For photochemical transformation of lower energy reactants into higher energy products, i.e. conversion of light energy into chemical energy.

(iii) For chemical generation of excited states in highly exoergonic reactions in order to convert chemical energy into light energy (chemiluminescence).

1.4 Theoretical Aspects of Outer-Sphere Thermal Electron-Transfer Reactions: An Outline of Marcus Theory

The Marcus formulation is the most widely used among several other classical models. It has enjoyed a wide popularity over two decades, even after the appearance of the quantum model due to[27,38] (i) its conceptually simple basis, (ii) its reasonably good predictive power and amenability to experimental tests, (iii) the relative ease with which the intrinsic barriers can be calculated. On the other hand, it uses input data that are sometimes difficult to obtain or estimate, as in other kinetic theories of similar character.[37]

Marcus[28-31] attacked the problem of estimating the rate constant for an outer-sphere electron transfer (1.14) between two

$$D + A \rightarrow D^+ + A^- \qquad (1.14)$$

transition metal complexes, one acting as donor (D) and the other as acceptor (A). Equation (1.14) can be discussed in terms of elementary steps as shown in scheme (1.15), where the electronic states of D and

$$\underset{\text{reactants}}{D + A} \underset{k_{-d}}{\overset{k_d}{\rightleftharpoons}} \underset{\text{precursor complex}}{D \ldots A} \underset{k_{-e}}{\overset{k_e}{\rightleftharpoons}} \underset{\text{successor complex}}{D^+ \ldots A^-} \xrightarrow{k_s} \underset{\text{products}}{D^+ + A^-} \qquad (1.15)$$

A are left unspecified, k_d, k_{-d} and k_s are diffusion or dissociation rate constants, and k_e, k_{-e} are the unimolecular rate constants for the forward and back-electron transfer in the encounter. The rate constant of the electron-transfer step of (1.15) can be expressed by an equation which is formally the same as that used in the absolute reaction rate theory.[32,35,41] According to this theory, the rate constant for a unimolecular reaction is given by

equation (1.16), where k_e^o is the frequency factor and ΔG^* is the free energy required to reorganise the coordination shells of the

$$k_e = k_e^o \exp(-\Delta G^*/RT) \qquad (1.16)$$

reactants prior to the electron transfer, and R and T have their usual meanings. The frequency factor is given by equation (1.17), where κ is the so-called transmission coefficient and k_BT/h is a universal

$$k_e^o = \kappa \frac{k_BT}{h} \qquad (1.17)$$

frequency factor for reaction between two uncharged reactants in solution (6×10^{12} s^{-1} at 25°C). The essence of the electron transfer problem is the fact that the equilibrium nuclear configuration of a species changes when it gains or loses an electron.[32,35,41] In the case of a metal complex, this configurational change involves changes in the vibrations and rotations of the solvent dipoles and, in most systems, changes in metal-ligand and intraligand bond lengths and angles as well. The changes in nuclear configurations give rise to an activation barrier to electron transfer because[32,35,41] nuclear motion occurs on a time scale (10^{-11} - 10^{-13} s) much longer than electronic motion (<10^{-15} s); (this is a statement of the Franck-Condon principle). Thus, the only possible region in which electron transfer can occur is near the crossing point of the zero-order potential energy surfaces of the initial and final states of the system. A cross-section of these surfaces is shown in Figure (1.6); the minima of the two curves correspond to the stable nuclear configurations of the reactants and products. The energy separation (E_{th}) between the

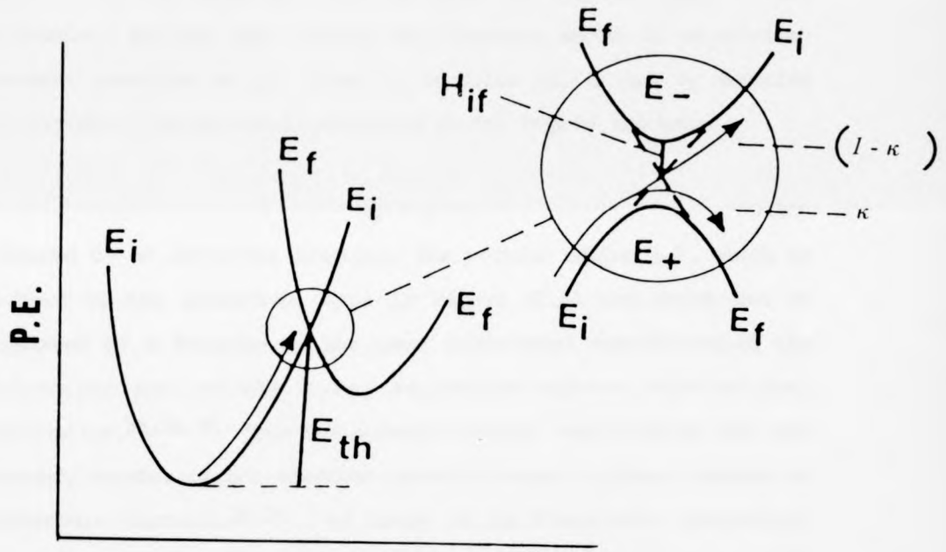

Figure (1.6) Schematic representation of potential energy changes during an electron-transfer process, E_i and E_f are the zero-order potential energy surfaces of the initial and final states. (From reference 26).

minimum of the initial state and the crossing point where the reaction can occur is called the reorganisation energy and it is usually taken to[26,35,41] equal $\Delta G^{\ddagger}$ which appears in equation (1.16). The parameter $\Delta G^{\ddagger}$ of the electron transfer reaction does not have the meaning of an activation energy because[33] it does not refer to a transition state but it is related to a non-equilibrium nuclear configuration of the reactants that has to be reached in order to obey the Franck-Condon principle. For the same reason, the frequency factor of an electron transfer reaction is not given by equation (1.17) but by equation (1.18), where the universal frequency factor (k_BT/h) has been

$$k_e^o = \kappa \nu_N \qquad (1.18)$$

replaced by an effective frequency for nuclear motion (ν_N), which is defined by the parabolic curve in Figure (1.6) and which can be expressed as a function of the inner vibrational coordinates of the molecules and of the outer solvation sphere vibrational frequencies.[32,34,35] Once the suitable nuclear configuration has been reached, whether or not electron transfer occurs is then a matter of electronic factors.[26,38] If there is no electronic interaction between the zero-order initial and final states, the surfaces will intersect and thus the reaction cannot take place. If there is an electronic interaction, the degeneracy at the intersection will be removed and two new surfaces will be formed[26,35,38] Figure (1.6). The separation between the two first-order surfaces is equal to $2H_{if}$, where H_{if} is the interaction energy[26,35,41] (electronic coupling matrix element). Marcus[28-31] assumed that H_{if} is small enough to be neglected in calculating E_{th}, but large enough so that the reactants are converted into products with unit probability in the intersection region. This is the so-called <u>adiabatic</u> assumption,

according to which the system always remains on the lower potential energy surface on passing through the intersection region. This is equivalent to saying that the transmission coefficient (κ)is unity. More generally, in the weak interaction limit, the second assumption has to be removed, and the possibility has to be considered that a system arriving from the initial state may continue along the original zero-order curve and then return without undergoing reaction. This so-called non-adiabatic behaviour may be taken into account by adopting a transmission coefficient of less than unity. Thus, in a classical adiabatic approach, the rate constant of the electron-transfer reaction converting the precursor into the successor complex, equation (1.15), is given[26,38] by equation (1.19).

$$k_e = \nu_N \exp(-\Delta G^{\ddagger}/RT) \qquad (1.19)$$

According to Marcus theory,[28-31] the reorganisational free energy ($\Delta G^{\ddagger}$) is made up by three parts, as in equation (1.20), the meaning of the individual terms being given below.

$$\Delta G^{\ddagger} = \Delta G_c^{\ddagger} + \Delta G_i^{\ddagger} + \Delta G_o^{\ddagger} \qquad (1.20)$$

$\Delta G_c^{\ddagger}$ is the free energy change due to electrostatic interaction between reactants in the transition state (equal to the work expended or gained in the process of moving the reactants from infinite distance to the colliding distance in the encounter complex). Eberson[27] has shown that $\Delta G_c^{\ddagger}$ decreases strongly with increasing ionic strength of the solution and for solutions of low ionic strength at 25°C, $\Delta G^{\ddagger}$ can be calculated according to equation (1.21), where values of the charges $|Z_1Z_2|$, the dielectric constant (ε) and the internuclear

$$\Delta G_c^{\ddagger} = \frac{331.3\ Z_1Z_2}{\varepsilon\ r_{12}} \qquad (1.21)$$

distance (r_{12}) are available.[27] Normally, $\Delta G_c^{\ddagger}$ can be neglected for many organic electron-transfer reactions and also for inorganic electron-transfer reactions if one of the reactants is uncharged.[26,38,41]

For a reaction between two complexes, $\Delta G_i^{\ddagger}$, expresses the free energy due to changes in the ligand geometry (bond lengthening and compression, etc.) required to satisfy the Franck-Condon principle. If it is assumed that the vibrations of the coordination shells are harmonic, at least to the intersection region, the inner-shell reorganisation energy can be easily estimated.[28] It can be written in terms of vibrational partition functions for the participating species (Q_A, Q_D and $Q_{\ddagger}^{V}$) as in equation (1.22) in which $\Delta U_i^{\ddagger}$ is the difference in zero-point energies between the transition state and reactants A and D. The partition functions are set equal to one, as an approximation for weakly interacting molecules, giving equation (1.23) from which the final set of equations (1.24-1.27) for expressing

$$\Delta G_i^{\ddagger} = -RT \ln \left(\frac{Q_{\ddagger}^{V}}{Q_A Q_D} \right) + \Delta U_i^{\ddagger} \qquad (1.22)$$

$$\Delta G_i^{\ddagger} = \Delta U_i^{\ddagger} \qquad (1.23)$$

$\Delta G_i^{\ddagger}$ was derived by statistical mechanics.[28]

$$\Delta G_i^{\ddagger} = m^2 \lambda_i \qquad (1.24)$$

$$m = -0.5 - \frac{\Delta G^{o}}{2\lambda} \qquad (1.25)$$

$$\lambda = \lambda_i + \lambda_o \qquad (1.26)$$

$$\lambda_i = \sum_j \frac{k_j^R k_j^P}{k_j^R + k_j^P} (q_j^R - q_j^P)^2 \qquad (1.27)$$

λ_i is the inner-sphere reorganisation energy (1.24), λ_o (1.26) is the sum of the solvent and ionic atmosphere reorganisation energies and λ (1.25, 1.26) is the total reorganisation energy. ΔG^o is introduced to simplify equation (1.25) and corresponds to the free-energy change for the reaction in the medium used; ΔG^o is not necessarily equal to the standard free energy change, but nevertheless in most cases it is put equal to it.[27] Equation (1.27) contains as the variable k_j^R and k_j^P the force constants of the j_{th} vibrational coordinate in a species participating as reactant and product, respectively, and $(q_j^R - q_j^P)$, the change in the bond lengths and bond angles in going from reactant to product.

A simple example from Eberson's review will help to clarify the meaning of (1.24) - (1.27). For a self-exchange reaction, i.e. a symmetrical electron transfer reaction with $\Delta G^o = 0$, an electron is transferred between $Fe(H_2O)_6^{2+}$ and $Fe(H_2O)_6^{3+}$ in their equilibrium configurations (1.28). If we consider the change in the Fe-O bond distance only, equation (1.27) gives the simplified expression (1.29), in which k_1 and k_2 are the force constants of the Fe-O bonds of the

$$\overset{*}{Fe}(H_2O)_6^{2+} + Fe(H_2O)_6^{3+} \longrightarrow \overset{*}{Fe}(H_2O)_6^{3+} + Fe(H_2O)_6^{2+} \qquad (1.28)$$

$$\lambda_i = \frac{12\, k_1\, k_2}{k_1 + k_2} (q_1 - q_2)^2 \qquad (1.29)$$

reactants and q_1, q_2 their equilibrium distances (with 2 x 6 = 12 Fe-O bonds in the transition state). Thus equation (1.24) becomes (1.30) and with values for k_1, k_2, q_1 and q_2 appropriate to $Fe(H_2O)_6^{2+}$ and

$$\Delta G_i^{\ddagger} = (0.5)^2 \frac{12\ k_1\ k_2}{k_1 + k_2} (q_1 - q_2)^2 \qquad (1.30)$$

$Fe(H_2O)_6^{3+}$ of 1.49 and 4.16 N cm^{-1} ; 2.21 and 2.05 Å, one obtains $\Delta G_i^{\ddagger}$ = 50 kJ mol^{-1}.[27]

For organic molecules it is often assumed[26,27,38,41] that the inner-sphere reorganisation energy, $\Delta G_i^{\ddagger}$, is equal to zero, which is another way of saying that no bond lengths and angles are changed on electron removal from, or addition to, an organic species.

The free energy change due to solvent reorganisation $\Delta G_o^{\ddagger}$ was estimated from a classical dielectric continuum model of the solvent[27,38,41], giving (1.31) and (1.32), where (e) is the change in the charge of each reactant, r_{12} is the distance between the centres

$$\Delta G_o^{\ddagger} = m^2 \lambda_o \qquad (1.31)$$

$$\lambda_o = e^2 \left(\frac{1}{2r_1} + \frac{1}{2r_2} - \frac{1}{r_{12}}\right)\left(\frac{1}{\varepsilon_o} - \frac{1}{\varepsilon}\right) \qquad (1.32)$$

of the two reactants in the encounter complex (usually taken as equal to the close contact distance, $r_1 + r_2$), ε_o is the optical dielectric constant (the square of the refractive index) and ε is the static dielectric constant of the solvent. In the case of reaction (1.28) in aqueous solution, the value of $\Delta G_o^{\ddagger}$ calculated from (1.31) is 27 kJ mol^{-1}.[38]

For an exchange reaction (1.28), the free activation energy

$\Delta G^{\ddagger}$ is related to the horizontal displacement of the curvature of the two curves representing the initial and final states of the system[26,38], Figure (1.7a). For the more general case of cross-electron transfer reactions[26,38] (i.e. electron transfer reactions with net chemical change, equation (1.33)), it is clear that the free activation energy depends not only on the horizontal

$$Fe(H_2O)_6^{2+} + Ru(NH_3)_6^{3+} \longrightarrow Fe(H_2O)_6^{3+} + Ru(NH_3)_6^{2+} \qquad (1.33)$$

displacement and curvature of the two curves, but also on the standard free energy change (ΔG^{o}) which represents the vertical displacement of the minima of the two curves assuming a negligible entropy change,[26] Figure (1.7b).

One difficulty with this model when applied to organic molecules is their non-spherical shape. Octahedral complexes are reasonably well-approximated as structureless, spherical objects but aromatic hydrocarbons and their radical ions have been treated in two ways.[27] In one, the spherical approximation is retained and an "effective" radius of the sphere is estimated from the molecular volume calculated by a simple method, equation (1.34) in which (M) is the molecular weight and (d) is the density.

$$r = \left(\frac{3M}{4\pi dN}\right)^{1/3} \qquad (1.34)$$

Alternatively a more realistic geometry based on known molecular dimensions is introduced and discussed in detail recently by Eberson.[27]

The complete expression for $\Delta G^{\ddagger}$ (1.35) can be obtained after rearrangement by combining (1.20), (1.21), (1.24), (1.25) and (1.31).

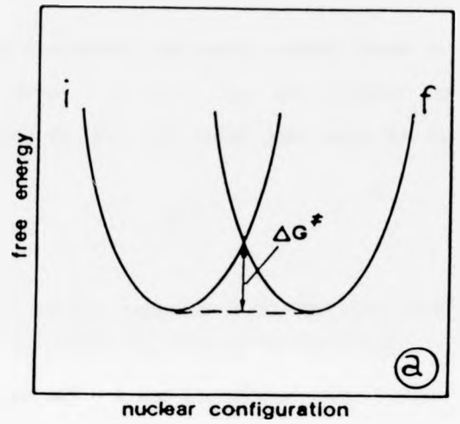

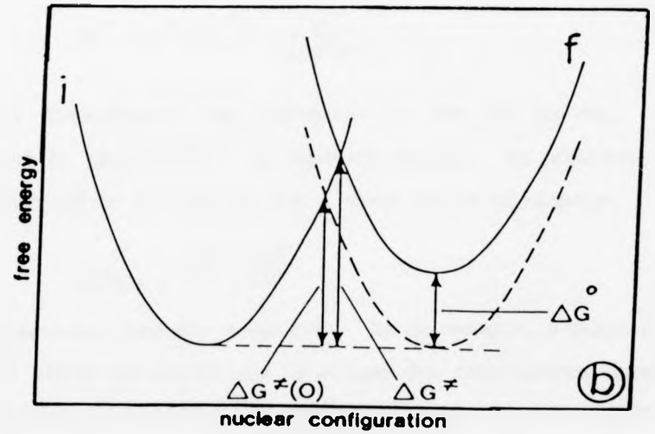

Figure (1.7) Schematic representations of the energy surfaces of the initial (i) and final (f) states for self-exchange (a) and cross-electron transfer (b) reactions. (From reference 38).

For a reaction involving at least one uncharged species, as for many

$$\Delta G^{\ddagger} = \frac{Z_1 Z_2 e^2}{\epsilon\, r_{12}} + \frac{\lambda_i + \lambda_o}{4}\left[1 + \frac{\Delta G^{o}}{\lambda_i + \lambda_o}\right]^2 \qquad (1.35)$$

organic electron transfers, the electrostatic term is considered zero and on substituting $\lambda = \lambda_i + \lambda_o$, one obtains the famous Marcus quadratic equation (1.36). One often also sees the alternative form

$$\Delta G^{\ddagger} = \frac{\lambda}{4}\left[1 + \frac{\Delta G^{o}}{\lambda}\right]^2 \qquad (1.36)$$

(1.37) in which $\Delta G^{\ddagger}(0)$ replaces $\lambda/4$. The intrinsic reorganisation barrier $\Delta G^{\ddagger}(0)$ is simply the change in activation free energy ($\Delta G^{\ddagger}$) for a process when $\Delta G^{o} = 0$ and is related only to the

$$\Delta G^{\ddagger} = \Delta G^{\ddagger}(0)\left[1 + \frac{\Delta G^{o}}{4\Delta G^{\ddagger}(0)}\right]^2 \qquad (1.37)$$

horizontal displacement and curvature of the two curves, Figure (1.7a), and is given[30,38,41] by equation (1.38). In practice it is assumed that $\Delta G^{\ddagger}(0)$ is constant for a whole series of closely-

$$\Delta G^{\ddagger}(0) = \frac{\Delta G_A^{\ddagger} + \Delta G_D^{\ddagger}}{2} \qquad (1.38)$$

related electron – transfer reactions. As an example, a value of 2.4 kcal mol^{-1} (10.0 kJ mol^{-1}) has been used for fluorescence quenching of hydrocarbons by electron donors.[15,16] Values of $\Delta G^{\ddagger}(0)$ of 63 kJ mol^{-1} or higher have been proposed[39] for ground-state electron transfer reaction of alkylmetals and electron acceptors. The profound effect of the value of $\Delta G^{\ddagger}(0)$ on the

activation free energy $\Delta G^{\ddagger}$ is shown in Figure (1.8) in order to illustrate the relative simplicity of the Marcus equation (1.37). The effect of $\Delta G^{\ddagger}(0)$ on the rate constant of excited state quenching will be discussed in section (1.5).

All non-bonding electron-transfer processes between two different species can actually be formulated as cross-reactions of two self-exchange reactions. Thus, the cross-reaction of (1.39) and (1.40) is (1.41) by neglecting a small electrostatic effect. Assuming that:[38,41]

$$D \ldots D^{+} \overset{k_{11}}{\rightleftharpoons} D^{+} \ldots D \qquad (1.39)$$

$$A \ldots A^{-} \overset{k_{22}}{\rightleftharpoons} A^{-} \ldots A \qquad (1.40)$$

$$D \ldots A \overset{k_{12}}{\rightleftharpoons} D^{+} \ldots A^{-} \qquad (1.41)$$

(i) the rate constants of unimolecular reactions k_{11}, k_{22} and k_{12} can be expressed by a classical adiabatic equation (1.19); **(ii)** the pre-exponential term is the same for (1.39), (1.40) and (1.41); **(iii)** the intrinsic barrier $\Delta G^{\ddagger}(0)$ of the cross reaction (1.41) is given by the average of the intrinsic barriers of the exchange reactions, equation (1.38), and **(iv)** the free activation energy of the cross-reaction is given by the Marcus equation (1.37), the following relations are obtained:

$$k_{12} = (k_{11} \cdot k_{22} \cdot K_{12} \cdot f)^{\frac{1}{2}} \qquad (1.42)$$

$$\ln f = \frac{(\ln K_{12})^2}{4 \ln (k_{11}\, k_{22}/\nu_N^2)} \qquad (1.43)$$

$$\log f = \frac{-1}{2.303\, RT} \cdot \frac{(\Delta G^{o}_{12})^2}{(\lambda_{11} + \lambda_{12})} \qquad (1.44)$$

where K_{12} is the equilibrium constant for the cross-reaction (1.41). Equation (1.42) is the so-called Marcus cross-relation.[29,30] Finally, equations (1.43) and (1.44) can be combined and rewritten to give (1.45); this useful relation tells us that a plot of the left hand side versus ΔG^{o}_{12} should be a straight line with slope 0.5

$$\Delta G^{\ddagger}_{12} + (0.5)(2.303)RT \log f = 0.5(\Delta G^{\ddagger}_{11} + \Delta G^{\ddagger}_{22}) + 0.5\ \Delta G^{o}_{12} \qquad (1.45)$$

and intercept equal $\Delta G^{\ddagger}(0)$, since $\Delta G^{\ddagger}(0) = 0.5(\Delta G^{\ddagger}_{11} + \Delta G^{\ddagger}_{22})$; equation (1.38). When $|\Delta G^{o}_{12}| \leqslant \Delta G^{\ddagger}(0)$ the parabolas of figure (1.8) can be approximated as a straight line with slopes of 0.5; this approximation[27] becomes better and has a wider range of validity with increasing value of $\Delta G^{\ddagger}(0)$.

The derivation (1.42) is very popular among inorganic and bioinorganic chemists who regularly use it to calculate rates of rections that would otherwise be difficult to measure.[37] This equation (1.42) is also used in reverse, i.e. to calculate log K_{12} from rate data and hence to obtain otherwise unknown redox potentials[43] through equation (1.46) where n is the number of

$$\log K_{12} = \frac{\Delta G^{o}}{2.303\ RT} = \frac{-nFE^{o}}{2.303\ RT} \qquad (1.46)$$

electrons and F is the Faraday constant.

Recently Ratner and Levine[40] have shown that the Marcus cross-relation (1.42) can be derived rigorously for the case that f = 1 by a thermodynamic treatment without postulating any microscopic model of the activation process.

Within the classical approach, the nonadiabaticity can formally be taken into account by using the transmission coefficient κ of the absolute reaction rate theory, equation (1.47), and relating it to the

$$k_e = \kappa\ \nu_N \exp(-\Delta G^{\ddagger}/RT) \qquad (1.47)$$

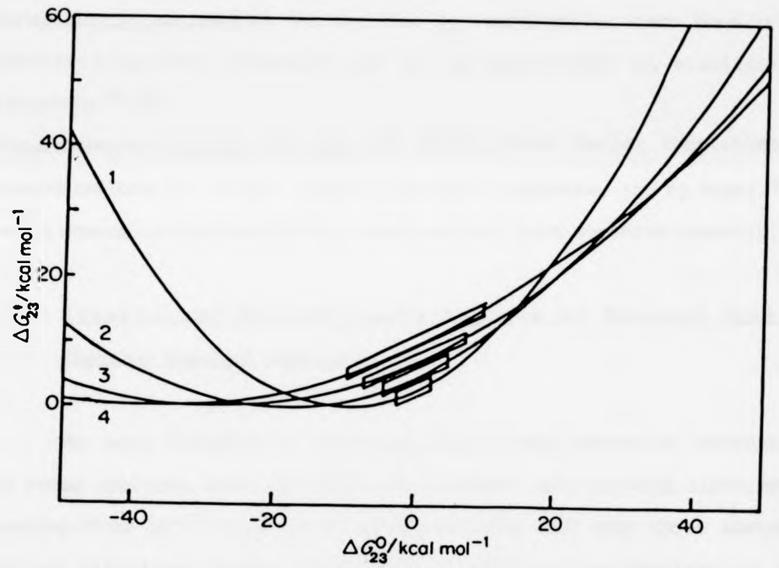

Figure (1.8) Plots of $\Delta G_{23}^{\ddagger}$ against ΔG_{23}^{o} according to the Marcus equation (1.60) for $\Delta G_{23}^{\ddagger}(0)$ equal to 2.4 (1), 4.8 (2), 7.2 (3) and 9.6 (4) kcal mol^{-1}. (From reference 27).

interaction energy between the two zero-order surfaces, Figure (1.6), by means of the semiclassical Landau-Zener theory.[33,38,41] An important difference between adiabatic and nonadiabatic classical expression has to be emphasized. In the adiabatic expression (1.19), the pre-exponential factor is a nuclear frequency and thus the electron-transfer process resembles an ordinary chemical reaction which is consummated by a nuclear motion. By contrast, in the nonadiabatic expression (1.47), the pre-exponential term does not contain a nuclear frequency but it is essentially an electronic frequency.[38,41]

Comprehensive reviews by Sutin,[41] which cover deeper theoretical considerations of thermal electron-transfer reactions, and by Meyer,[42] which covers excited-state electron-transfer, have appeared recently.

1.5 Kinetic and Thermodynamic Aspects of Excited State Electron-Transfer Reactions

The main features of electronically excited states as reactants in redox reaction are: **(i)** they are transient species with lifetimes ranging from 10^{-12} - 10^{-3}s in fluid solution and only those states having lifetimes longer than 10^{-10} - 10^{-9}s can be involved in a bimolecular electron-transfer quenching;[23,24] **(ii)** an excited state always has both a higher electronic affinity and a lower ionisation potential than the corresponding ground state molecule. The direction of the electron transfer depends on the sum of the ionisation potential and electron affinity of the individual reactants. The reactant with the greater sum always acts as oxidant (A) and that with

the small sum as reductant (D), irrespective of which of the reactants is in the excited state,[44] **(iii)** the equilibrium nuclear geometry of the excited state may be more or less different from that of the corresponding ground state and they are equal only when the Stokes' shift is zero, when the reorganisation parameters of the ground and excited states toward redox reactions are equal,[23,24] **(iv)** formation of an excited state usually involves population of high energy molecular orbitals which may well occupy a greater space or be highly delocalised and the latter may lead to changes in dipole moment, internal degrees of freedom, etc.[22]

The kinetic and thermodynamic aspects of excited state redox reactions were first discussed by Rehm and Weller,[15,16] who studied the electron transfer quenching of the fluorescence of aromatic compounds by a number of one-electron organic donors in acetonitrile solution; their kinetic scheme, which follows, has been widely adopted.[15,16]

$$\begin{array}{ccccc} & {}^1A^* & + D & \underset{k_{21}}{\overset{k_{12}}{\rightleftharpoons}} & ({}^1A^* \ldots D) \\ h\nu & \downarrow\uparrow 1/\tau_o & & & \text{encounter complex} \\ & A & & & \end{array} \quad \underset{k_{32}}{\overset{k_{23}}{\rightleftharpoons}} \quad \begin{array}{c} (A^{\cdot -} \ldots D^{\cdot +}) \\ \text{solvated ion pair} \\ \downarrow k_{30} \\ A^{\cdot -} + D^{\cdot +} \text{ or } A + D \end{array}$$

The electron transfer quenching originates from a weakly bound encounter complex formed by interaction between the excited singlet state molecule ($^1A^*$) and the ground state molecule (D). In the above scheme ($^1/_{\tau_o}$) is the decay fluorescence constant in the absence of quencher, k_{12} and k_{21} are the diffusion and dissociation rate constants of the encounter complex, k_{23} and k_{32} are the rate constants for forward- and back-electron transfer in the encounter complex, and k_{30} comprises all the possible ways by which

the solvated ion pair can be consumed. Using steady-state approximations, the following equation (1.48) is obtained for the overall experimental bimolecular quenching rate constant, k_q.

$$k_q = \frac{k_{12}}{1 + \frac{k_{21}}{k_{23}} + \frac{k_{21}}{k_{30}} \cdot \frac{1}{K_{23}}} \tag{1.48}$$

All the three electron transfer steps (k_{23}, k_{32}, k_{30}) are assumed to occur by the same adiabatic outer-sphere type mechanism, and according to absolute rate theory[45] their rate constants are given by:

$$k_{ij} = \kappa^{o}_{ij} \exp(-\Delta G^{*}_{ij}/RT) \tag{1.49}$$

where κ^{o}_{ij} is the collisional frequency factor and assumed to be the same for the three electron-transfer steps and κ^{o}_{ij} usually taken equal[15,16] to k_{30} since the free energy of activation (ΔG^{*}_{30}) for k_{30} leading to ground state products is assumed to be close to zero, so that $k_{30} = \kappa^{o}_{ij} = 5 \times 10^{10}\ s^{-1}$. Using a classical approach, k_{23} and $1/K_{23} = k_{32}/k_{23}$ are given by equation (1.50) and (1.51).

$$k_{23} = k_{30} \exp(-\Delta G^{*}_{23}/RT) \tag{1.50}$$

$$1/K_{23} = k_{32}/k_{23} = \exp(\Delta G^{o}_{23}/RT) \tag{1.51}$$

Substitution of equation (1.50) and (1.51) into equation (1.48) leads to equation (1.52), ΔG^{*}_{23} and ΔG^{o}_{23} are the free energy of

$$k_q = \frac{k_{12}}{1 + \frac{k_{21}}{\kappa^{o}_{23}} \left[\exp\left(\frac{\Delta G^{*}_{23}}{RT}\right) + \exp\left(\frac{\Delta G^{o}_{23}}{RT}\right)\right]} \tag{1.52}$$

activation and the standard free energy change for the electron transfer step (k_{23}). The diffusion-controlled rate constant k_{12} is given by the Debye equation[46] (1.53), where η is the viscosity of the solvent (in poise). While the rate constant for the dissociation

$$k_{12} = \frac{8\ RT}{3000\ \eta} \qquad (1.53)$$

of the encounter complex can be estimated by the Eigen equation[47] (1.54), where r, the encounter distance, is usually taken[15,16] as

$$k_{21} = k_{12}\ \frac{3}{4\pi\ r^3 N} \qquad (1.54)$$

7 Å with N being the Avogadro number. Thus the simplified form of the Rehm and Weller treatment is equation(1.55), from which k_q is expected to be depend only on ΔG^{o}_{23} and $\Delta G^{\ddagger}_{23}$.

$$k_q = \frac{20 \times 10^9\ M^{-1}\ s^{-1}}{1 + 0.25\left[\exp\left(\frac{\Delta G^{\ddagger}_{23}}{RT}\right) + \exp\left(\frac{\Delta G^{o}_{23}}{RT}\right)\right]} \qquad (1.55)$$

The ΔG^{o}_{23} for the overall net electron-transfer reaction is related to redox potentials of the excited singlet state and the quencher according to equation (1.56).

$$\Delta G^{o}_{23}(\text{kJ mol}^{-1}) = 96.48\ [E^{o}D/D^{\cdot+} - E^{o}A^{\cdot-}/A - \frac{e^2}{\varepsilon r} - \Delta^1 E_{o,o}] \qquad (1.56)$$

where $\Delta^1 E_{o,o}$ is the zero-zero spectroscopic energy of the fluorescer (in eV), $\frac{e^2}{\varepsilon r}$ is the Coulombic energy released by bringing the two radical ions to the encounter distance, which has been taken[15,16] as 0.06 eV in acetonitrile, $E^{o}D/D^{\cdot+}$ and $E^{o}A^{\cdot-}/A$ are the one-electron oxidation and reduction potentials of the donor and the acceptor (in eV), respectively.

Rehm and Weller,[15,16] on the basis of many experimental results, derived an empirical relationship (1.57) which correlated ΔG^{o}_{23} with $\Delta G^{\ddagger}_{23}$ on the assumption that the latter is a monotonic function of ΔG^{o}_{23}.

$$\Delta G^{\ddagger}_{23} = \frac{\Delta G^{o}_{23}}{2} + \left[\left(\frac{\Delta G^{o}_{23}}{2}\right)^{2} + (\Delta G^{\ddagger}_{23}(0))^{2}\right]^{\frac{1}{2}} \qquad (1.57)$$

Here $\Delta G^{\ddagger}_{23}(0)$, is the reorganisation intrinsic barrier which was found[15,16] experimentally to be 10.0 kJ mol^{-1} (2.4 kcal mol^{-1}) and this barrier is related to the change in the nuclear position that must occur prior to the electron transfer step. The intrinsic energy barrier is equal to the value of $\Delta G^{\ddagger}_{23}$ when $\Delta G^{o}_{23} = 0$, Figure (1.9b). The correlation between log k_q and ΔG^{o}_{23} for the electron transfer quenching according to equations (1.55) and (1.57), is demonstrated in Figure (1.10), which consists of: (i) a plateau region for sufficiently exoergonic reaction ($\Delta G^{o}_{23} < 0$, $\Delta G^{\ddagger}_{23} \gtrsim 0$) when the rate of quenching is given by equation (1.58) (ii) an inter-

$$k_q = \frac{k_{12}\, k_{30}}{k_{30} + k_{21}} \qquad (1.58)$$

mediate region centred at $\Delta G^{o}_{23} \approx 0$; $\Delta G^{\ddagger}_{23} = 10.0$ kJ mol^{-1} in which log k_q increased in a complex but monotonic way as ΔG^{o}_{23} becomes more negative and, (iii) a linear region (slope = $-1/2.303\ RT = -16.9\ eV^{-1}$ for sufficiently endoergonic reactions ($\Delta G^{o}_{23} > 0$) when the rate of quenching is given by equation (1.59).

$$k_q = \frac{k_{12}\, k_{30}}{2\, k_{21}} \exp(-\Delta G^{o}_{23}/RT) \qquad (1.59)$$

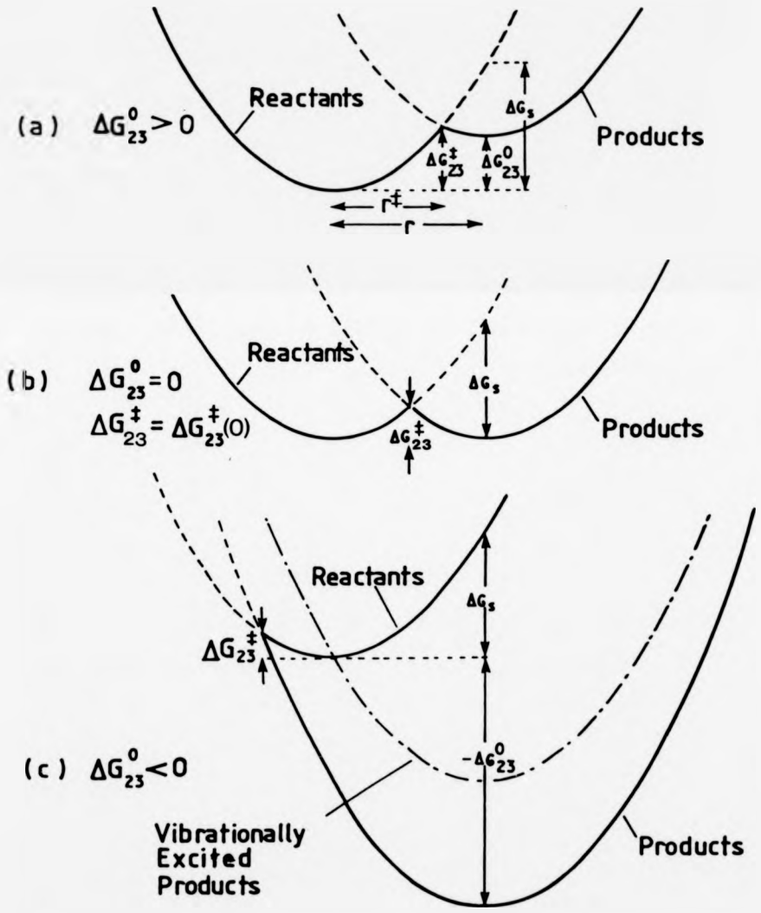

Figure (1.9) Schematic diagram showing the increase in the value of $\Delta G^{\ddagger}_{23}$ for outer-sphere electron-transfer reactions, in which the activated complex occurs at the intersection of similar solvent or ligand reorganisation free energy parabolas (ΔG_S), as the value of ΔG^{o}_{23} increases from (c) the exoergonic region to (b) the isoergonic region then to (a) the endoergonic region. (From reference 4).

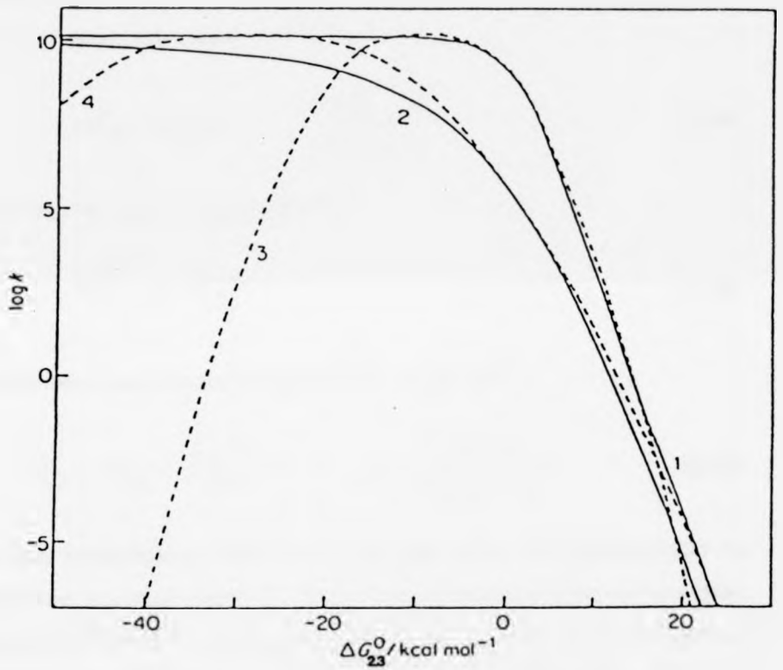

Figure (1.10) Rehm and Weller (——) and Marcus (---) plots for $\Delta G_{23}^{\ddagger}(O)$ = 2.4 (1 and 3) and 7.2 (2 and 4) kcal mol^{-1}. (From reference 27).

A number of excited state redox reactions of organic molecules have been found to obey the Weller equations (1.52) and (1.57).[48-58] The other free energy relationships which have been proposed in connection with electron transfer process involving excited states in solution are:

(i) Marcus' quadratic equation[29,30]

$$\Delta G^{\ddagger}_{23} = \Delta G^{\ddagger}_{23}(0) \left[1 + \frac{\Delta G^{o}_{23}}{4\Delta G^{\ddagger}_{23}(0)}\right]^2 \qquad (1.60)$$

(ii) Polanyi's linear equation[59,60]

$$\Delta G^{\ddagger}_{23} = \alpha\ \Delta G^{o}_{23} + \beta \qquad (1.61)$$

(iii) Scandola and Balzani's hyperbolic equation[61]

$$\Delta G^{\ddagger}_{23} = \Delta G^{o}_{23} + \frac{\Delta G^{\ddagger}_{23}(0)}{\ln 2} \ln \{1 + \exp \left[\frac{-\Delta G^{o}_{23} \ln 2}{\Delta G^{\ddagger}_{23}(0)}\right]\} \qquad (1.62)$$

The Marcus relationship equation (1.60) has been used successfully to rationalise kinetic data on many ground-state electron-transfer reactions.[32,36,62,63] A peculiar and famous feature of this equation is the prediction of an increase of $\Delta G^{\ddagger}_{23}$ when ΔG^{o}_{23} becomes less than $-4\,\Delta G^{\ddagger}_{23}(0)$. When used in conjunction with equation (1.55), it predicts a dramatic decrease in log k_q with increasing exoergonicity (to give the so-called 'Marcus inverted region'), Figure (1.10). Experimental evidence for or against such an inverted region cannot usually be obtained in the case of ground-state electron-transfer reaction in fluid solution because ΔG^{o}_{23} is not sufficiently negative.

However analysis of data for excited-state electron-transfer reactions[15,16,48-58] demonstrates that the decrease in reaction rate predicted by equation (1.60) for highly exoergonic reaction does not take place. Several explanations have been put forward to account for this discrepancy within the framework of the Marcus theory. Recently Marcus and Sider[64] suggested that exothermic processes take place over larger distances than the collision model implies. This will make $\Delta G^{\ddagger}_{23}(0)$ larger and hence $\Delta G^{\ddagger}_{23}$ small, thereby reducing the extent of inversion. However, increasing the encounter distance causes a strong decrease of the value of κ^{o} in equation (1.49), which would make the reaction nonadiabatic.[27] Another explanation includes the existence of a competing mechanism in the highly exoergonic region, such as H-atom transfer,[65,66] exciplex formation,[18] formation of products in excited electronic states and also nuclear tunnelling of the reactants to vibrationally excited states of the products.[65,67-69]

One feature of the linear free energy equation (1.61), with α and β being empirical parameters, is that it breaks down for very large positive or negative value for ΔG^{o}_{23}. The view has been expressed[27,70] that such linear relationship can be regarded as approximations of the other free energy relationships over narrow ranges of ΔG^{o}_{23}, depending on the value of $\Delta G^{\ddagger}_{23}(0)$.

Scandola and Balzani[71] developed a free energy relationship, equation (1.62), by the bond energy-bond order method for a function first derived by Marcus[72] for atom transfer reactions and formulated latter empirically by Agmon and Levine.[73,74] Equation (1.62), in

conjunction with equation (1.55), gives almost the same plot of log k_q versus ΔG^{o}_{23} as the Weller relationship, Figure (1.11). According to Scandola and Balzani[71] (1.62) should be preferred over equation (1.57) since the latter is empirical. In general, the non-linear equations (1.57), (1.60) and (1.62) are closely similar around $\Delta G^{o}_{23} = 0$ but they differ for very negative and very positive ΔG^{o}_{23} values, when equations (1.57) and (1.62) give linear, instead of a quadratic dependence of log k_q on ΔG^{o}_{23}, Figures (1.10) and (1.11).

The apparent contradiction about the validity of the linear equation (1.61) and the non-linear equations (1.57), (1.60) and (1.62) has also been explained[70] in the following way. When $\Delta G^{\ddagger}_{23}(O)$ is very large, over a wide range in ΔG^{o}_{23} of the curve corresponding to equations (1.55) and (1.62), the curves can be approximated as tangents, Figure (1.11), with slopes given by equation (1.63). These tangents are exactly the straight lines which can be obtained from

$$\gamma = \frac{1}{2.303\ RT\ [1 + \exp(-\ln 2 \frac{\Delta G^{o}_{23}}{\Delta G^{\ddagger}_{23}(O)})]} \qquad (1.63)$$

equation (1.55) using the Polanyi equation, (1.61). Thus the experimental values of the slope (α) and the intercept (β) have been related to ΔG^{o}_{23} and $\Delta G^{\ddagger}_{23}(O)$ by:

$$\alpha = \frac{1}{[1 + \exp(-\ln 2 \frac{\Delta G^{o}_{23}}{\Delta G^{\ddagger}_{23}(O)})]} \qquad (1.64)$$

$$\beta = \frac{\Delta G^{o}_{23}}{1 + \exp(\ln 2 \frac{\Delta G^{o}_{23}}{\Delta G^{\ddagger}_{23}(O)})} + \frac{\Delta G^{\ddagger}_{23}(O)}{\ln 2} \ln \frac{1}{\alpha} \qquad (1.65)$$

Figure (1.11) Plot of Scandola and Balzani equation (1.62) in conjunction with equation (1.55). The response of log k to changes in ΔG°_{23} as the value of $\Delta G^{\ddagger}_{23}(0)$ is varied. (From reference 70).

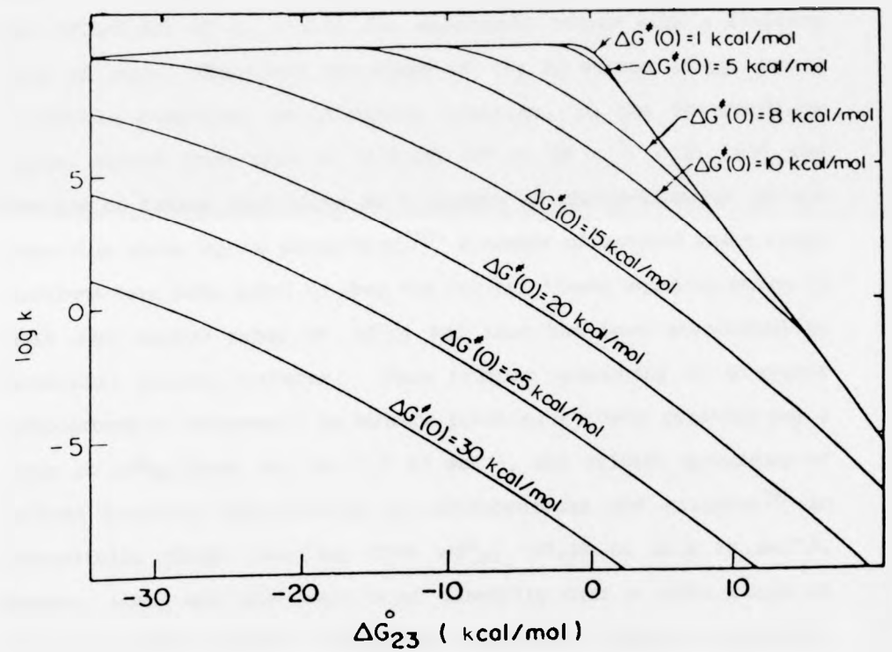

and

$$\alpha = -2.303\ RT\ \gamma \qquad (1.66)$$

where (β) is equal to $\Delta G^{\ddagger}_{23}(0)$ only for the tangent at $\Delta G^{o}_{23} = 0$, being less than $\Delta G^{\ddagger}_{23}(0)$ for all the other tangents. For $\Delta G^{o}_{23} = 0$, the slope of the tangent is $-0.5/2.303\ RT$ ($\alpha = 0.5$) and will be more negative than $-0.5/2.303\ RT$ ($\alpha > 0.5$) for endoergonic region, and less negative than $-0.5/2.303\ RT$ ($\alpha < 0.5$) for exoergonic region with a limiting value of zero. Therefore the slope of log k_q versus ΔG^{o}_{23}, for a reversible complete, one-electron transfer, in the intermediate region, varies from zero to $-1/2.303\ RT$ or ($0 < \alpha < 1$), and the practice of taking this slope as a measure of charge-transfer in the transition state may be misleading.[70] A number of excited state redox reactions have been found to obey the Polanyi linear equation which is valid over a narrow range of ΔG^{o}_{23} and this has been attributed to favourable charge transfer. Thus triplet quenching of aromatic hydrocarbons by quinones[75] in benzene provides a linear relation for a range in ΔG^{o}_{23} from -9.6 to 7.7 kJ mol^{-1}, and triplet quenching of various aromatic hydrocarbons by nitrobenzenes and quinones[76] in acetonitrile gives linearity from ΔG^{o}_{23} -19.29 to 38.6 kJ mol^{-1}. However, there are also reports of linearity over a wider range of ΔG^{o}_{23} and this has been attributed either to charge or electron transfer quenching depending on the observation of radical ion products. Thus the range of linearity spans from -90 to 90 kJ mol^{-1} in the fluorescence quenching of various aromatic hydrocarbons by inorganic anions[77,78] and from -25 to 90 kJ mol^{-1} in the quenching of triplet ketones by inorganic anions.[79]

Linear plots covering a range in ΔG^{o}_{23} of 90 kJ mol^{-1} are also reported by Kuzmin et al.[80,81] for fluorescence quenching of 9, 10-dicyanoanthracene in heptane and of exciplexes in benzene. Triplet quenching of methylene blue by aliphatic and aromatic amines in methanol was found[82] to correlate linearly with ionisation potential covering a range of ΔG^{o}_{23} = 90 kJ mol^{-1}. Recently, the Polanyi equation has been successfully applied in the quenching of excited uranyl ion by organosulphur, organohalogen and organometal species[83] and the mechanism of quenching explained in terms of full one-electron transfer, and the intermediacy of an exciplex based on identification of the radical cation products resulting from the quenching process.

The rate constant of the electron transfer step (k_{23}) in the Weller scheme has been taken as a measure of comparison of the reactivities of excited states of organic molecules. The difference in quenching rate constants of excited singlet (k_q^S) and triplet state (k_q^T) of the same molecules was studied for several dye molecules such as thionine[53,84,85], methylene blue[52], o-methylfluorescein methyl ether[84] and acridine orange[54,86] with organic reductants. In all these studies the authors conclude that triplet state displays lower reactivity than the excited singlet state. Many explanations have been proposed for this trend; among them are (i) the back electron-transfer (k_{30}) to a ground state is spin-forbidden in the case of the triplet and there is therefore a slower deactivation of the triplet exciplex than the singlet exciplex,[54] (ii) the excited singlet and triplet states differ in position and curvature in their potential energy minima, resulting in different activation free

enthalpies for singlet and triplet electron transfer reactions,[84] (iii) the higher energy of the excited singlet state as compared with the triplet state affects the redox potential of the excited states and therefore the value of ΔG^{o}_{23} for the electron transfer step in the encounter complex between the excited states and the reductants.[53,85,86] Recently, the dependence of the rate of quenching in excited flavin by organic reductants has been investigated by Vogelmann et al.[87] who concluded that the lower reactivity of triplet state as compared with the excited singlet state is consistent with equation (1.67). This equation (1.67) reflects clearly the difference in reactivity in electron transfer quenching as due to the

$$\text{Log}\ \frac{k_q^S}{k_q^T} = \frac{-1}{2.3\ RT}\ [\Delta^1 E_{o,o} - \Delta^3 E_{o,o}] \qquad (1.67)$$

difference in energy between the two excited states. In most of the examples given above, the overall trends typical of the Weller plot for singlet excited states are shifted slightly to a negative value of ΔG^{o}_{23} for the corresponding triplet states. However, a comparison of the quenching of excited singlet and triplet states of various aromatic hydrocarbons by europium ion as acceptor shows[88] the plateau value of the triplet quenching rates is~10^6 $dm^3\ mol^{-1}\ s^{-1}$, which is anomalously low, while the singlet excited states almost fit to the Weller plot. The different behaviour was explained[88] on the basis of the higher polarisability of the singlet state. The same explanation was used previously to interpret the higher quenching rate constant of fluorescence of biacetyl compared with that of phosphorescence by inorganic anions.[89]

Eberson[27,90] has argued that the widely accepted value of $\Delta G^{\ddagger}_{23}(0)$ of 10.04 kJ mol^{-1} (2.4 kcal mol^{-1}) need not and indeed should not be valid for all electron-transfer reactions. Recent studies have confirmed this view, thus the fluorescence quenching of chlorophyll a by quinones[55] requires $\Delta G^{\ddagger}_{23}(0)$ = 20.92 kJ mol^{-1} to achieve a good fit to the Rehm-Weller equation, while even higher values of $\Delta G^{\ddagger}_{23}(0)$ are required to fit the fluorescence quenching data of anthraquinone radical anion (41.8 kJ mol^{-1}) and thianthrene radical cation (64 kJ mol^{-1}) by organic acceptors and donors respectively in terms of the Marcus equation.[91,92] The reader is also referred to p.53.

1.6 Solvatochromic Effects in the Fluorescence and Absorption Spectra of Aromatic Compounds

Solvatochromism, i.e. solvent-induced changes of absorption and especially emission spectra provides the simplest and most well-established probe of the change in electron distribution on excitation to the S_1 state, and hence a method of evaluating the dipole moment of the S_1 state.[93-103] Generally, the S_1 states of aromatic compounds possess dipole moments (μ_e) which are larger than in the S_o state (μ_g). As a result, the absorption of a photon by a fluorophore results in the essentially instantaneous creation of a dipole, which perturbs the environment surrounding the fluorophore. This process is called solvent relaxation.[3,93,103] Because nuclear motions are involved, solvent relaxation occurs approximately at the same time as vibrational relaxation, taking about 10^{-14} - 10^{-12} s , and the process is rapid by comparison with the lifetime of the S_1 state (~10^{-8} s). Consequently, fluorescence originates from the excited solute molecule in a thermally equilibrated solvent

Eberson[27,90] has argued that the widely accepted value of $\Delta G^{\ddagger}_{23}(0)$ of 10.04 kJ mol^{-1} (2.4 kcal mol^{-1}) need not and indeed should not be valid for all electron-transfer reactions. Recent studies have confirmed this view, thus the fluorescence quenching of chlorophyll a by quinones[55] requires $\Delta G^{\ddagger}_{23}(0)$ = 20.92 kJ mol^{-1} to achieve a good fit to the Rehm-Weller equation, while even higher values of $\Delta G^{\ddagger}_{23}(0)$ are required to fit the fluorescence quenching data of anthraquinone radical anion (41.8 kJ mol^{-1}) and thianthrene radical cation (64 kJ mol^{-1}) by organic acceptors and donors respectively in terms of the Marcus equation.[91,92] The reader is also referred to p.53.

1.6 Solvatochromic Effects in the Fluorescence and Absorption Spectra of Aromatic Compounds

Solvatochromism, i.e. solvent-induced changes of absorption and especially emission spectra provides the simplest and most well-established probe of the change in electron distribution on excitation to the S_1 state, and hence a method of evaluating the dipole moment of the S_1 state.[93-103] Generally, the S_1 states of aromatic compounds possess dipole moments (μ_e) which are larger than in the S_0 state (μ_g). As a result, the absorption of a photon by a fluorophore results in the essentially instantaneous creation of a dipole, which perturbs the environment surrounding the fluorophore. This process is called solvent relaxation.[3,93,103] Because nuclear motions are involved, solvent relaxation occurs approximately at the same time as vibrational relaxation, taking about 10^{-14} - 10^{-12} s , and the process is rapid by comparison with the lifetime of the S_1 state (~10^{-8} s). Consequently, fluorescence originates from the excited solute molecule in a thermally equilibrated solvent

cage configuration which is lower in energy than Franck-Condon excited state, and generally somewhat lower than vibrationally relaxed unsolvated or weakly solvated excited molecule. When fluorescence occurs, it terminates in the ground electronic state of the solute molecule, but because of the rapidity of the electronic transition, the molecule remains momentarily in the (excited state) equilibrium solvent cage (i.e. higher in energy than the thermally relaxed ground state). Rapid solvent relaxation then occurs (10^{-14} - 10^{-12} s), and the solute molecule ultimately returns to the (ground state) equilibrium solvent cage. Because the solvent relaxed excited state is lower in energy than the Franck-Condon excited state, and the Franck-Condon ground state is higher in energy than the solvent relaxed ground state, Figure (1.12), fluorescence often occurs at considerably longer wavelengths than would be expected on the basis of vibrational relaxation.[3,93,103] This type of behaviour is characteristic of most $\pi \rightarrow \pi^*$ and intramolecular charge-transfer transitions.[3,93] In the event that the electronic dipole moment is lower in the Franck-Condon excited state than in the ground state, increasing solvent polarity will stabilise the ground state to a greater degree than the excited state and the absorption spectrum will show a blue shift with increasing solvent polarity. This type of behaviour is generally observed in $n \rightarrow \pi^*$ transitions because of the preferred stabilisation of the non-bonding orbital in the ground state.[3,93] Therefore, in general, fluorescence emissions from molecules which become highly polar in the S_1 state tend to show a greater wavelength dependence on solvent polarity than do the corresponding absorption spectra because of relatively greater solvent relaxation stabilisation of the S_1 state,[3,103] Figure (1.12).

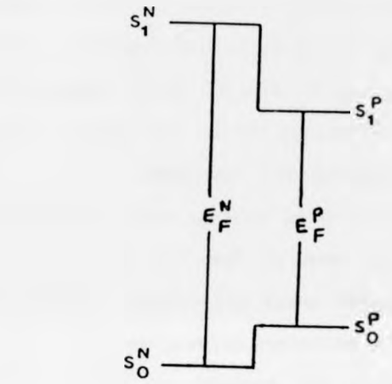

(a)

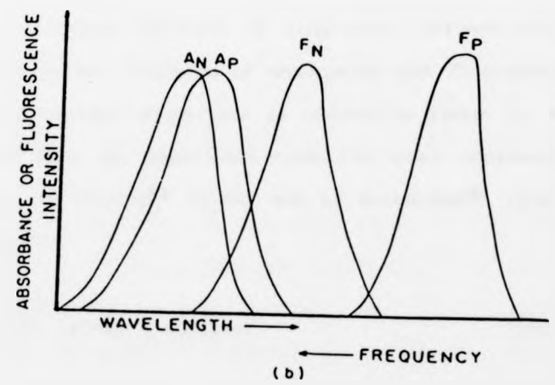

(b)

Figure (1.12) (a) The effect of solvent upon the energy of the fluorescent transition (E_F) of a molecule which is more polar in the excited state (S_1) than in the ground state (S_O). Superscript (N) denotes non-polar solvent; superscript (P) denotes polar solvent.

(b) Representation of the fluorescence bands F_N and F_P which might be expected to correspond to the transition depicted in (a). The corresponding $S_O \rightarrow S_1$ absorption bands (A_N and A_P) are also shown, illustrating the relative failure of the mirror image relationship between absorption and fluorescence in polar solvents. (From reference 3).

The derivations of the solvatochromic equations[98-104] of absorption and fluorescence are based principally on the magnitude of the interaction of solute with solvent, which is in turn related to the values of μ_g and μ_e, and the reactive fields around the dipoles. These fields have been divided into electronic factors and solvent reorientation; the electronic field depends on the dipole moment and the solvent refractive index (n) while the solvent reorientation factor depends on the dipole moment and the dielectric constant (ε). Numerous approximations have been invoked in deriving solvatochromic equations, as comprehensively reviewed by Amos and Burrows[100] and latterly by Koutek.[101,102] Despite the known limitations[105] of the absorption shift method for quantitative evaluation of μ_e, studies are still continuing[102,106,107] to improve the reliability of the estimated μ_e values. Koutek[101] has evaluated statistically sixteen equations based on existing theories of long-range solvent-solute interactions which correlate energies of absorption and fluorescence with such macroscopic solvent properties as refractive index (n) and dielectric constant (ε); he concluded that the near-equivalent approaches of Bilot and Kawski[94] (1.68) and of Bakhshiev[95] (1.69), afforded optimum results.

$$\Delta\bar{\nu}_{SS} = \frac{(\mu_e - \mu_g)^2}{h\ c\ a^3}\ [B\text{-}K] + \text{constant} \qquad (1.68)$$

where

$$B\text{-}K = \frac{(\frac{\varepsilon - 1}{2\varepsilon + 1}) - (\frac{n^2 - 1}{2n^2 + 1})}{(1 - \beta.\ \frac{n^2 - 1}{2n^2 + 1})^2\ (1 - \beta.\ \frac{\varepsilon - 1}{2\varepsilon + 1})}$$

$$h\ c\ \Delta\bar{\nu}_{SS} = \frac{2(\mu_g^2 - \mu_e^2 - 2\mu_g\mu_e\ \cos\alpha)}{h\ c\ a^3}\ .\ F(\varepsilon,n)\ .\ F(n^2) + \text{constant} \qquad (1.69)$$

where

$$F(\varepsilon,n) = \left(\frac{\varepsilon-1}{\varepsilon+2} - \frac{n^2-1}{n^2+2}\right)$$

$$F(n^2) = \left(\frac{2n^2+1}{n^2+2}\right)^2$$

The Stokes' shift $\Delta\bar{\nu}_{SS}$ (i.e. the energy of absorption $\bar{\nu}_A$ minus the energy of fluorescence $\bar{\nu}_F$) has been related to polarisability functions through μ_g and μ_e. Other terms are as follows: β - a factor approximated by unity, a - the solute cavity radius, α - the angle between μ_g and μ_e, h and c are the normal universal constants. However, all the treatments agree on certain essentials, i.e. (i) the increase of the Stokes' shift with solvent polarity results from an increase in the dipole moment of the S_1 over that of S_o state; (ii) fluorescence from unsubstituted aromatic hydrocarbons (Ar-H) will show little sensitivity to solvent because of the high symmetries of both S_o and S_1 states; (iii) substitution of (ArH) by good electron donor or acceptor groups will induce large solvatochromic effects in fluorescence because of the increase of intramolecular charge-transfer in the S_1 state.

These solvent-sensitive properties have been extensively utilised, particularly as probes of biological systems,[103] to draw conclusions about the nature of the site occupied by the probe molecule. Kosower and co-workers[108-110] have investigated the solvent sensitivity of the fluorescence of 6-N-arylaminonaphthalene-2-sulphonate by plotting the emission energies against Dimroth's empirical solvent polarity $E_T(30)$, which reveals two distinct sloping regions; this they interpreted in terms of two emitting

states, a locally-excited naphthalene-centred state in less polar solvents (lower slope), and a charge-transfer state in polar solvents (higher slope). A recent investigation[111] on 1-aminonaphthalenes supported a previous study[112] on 5-dimethylaminonaphthalene -1-sulphonate which suggests that a combination of solute-solvent interaction and geometrical change within the amino substituent could result in the charge-transfer character of S_1. An excited, twisted charge-transfer singlet state has been suggested for many aromatic molecules following Kosower's observation of the two separate correlations with the solvent parameter $E_T(30)$.[113,121-123]

The two solvent parameters most successful in predicting fluorescence maxima are $E_T(30)$, also known as the Dimroth and Reichardt-Dimroth parameter,[114,115] and the Z-parameter of Kosower,[116,117] both of which are based on the high solvent-sensitivity of charge-transfer absorptions in pyridiniumphenol betaine and 1-ethyl-4-carbomethoxypyridinium iodide, respectively. One shortcoming of these scales is that they incorporate both hydrogen-bonding effects as well as solvent polarity in the case of protic solvents, and a multiparameter approach has been proposed to separate the effects due to the solvent polarity, hydrogen-bond donor ability and hydrogen-bond acceptor ability on spectral and kinetic properties.[118-120]

Finally, solvent effects on fluorescence spectra have been reviewed in depth recently[103] and are classified in terms of general and specific effects; the former are determined by electronic polarisability (described by n) and molecular polarisability (described by ϵ) while the latter are attributed to hydrogen-bonding, acid-base chemistry or charge-transfer interactions as appropriate.

There have been few systematic investigations of solvatochromic effects upon $T_1 \longrightarrow T_n$ absorption spectra of aromatic compounds. The reported studies are the red-shift of 90 nm in going from n-hexane to N-methylformamide for 1-nitronaphthalene,[124] indicating an increase in dipole moment of 5.6 D. Garner and Wilkinson[125] reported a small blue-shift in the $T_1 \rightarrow T_n$ absorption spectrum of xanthone in going from cyclohexane (λ_{max}. 610 nm) to H_2O - EtOH (10% H_2O by weight), (λ_{max}. 590 nm).

1.7 General Object of this Work

One of the main objectives of the present work was to collect a considerable bank of experimental data for selected systems in which electron-transfer quenching occurs, and to match these against rate constants predicted by the various theoretical expressions. It should be possible to test the validity of the Marcus model against that of the Rehm and Weller model; the Scandola model is probably not distinguishable from that of Rehm and Weller; the semi-empirical Polanyi expression may turn out to offer a better rationalisation, but it cannot be used in a predictive manner.

CHAPTER 2

EXPERIMENTAL

2.1 INSTRUMENTATION

2.1.1 Fluorescence Intensities and Spectra

Fluorescence studies were carried out using a Perkin Elmer MPF-3 double beam spectrofluorimeter, fitted with either a Hamamatsu R666S photomultiplier tube for λ (500-1000 nm) or with a R.C.A. I.P.28 photomultiplier tube for λ up to 600 nm. This instrument uses right-angle illumination, which reduces effects from scattered light, sample cell fluorescence and the portion of the excitation beam which is transmitted. The double-beam configuration of this model means that the spectra are automatically corrected for lamp intensity fluctuation.

The excitation source for this model is a 150 W xenon lamp, from which the emitted light passes through an excitation monochromator which provides an excitation wavelength between 220 nm and 800 nm selected with a bandwidth of between 1 nm and 40 nm. The emission monochromator is identical to the excitation unit and activates a photomultiplier the signal from which is fed to a chart recorder. The emission or excitation wavelengths can be scanned at preset speeds by means of a motor to give either emission or excitation spectra, depending upon whether the emission or excitation wavelength control is engaged.

2.1.2 Laser Flash Photolysis

The flash photolysis technique has been employed extensively in the study of fast reaction since it was first reported by Norrish and Porter in 1949.[126] Flash photolysis is a relaxation method in which

a high energy pulse of light produces a momentarily large number of molecules in their excited state, which absorb a following analysing pulse or 'spectroflash' to give an excited state absorption (ESA) spectrum which can either be recorded on a spectrograph or as time-dependent kinetics at a pre-selected monitoring wavelength by attaching the photomultiplier detector output to an oscilloscope (spectrophotometric method). Alternatively for luminescent species, an excited state emission spectrum can be obtained by employing a photomultiplier coupled to an oscilloscope without using the analysing beam. The limitation of the technique employing conventional light sources is the duration of the high energy lamp pulse; by using a 'chopper' the pulse width can be reduced, but the energy is also greatly decreased. However, with the development of the laser and the production of a laser flash photolysis assembly in 1967,[127] events in the nanosecond time scale can be studied. With the further development of lasers, processes in the picosecond time domain are accessible.[128]

Two types of nanosecond laser have been employed in this work, i.e. a rare gas halide excimer laser and a solid state Q-switched ruby laser (both supplied by Applied Photophysics Ltd., London, although the former was built by Oxford Lasers Ltd.). All the work was carried out using the model KX_2 excimer laser and the ruby laser was used only in the construction of (ESA) spectra of heterocyclic ketones where the absorbances of the solvents are relatively high at 249 nm.

The rare gas halide excimer laser assembly is depicted in Figure (2.1). In all cases the gas mixture used was krypton and fluorine. The laser cavity is filled with 200 mbar of 10% fluorine in helium, 200 mbar of krypton and 1 bar of helium. The laser cavity is coupled to a gas purifier kept at ~ 106 K which removes unwanted products

formed by the lasing action. Lasing is achieved by discharging a high voltage ($\sim$ 35 kV) across a spark gap. The excitation mechanisms of rare gas halide lasers are complex and not fully understood, however, the following reactions for KrF are thought to be involved:

$$Kr + e \rightarrow Kr^+ + 2e$$

$$F_2 + e(slow) \rightarrow F^- + F$$

$$F^- + Kr^+ + He \rightarrow (KrF)^* + He$$

$$(KrF)^* + h\nu \rightarrow Kr + F + 2h\nu$$

The high efficiency of the overall process results from the fact that Kr^+ is formed very efficiently in a high-current glow discharge, and of the energy stored in Kr^+ approximately 30% reappears in the emitted photon. The ultraviolet output (249 nm, 250 mJ/pulse of 15 ns duration) is focused and deflected onto the sample cell. For (ESA) the laser beam is focused onto the sample cell positioned at right-angles to the analysing beam from a water-cooled 250 W xenon high pressure lamp by means of a beam splitter and iris. Absorption of the laser pulse by the sample produces a high yield of excited state molecules which in turn absorb the analysing light, resulting in a transient change in the intensity of the beam, corresponding to the lifetime of the excited state. The change in intensity of the beam is monitored at a preset wavelength by the analysing high-radiance monochromator and photomultiplier tube (either a model Hamamatsu R666S or an R.C.A. model I.P.28). The monochromator can be preset to any wavelength between 200 and 888 nm with a bandpass of between 1 and 20 nm. The light gathering power of > 0.25 allows a satisfactory photomultiplier signal-to-noise ratio to be attained with a reasonable

bandwidth. The transient photomultiplier output is recorded on a Tektronix 7623 storage oscilloscope, equipped with 7A15A (Y) and 7B50(X) amplifiers. Triggering of the oscilloscope is made internally. The stored trace on the Tektronix 7623 oscilloscope is photographed using Polaroid Type 46-L film employing a Telford Type A oscilloscope camera. The film transparencies are then fixed using a 'Polaroid Dippit' containing a fixing solution of 0.03 mol dm^{-3} of tin(IV) tetrachloride in 2-propanol. The negatives are then enlarged two times using a Johnson V/4-5 enlarger onto graph paper and the transient curves digitised by hand ready for analysis.

The ruby laser assembly is depicted in Figure (2.2). The red output (694 nm, ~ 1 J/pulse of 20 ns duration) of the Q-switched laser pulse is frequency doubled by using a rubidium dihydrogen arsenate (RDA) crystal, thermostatted at 323 K, to give a ~ 75 mJ/pulse at 347 nm. The pulse then passes through a saturated copper sulphate solution to remove any remaining red output before being deflected and focused on to the sample cell. For (ESA) studies the laser beam is focused onto the sample cell in a co-linear alignment with the analysing light instead of using right-angle analysis. Triggering is achieved by the use of a photodiode, placed near to the front face of the laser head. The output from the photodiode is split between the Tektronix 7623 storage oscilloscope and a second oscilloscope (Iwatsu model DMS-510) which exhibits a profile of the structure and intensity of the laser pulse, enabling any fluctuations in pulse amplitude to be observed, and gives warning of multiple laser pulsing. The ruby laser head consists of a partially reflecting front mirror and totally internally reflecting rear mirror which acts as an optical resonator. In between these is placed a reflecting cavity containing a ruby rod (6" x ½")

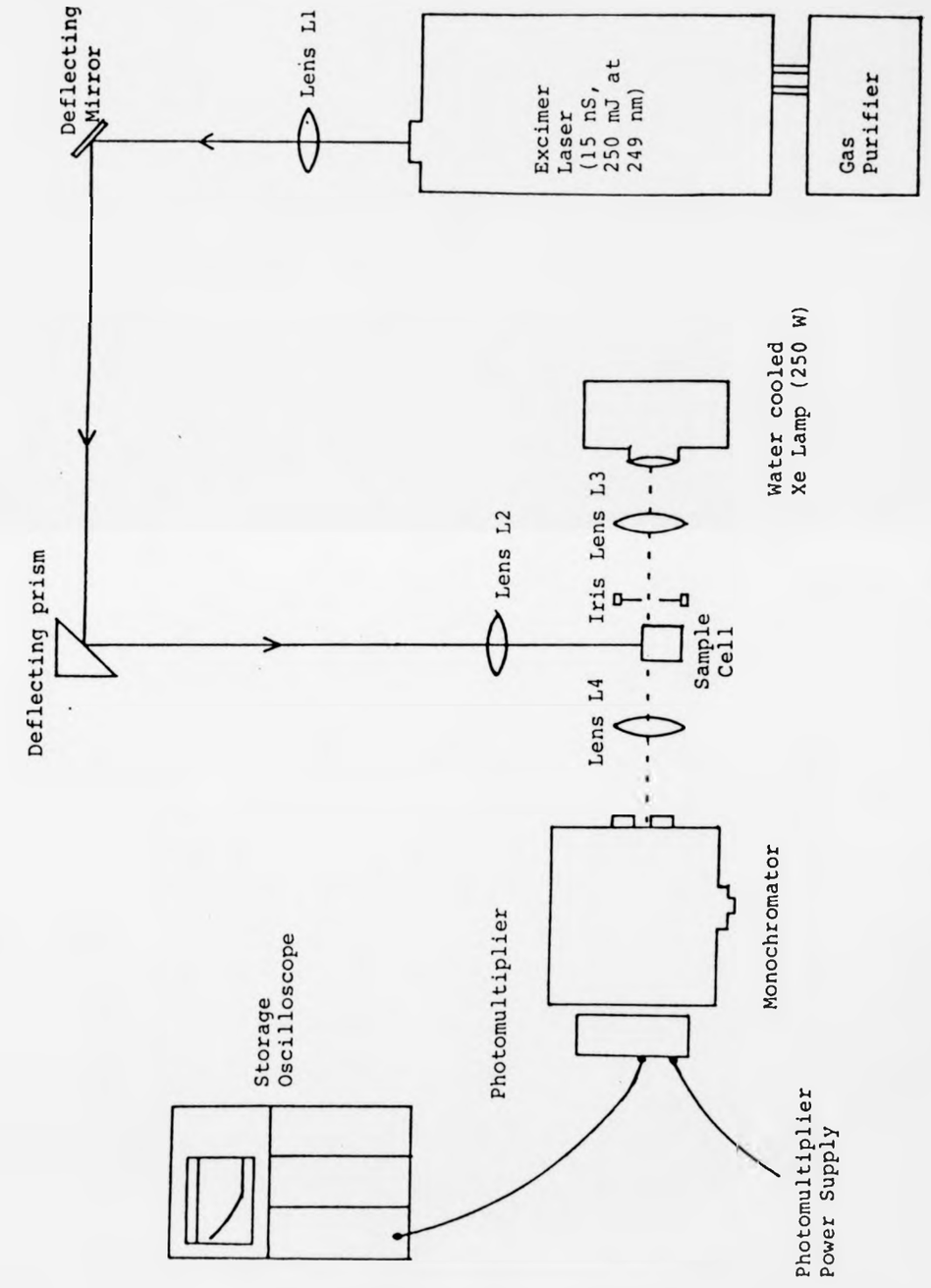

Figure (2.1) Rare gas halide excimer laser flash photolysis assembly.

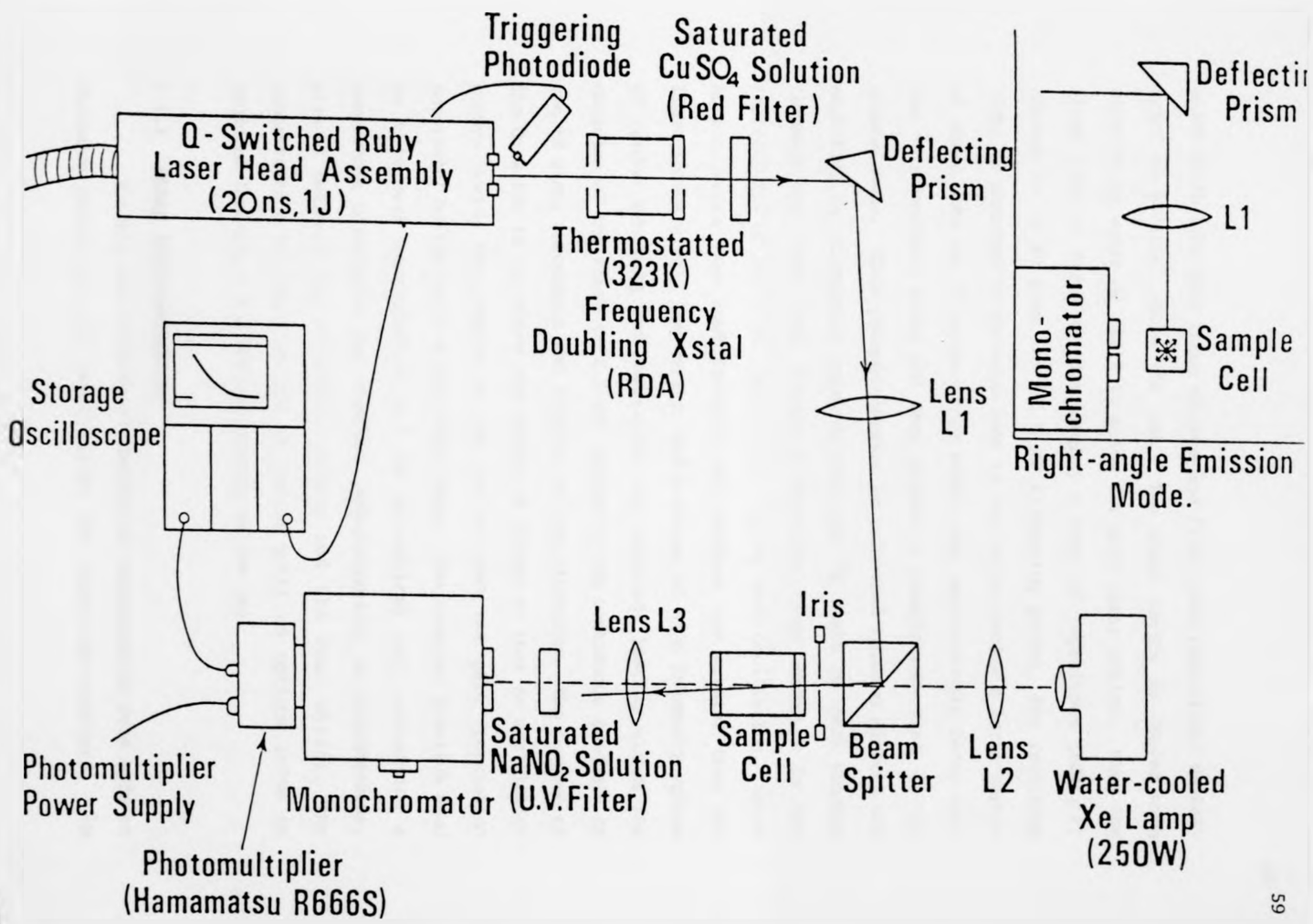

Figure (2.2) Ruby laser flash photolysis assembly.

which is in line with these mirrors and flash tube (Noblelight VR-E46) lying in parallel above the rod. The whole cavity is cooled with circulating water at 288 K to allow for good laser action. When the flash tube is fired by discharging a bank of capacitors (680 μ F) through it (2 kV plus initial 5 kV triggering pulse), the resulting light is absorbed by chromium ions in the rod to excite a large number of these into the ^4F states from which they spontaneously decay into the ^2E metastable state and then gradually phosphoresce back to the ground state. This phosphorescence is reflected between mirrors and amplified by stimulated emission from the ^2E state on each passage through the laser rod, losing a fraction (1-R) where R is the reflectivity of the front face mirror, during each oscillation. Laser action occurs when amplification and feedback are greater than the light losses within the cavity, and a series of high intensity spikes of random intensity and separation are produced, lasting almost the duration of the flash ($\sim$1.5 ms) caused by the continuous feedback to the ^2E state throughout the lifetime of the flashlamp. The purpose of the Q-switch is to reduce the number of pulses so that no oscillation occurs during the pumping of the rod so that the gain (population inversion) builds up to a very high value. The chemical Q-switch used in this work consisted of a 1 cm cylindrical cell containing a reversible bleachable dye (vanadyl phthalocyanine) in nitrobenzene, placed between the reflector cavity and the rear mirror. The concentration of the Q-switch is varied until an optimum pulse is produced (usually $\sim$ 0.3 optical density at 694 nm).

2.1.3 Other Instrumentation

Visible and ultraviolet absorption measurements were made on Shimadzu model 365 and Perkin-Elmer 552 spectrophotometers. ^1H

n.m.r. spectra were taken on a Perkin-Elmer R-34 (220 MHz) instrument. Mass spectra were obtained on Kratos Ltd., model MS80 instrument. Fluorescence lifetimes were measured by time-correlated single photon counting using a picosecond excitation source at the Royal Institution (London). Two measurements were performed by Mr. L. Chewter, on solutions of 2-aminoanthracene in methanol and cyclohexane, which had been deoxygenated by three freeze-pump-thaw cycles, while the remaining singlet lifetime measurements were performed by Dr. S. Meech using purified nitrogen gas (bubbled for 15 minutes) for deoxygenation; to both I express my thanks. (See Appendix II).

2.2 Syntheses

N,N-Dimethyl-2-aminoanthracene (2-DMA) was synthesised by thermolysis under reduced pressure (180°C, 0.1 mm Hg) of 2-dimethylaminoanthracene methiodide. Recrystallisation from acetone/water gave an 82% yield of bright yellow crystals, m.p. 155°C (Lit.[129] 155°C). 2-Dimethylaminoanthracene methiodide was prepared by mixing 1.93 g (0.01 mol) of 2-aminoanthracene (2-AA) and 1.68 g (0.02 mol) sodium hydrogen carbonate and heating to 110°C in 31 cm^3 (0.50 mol) of methyl iodide with a trace of methanol for 8 hours following the literature procedure,[129] but with a yield of only 13.8%, m.p. 208-211°C (Lit.[129] 215°C). The structure of 2-DMA was confirmed spectroscopically and by elemental analysis. The mass spectrum showed base peak 221 (100%), 205 (12.66%), 178 (27.67%), 165 (14.32%), 151 (3.15%); ^1H n.m.r. ($CDCl_3$) showed δ (ppm): 8.28 (1H,s, 10-H), 8.18 (1H, s, 9-H), 7.91 (4H, m), 7.35 (2H,m), 6.99 (1H, s, 3-H), 3.08 (6H, s, 2Me), and the result of elemental analysis was:

	C%	H%	N%
Found:	86.54	6.84	6.59
Calculated:	86.83	6.83	6.33

Symmetrical alkyltin compounds were prepared by the standard reaction of anhydrous tin(IV) tetrachloride with the corresponding alkyl Grignard reagent in diethyl ether.[130] Alkyl bromide (0.2 mol) was added to 100 cm^3 of diethyl ether containing magnesium turnings (0.2 mol) and a crystal of iodine. The ethereal solution was refluxed for four hours and then cooled to 0°C before tin(IV) tetrachloride (0.025 mol) in benzene was carefully added. Excess Grignard reagent was hydrolysed using ammonium chloride (20 g) in 100 cm^3 of water and the resulting solution left to stand overnight. The organic layer was then separated, dried over magnesium sulphate, filtered and the excess diethyl ether distilled off. The alkyltin compounds were then distilled under reduced pressure as follows:

Compound	Boiling Point/°C
Et_4Sn	78/13 mm Hg
$n\text{-}pr_4Sn$	110/10 mm Hg
$i\text{-}Pr_4Sn$	103/10 mm Hg
$n\text{-}Bu_4Sn$	103/10 mm Hg
$s\text{-}Bu_4Sn$	130/10 mm Hg

RMe_3Sn compounds were prepared by the same procedure used for preparing the symmetrical alkyltins by replacing tin(IV) tetrachloride with trimethyltin chloride.[130] The following unsymmetrical alkyltin compounds were prepared:

Compound	Boiling Point/°C
$EtMe_3Sn$	105/760 mm Hg
$n\text{-}BuMe_3Sn$	43/43 mm Hg

The alkyltin compounds were analysed using ^1H n.m.r., mass spectrometry and in some cases elemental analysis as follows:

Compound	Calculated		Found	
	C%	H%	C%	H%
Et_4Sn	40.93	8.52	40.62	8.79
$n\text{-}pr_4Sn$	49.54	9.63	49.34	9.71
$i\text{-}pr_4Sn$	49.54	9.63	48.12	9.72
$n\text{-}Bu_4Sn$	55.40	10.38	55.16	10.49

All the above alkyltin compounds were prepared by Mr. H.G. Beaton. The alkyllead compounds were gifts from the Associated Octel Co. Ltd., (Ellesmere port).

2.3 Purity of Chemicals

All organic solvents used were either of spectroscopic or AnalaR grade and were used without further purification. Purifed water was obtained by refluxing doubly distilled water over alkaline potassium permanganate for 48 hours and again doubly distilling. The following commercially available compounds were purified by recrystallisation (2x) from the solvents indicated:

Compound	Solvent	m.p./°C	Literature m.p./°C	Ref.
2-Aminoanthracene	Benzene	237-240	238-239	129
9,10-Dicyanoanthracene	Toluene	335	335	131
Thioxanthone	Petroleum ether	212-215	212	132
Xanthone	Ethanol	173-175	174	132
N-Methylacridone	Ethanol	205-207	203.5	133
Triphenylphosphine	Diethyl ether	78-80	80	133
1,4-Benzoquinone	Petroleum ether	115-116	115	133
1,3,5-Trinitrobenzene	Acetone/Water	117-120	121-122	132
4-Nitroanisole	Petroleum ether	54-55	54	132
4-Cyanopyridine	Petroleum ether	79-82	83	132

Liquid compounds were purified by simple distillation at boiling points as follows (which were in agreement with the literature 132-133).

Compound	Boiling point/°C
Iodobenzene	188
Benzonitrile	188-192
Bromobenzene	156-157
Pyridine	114-116
Quinoline	234-236
1-Nitropropane	128-131

Other chemical compounds were of the highest grade available commercially and were used without further purification.

2.4 Sample Preparation

All the experiments carried out in this work were done at room temperature. For this purpose a 1 cm x 1 cm quartz fluorescence cell fitted with a narrow-bore Teflon tap was used (6 cm^3 volume). Since all the samples used were sensitive to oxygen, deoxygenation was required before use. This was achieved either by bubbling the samples with high purity argon (B.O.C. 99.999%) or with purified nitrogen gas for 15-20 minutes. In fluorescence work the concentration of the fluorophores was $\sim 10^{-5}$ mol dm^{-3} and was kept constant through a series of fluorescence quenching experiments. In contrast, the concentrations required for laser measurements were adjusted to give an absorbance of about 2.0 at 249 nm (excimer laser) to ensure

substantial absorption of the laser pulse near the front of the cell.

Since the excited-state lifetimes measurements are extremely sensitive to impurities, all the glassware used were cleaned frequently in chromic acid solution to remove any trace of organic impurities.

2.5 Analysis of Results

2.5.1 Fluorescence Studies

The results from fluorescence quenching experiments were analysed in terms of the Stern-Volmer equation (2.1)

$$\frac{I_{fo}}{I_f} = 1 + K^{SV}\,[Q] \qquad (2.1)$$

where

I_{fo} is the intensity of fluorescence in the absence of any added quencher.

I_f is the intensity of fluorescence in the prescence of added quencher at concentration [Q].

K^{SV} is the Stern-Volmer constant, $K^{SV} = k_q\ \tau_o$, where k_q is the quenching rate constant and τ_o is the lifetime of the fluorescence in the absence of any added quencher.

Stern-Volmer constants were evaluated by least squares analysis using at least five concentrations (and usually about eight) of the quencher molecule, and correlation coefficients were always > 0.96.

The singlet excitation energy $\Delta^1E_{o,o}$ was estimated from the crossing point of the absorption and fluorescence spectra of the fluorophore.

Values of τ_o were measured by time-correlated single photon counting at the Royal Institution (London) using computer techniques to analyse the normal first-order decay of the fluorescence. The diffusion rate constant (k_{12}) and the intrinsic energy barrier ($\Delta G^*_{23}(O)$) derived from the Rehm-Weller plots were obtained by a best fitting procedure using a computer program developed by Mr. A. W. Parker, to whom I express my thanks, (see Appendix I).

2.5.2 Excited-State Absorption Measurements

Transient absorption spectra were recorded by measuring the initial intensity of absorbance as a function of monitoring wavelength, each reading being taken several times to allow for fluctuation in the intensity of the laser pulse, e.g. triplet-triplet absorption spectra were constructed on a point-to-point procedure by varying the monochromator wavelength.

For kinetic studies it is assumed that Beer's law is obeyed and the optical density (O.D.) at an instant (t) can be calculated from the transient absorption curve (see figure 2.3) as:

$$O.D. = \log I_{o/I_t} = \log X_{o/X} = \epsilon_\lambda c_t L \qquad (2.2)$$

so that the relative or absolute concentrations can be determined as a function of time, and the rate of the transient decay determined. In equation (2.2) I_o (initial intensity of the analysing light) and I_t (transmitted intensity at time t) are related to the oscilloscope deflections through:

I_o = k ('light-on' deflection - 'light-off' deflection) = k X_o

I_t = k ('transient' deflection - 'light-off' defelction) = kX

where k is a constant which depends on detector sensitivity and which need not be evaluated.

Normal first-order decay of ESA signals were analysed, after graphical enlargement of the traces two times, by computer techniques according to equation (2.3)

$$I_t = I_o \exp(-k_{obs}t) \qquad (2.3)$$

where k_{obs} is the first-order rate constant in s^{-1}, I_o is the initial intensity of the analysing beam, I_t is the transmitted intensity of analysing beam measured in terms of the photomultiplier voltage. The pertinent computer program (V1EØX) utilised a subroutine (VBØ1A) which involves a least-squares approximation to the relevant function. Initial estimates for k_{obs} were obtained by inspection of the transient decay, and I_o was calculated accurately and fed into the program.

The second-order quenching rates of triplets were obtained by a least-square procedure, from the coefficient ^3kq of equation (2.4), i.e. by plotting k_{obs} against quencher concentration [Q].

$$k_{obs} = k_1 + {}^3kq\ [Q] \qquad (2.4)$$

where k^{-1} is the triplet lifetime without any quencher added and k_{obs}^{-1} is the triplet lifetime in the presence of added quencher.

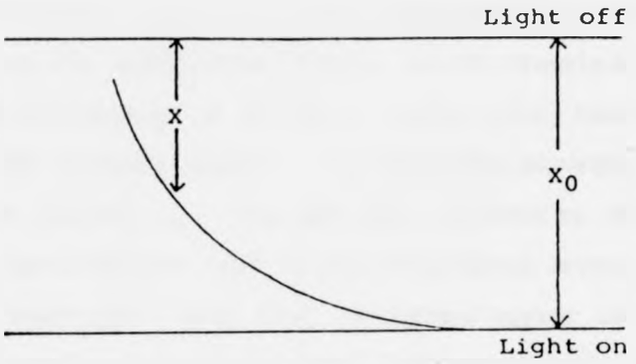

Figure (2.3) Representation of a transient absorption decay curve.

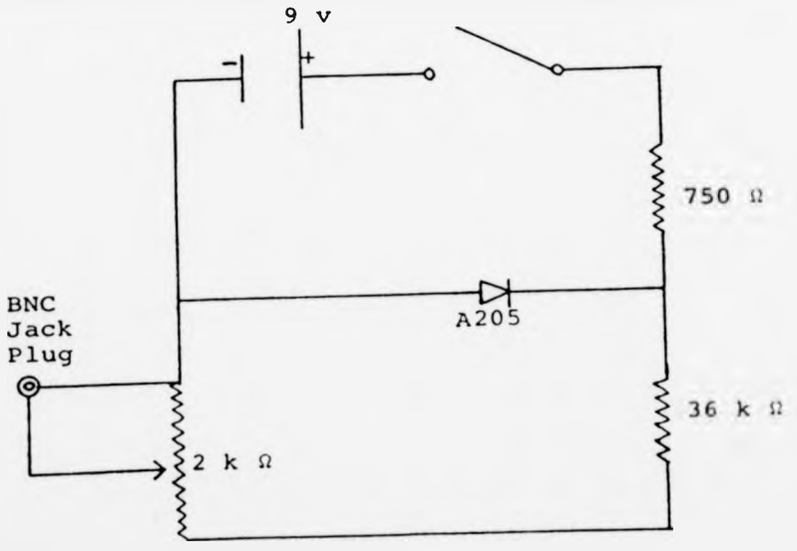

Figure (2.4) Circuit diagram for 'off-set box' used in recording weak transient absorptions.

In the measurement of weakly absorbing transients, one is normally restricted by the need to present I_o as a full-scale deflection on the oscilloscope screen. As the transient intensity is a constant percentage of I_o for a given time, then one way of enlarging the transient signal to allow more accurate measurements would be to increase I_o. This has been achieved by off-setting the zero-light level off the 'top' of the oscilloscope screen, which means that the 'light-off' trace will no longer appear on the screen. However, the use of an 'off-set box', which provides a precalibrated output voltage applicable to the Y amplifier of the oscilloscope, in place of the photomultiplier output, enables the 'light-off' level to be brought back on to the screen. This value can now be used to give the 'apparent' I_o value and by addition of the applied voltage from the 'off-set box', the true value of I_o in mV can be calculated. The circuit diagram of the 'off-set box' is shown in Figure (2.4).

CHAPTER 3

3.1 Electron-Donor and-Acceptor Quenching of the Fluorescence of 9,10-Dicyanoanthracene in Polar and Nonpolar Solvent: Results and Discussion

9,10-Dicyanoanthracene (DCA) has a reasonably good reduction potential and a high fluorescence quantum yield, and reductive quenching of ^{1}(DCA)* by electron-rich aromatic molecules in acetonitrile has been studied[50] in detail, demonstrating an excellent agreement with the treatment of Rehm and Weller.[15,16] A similar study of the quenching of ^{1}(DCA)* in heptane solution by Kuzmin et al.[80,81] shows that the linear free energy relationship of Polanyi affords a better fitting to their results. The Polanyi equation has also been used successfully in analysing the fluorescence quenching of various aromatic molecules by inorganic anions in aqueous ethanol.[77,78] Rather few examples have been reported of alkylmetals acting as quenchers of excited states, although Ph_3P has attracted some interest[131,134,135] as have mercury, tin and lead alkyls in respect of the heavy-atom effect.[136] Our aim in this study is to test the current theories of one electron-transfer quenching in polar and nonpolar solvent by examining the interaction of ^{1}(DCA)* with different type of quencher (both oxidative and reductive).

In Table 3.1 are presented fluorescence spectral and lifetime data for DCA in the solvents utilised in this study, together with values of the electronic excitation energy $\Delta^1E_{0,0}$ estimated from the crossing point of the absorption and fluorescence spectra of DCA in each solvent.

Table 3.1 Spectral and Lifetime Data for DCA

Solvent	τ_o/ns[a]	$\lambda_{exc.}$/nm[b]	λ_P/nm	$\Delta^1E_{0,0}$/eV[c,d]
MeOH	15.1	422	436, 457	2.897
MeOH/H_2O 1:1 (v/v)	14.8	400	442, 465	2.87
Cyclohexane	11.7	397	423, 448, 475	2.945

a Ref.(50) gives 15.3 ns in MeCN and Ref.(137) gives 11.2 ns in heptane.

b Excitation wavelength during quenching experiments.

c Obtained from intersection of absorption and fluorescence spectra.

d Ref.(50) gives 2.89 eV in MeCN and Ref.(131) gives 2.87 in benzene.

Fluorescence from ^{1}(DCA)* in O_2-free solution at room temperature (293 ± 1K) was quenched by a wide variety of donors in both 50% (v/v) MeOH-H_2O (inorganic anions and Ag^+, Table 3.2) and cyclohexane (organo-phosphorus, -antimony, -tin, -lead and -germanium compounds, Table 3.3). ^{1}(DCA)* is also a potential electron-donor, and it is quenched in MeOH solution by organic acceptors with half-wave potential more positive than -1.7 V vs. SCE, reaching the diffusion-controlled value when $E_{\frac{1}{2}} > -1.0$ V (Table 3.4). In all cases there was no evidence for any new emitting species such as an exciplex on addition of the quencher, and Stern-Volmer plots, Figures (3.1-3.3), give the values of K^{SV} (the Stern-Volmer constant) which were factorised using the relation $K^{SV} = k_q . \tau_o$ (τ_o = lifetime of ^{1}(DCA)* in absence of quencher).

Table 3.1 Spectral and Lifetime Data for DCA

Solvent	τ_o/ns[a]	$\lambda_{exc.}$ /nm[b]	λ_p/nm	$\Delta^1E_{0,0}$/eV[c,d]
MeOH	15.1	422	436, 457	2.897
MeOH/H_2O 1:1 (v/v)	14.8	400	442, 465	2.87
Cyclohexane	11.7	397	423, 448, 475	2.945

a Ref.(50) gives 15.3 ns in MeCN and Ref.(137) gives 11.2 ns in heptane.

b Excitation wavelength during quenching experiments.

c Obtained from intersection of absorption and fluorescence spectra.

d Ref.(50) gives 2.89 eV in MeCN and Ref.(131) gives 2.87 in benzene.

Fluorescence from ^{1}(DCA)* in O_2-free solution at room temperature (293 ± 1K) was quenched by a wide variety of donors in both 50% (v/v) MeOH-H_2O (inorganic anions and Ag^+, Table 3.2) and cyclohexane (organo-phosphorus, -antimony, -tin, -lead and -germanium compounds, Table 3.3). ^{1}(DCA)* is also a potential electron-donor, and it is quenched in MeOH solution by organic acceptors with half-wave potential more positive than -1.7 V vs. SCE, reaching the diffusion-controlled value when E_i > -1.0 V (Table 3.4). In all cases there was no evidence for any new emitting species such as an exciplex on addition of the quencher, and Stern-Volmer plots, Figures (3.1-3.3), give the values of K^{SV} (the Stern-Volmer constant) which were factorised using the relation $K^{SV} = k_q . \tau_o$ (τ_o = lifetime of ^{1}(DCA)* in absence of quencher).

Table 3.2 Fluorescence Quenching of ^{1}(DCA)* by Inorganic Anions in MeOH-H_2O (1:1 v/v) Solution

Donor	(number)	$E(D^{\cdot+}/D)/V$ [a] vs. NHE	ΔG^{o}_{23} /kJ mol^{-1}	k_q/dm^3 mol^{-1} s^{-1}
NO_2^-	(1)	1.0 ± 0.1 [b], 1.03 ± 0.04 [f]	-115.8	(6.17 ± 0.42) x 10^9
I^-	(2)	1.33 ± 0.03 [c], 1.4 ± 0.05 [b]	- 84.0	(8.28 ± 0.20) x 10^9
$S_2O_3^{2-}$	(3)	1.34 [e], 1.35 [f]	- 83.0	(5.62 ± 0.19) x 10^9
N_3^-	(4)	1.37 ± 0.02 [f], 1.87 [d]	- 80.1	(6.38 ± 0.20) x 10^9
SCN^-	(5)	1.601 [e], 1.66 [c], 1.50 [d]	- 57.8	(8.94 ± 0.23) x 10^9
CN^-	(6)	1.90 ± 0.3 [b]	- 29.0	(3.46 ± 0.47) x 10^9
Br^-	(7)	1.904 [e], 2.0 ± 0.1 [b,d]	- 29.0	(6.96 ± 0.16) x 10^9
OH^-	(8)	2.11 ± 0.09 [e], 1.9 ± 0.1 [b]	- 8.7	(4.22 ± 0.07) x 10^9
CO_3^{2-}	(9)	2.15 [e]	- 4.8	(2.98 ± 0.23) x 10^9
Cl^-	(10)	2.20 [e], 2.55 ± 0.1 [b,d]	0.0	(7.86 ± 0.21) x 10^8
Ag^+	(11)	2.25 [e], 1.987 [g]	+ 4.8	(6.61 ± 0.33) x 10^8
$CH_3CO_2^-$	(12)	2.32 [h], 2.41 [i]	+ 11.6	(7.07 ± 0.16) x 10^7
F^-	(13)	3.6 ± 0.1 [b]	+135.0	(2.78 ± 0.09) x 10^7

a The first figure listed was utilised in calculating ΔG^{o}_{23}.

b From ref.(142).

c From ref.(143).

d From ref.(78).

e From ref.(57).

f From ref.(144).

g From ref.(145) for 4 mol dm^{-3} $HClO_4$ solution.

h Calculated from data given in ref.(57).

i From ref.(146).

Table 3.3 Fluorescence Quenching of ^{1}(DCA)* by Organometallic Compounds in Cyclohexane Solution

Donor	(number)	I/eV	k_q/dm^3 mol^{-1} s^{-1}	k_q[f]/dm^3 mol^{-1}s^{-1}
$(p\text{-}MeC_6H_4)_3P$	(1)	7.60[a]	$(8.03 \pm 0.26) \times 10^9$	
Ph_3P	(2)	7.92[a]	$(11.67 \pm 0.21) \times 10^9$	
Et_4Pb	(3)	8.13[b]	$(10.10 \pm 0.23) \times 10^9$	
Ph_3Sb	(4)	8.18[c]	$(8.62 \pm 0.19) \times 10^9$	
Et_3MePb	(5)	8.26[d]	$(10.39 \pm 0.19) \times 10^9$	
$(s\text{-}Bu)_4Sn$	(6)	8.45[b]	$(8.97 \pm 0.13) \times 10^9$	
$(i\text{-}Pr)_4Sn$	(7)	8.46[b]	$(8.54 \pm 0.21) \times 10^9$	
$EtMe_3Pb$	(8)	8.65[d]	$(7.78 \pm 0.14) \times 10^9$	7.41×10^9
$(n\text{-}Bu)_4Sn$	(9)	8.76[b]	$(2.47 \pm 0.04) \times 10^9$	2.59×10^9
$(n\text{-}pr)_4Sn$	(10)	8.82[e]	$(1.53 \pm 0.03) \times 10^9$	1.46×10^9
Me_4Pb	(11)	8.90[b]	$(1.55 \pm 0.03) \times 10^9$	6.78×10^8
Et_4Sn	(12)	8.93[b]	$(1.55 \pm 0.05) \times 10^9$	5.09×10^8
$(n\text{-}Bu)Me_3Sn$	(13)	9.00[e]	$(5.12 \pm 0.26) \times 10^7$	2.60×10^8
$EtMe_3Sn$	(14)	9.10[b]	$(3.55 \pm 0.14) \times 10^7$	1.00×10^8
Et_4Ge	(15)	9.41[b]	$(1.02 \pm 0.05) \times 10^7$	5.15×10^6
Me_4Sn	(16)	9.69[b]	$(1.97 \pm 0.07) \times 10^7$	
Et_4Si	(17)	9.78[b]	$(7.21 \pm 0.07) \times 10^6$	

a From ref.(147).

b From ref.(148) and the compilation given therein.

c From ref.(149).

d From ref.(150).

e From ref.(151).

f Calculated from Polanyi equation (for parameters see text) and equation (3.3).

Table 3.4 Fluorescence Quenching of ^{1}(DCA)* by Organic Acceptors in MeOH Solution

Acceptor	(number)	$E_{\frac{1}{2}}$/V[a,b] vs. SCE	ΔG^{o}_{23}[f]/ kJ mol^{-1}	k_q/dm^3 mol^{-1} s^{-1}
Misonidazole	(1)	-0.395[c]	-80.3	(5.34 ± 0.20) x 10^9
1,3,5-Trinitrobenzene	(2)	-0.60	-60.3	(10.50 ± 0.28) x 10^9
Methyl viologen	(3)	-0.69[d]	-51.8	(9.53 ± 0.23) x 10^9
1,4-Dinitrobenzene	(4)	-0.70	-50.9	(15.64 ± 0.56) x 10^9
1,2-Dinitrobenzene	(5)	-0.83	-38.3	(10.25 ± 0.35) x 10^9
1,3-Dinitrobenzene	(6)	-0.91	-30.6	(16.41 ± 0.20) x 10^9
3-Methylnitrobenzene	(7)	-1.045	-17.6	(8.54 ± 0.28) x 10^9
Nitrobenzene	(8)	-1.147	-7.7	(6.37 ± 0.23) x 10^9
2-Methylnitrobenzene	(9)	-1.26	+3.2	(3.82 ± 0.10) x 10^9
2,3-Dimethylnitrobenzene	(10)	-1.318	+8.8	(3.40 ± 0.09) x 10^9
2,6-Dimethylnitrobenzene	(11)	-1.402	+16.9	(6.70 ± 0.27) x 10^8
4-Cyanopyridine	(12)	-1.44[e]	+20.7	(4.12 ± 0.10) x 10^8
1-Nitropropane	(13)	-1.458	+ 22.3	(4.44 ± 0.20) x 10^6
1-Nitropentane	(14)	-1.51	+ 27.3	(5.80 ± 0.10) x 10^6
2-Methyl-2-nitropropane	(15)	-1.70	+45.7	(1.61 ± 0.05) x 10^6

a Measured in MeCN or DMF vs. SCE using 0.1 mol dm^{-3} $R_4N^+ClO_4^-$ (R = Et or n-p_r) as supporting electrolyte.

b Except where indicated otherwise, values are taken from ref.(152).

c From ref.(153), measured in phosphate-buffered saline at pH = 7.2.

d From ref.(56) after correction for change of reference electrode from NHE to SCE.

e Calculated from data of ref.(140).

f Calculated using $E(D/D^{\cdot+})$ for DCA = 1.73 V (vs.SCE) from ref.(138) after correction for change of reference electrode from $Ag/AgNO_3$ to SCE.

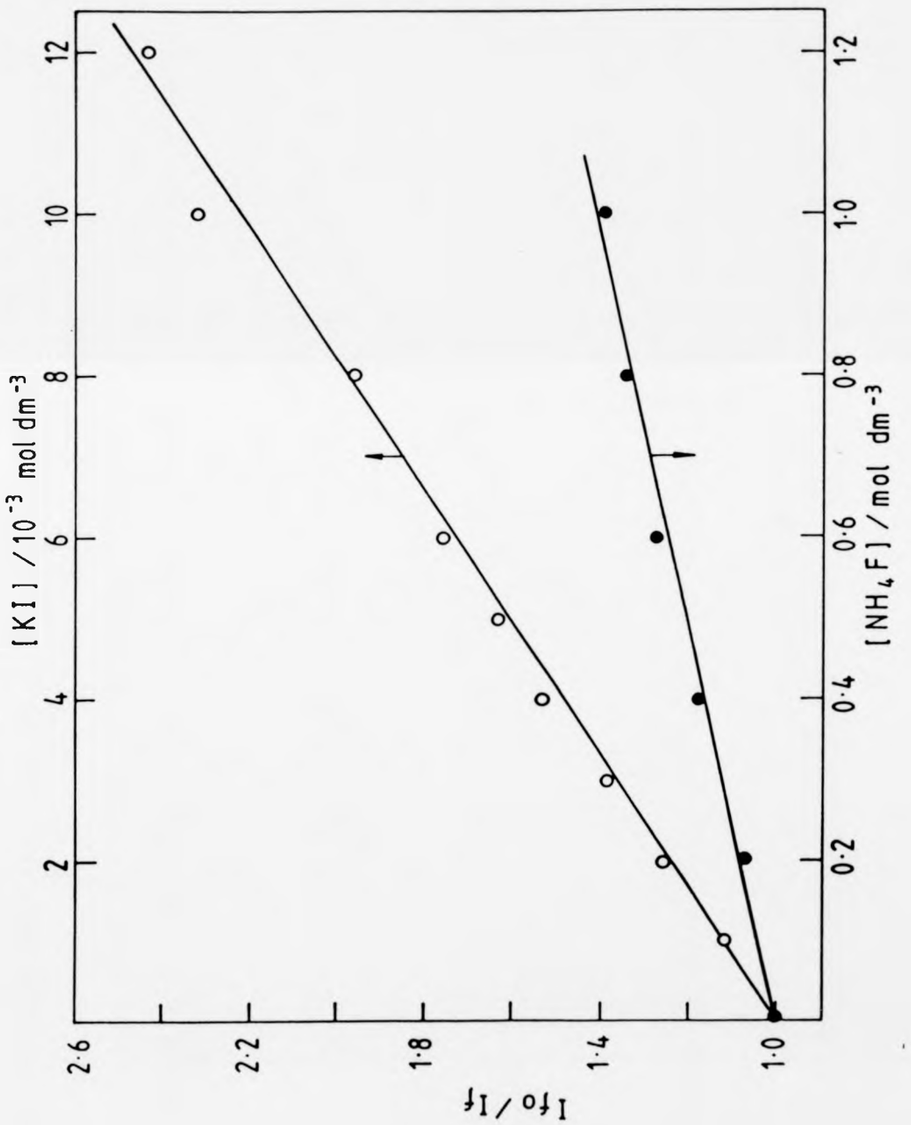

Figure (3.1) Typical Stern-Volmer plots for the fluorescence quenching of 9,10-dicyanoanthracene by inorganic anions in MeOH-H_2O (1:1 v/v) solution.

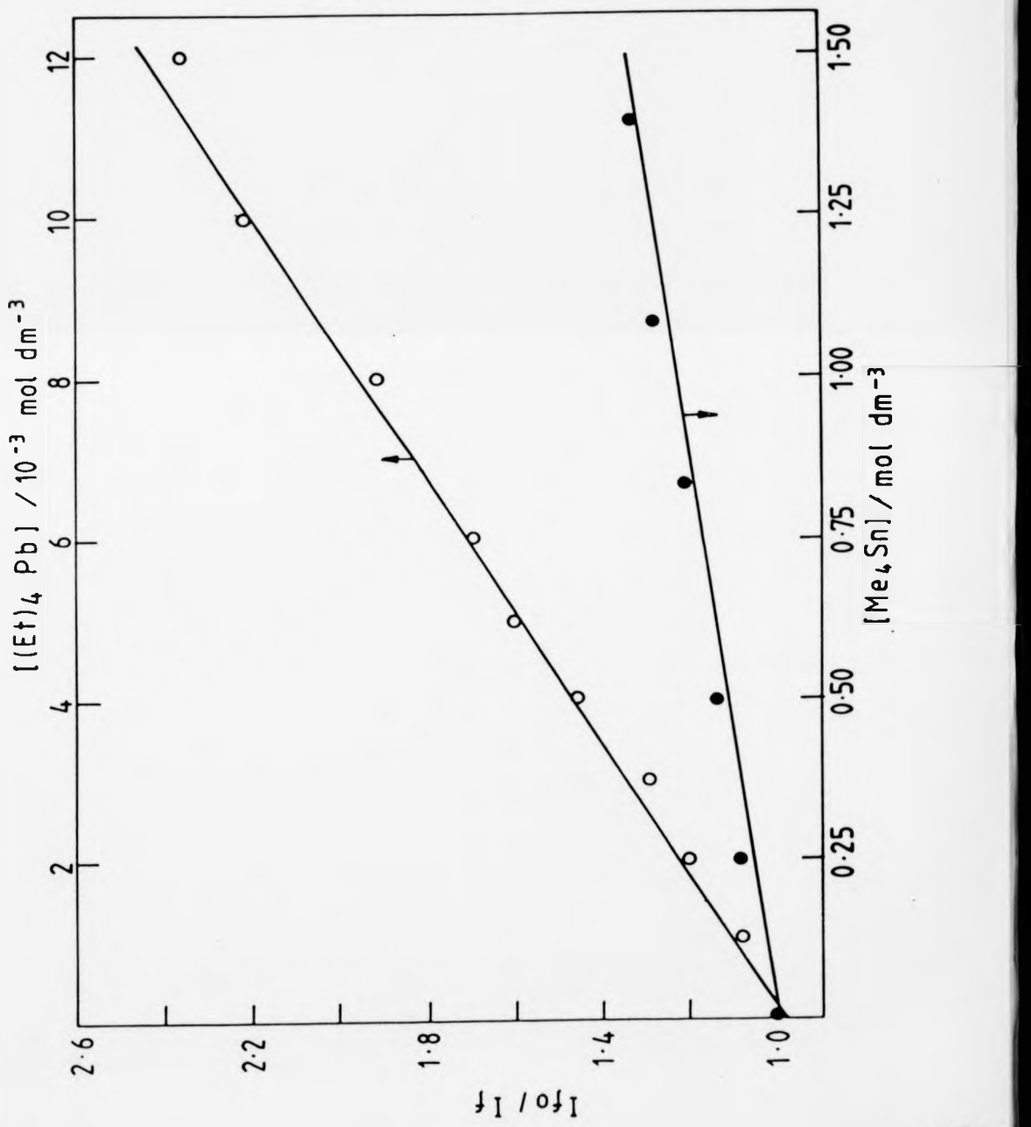

Figure (3.2) Typical Stern-Volmer plots for the fluorescence quenching of 9,10-dicyanoanthracene by alkylmetals in cyclohexane solution.

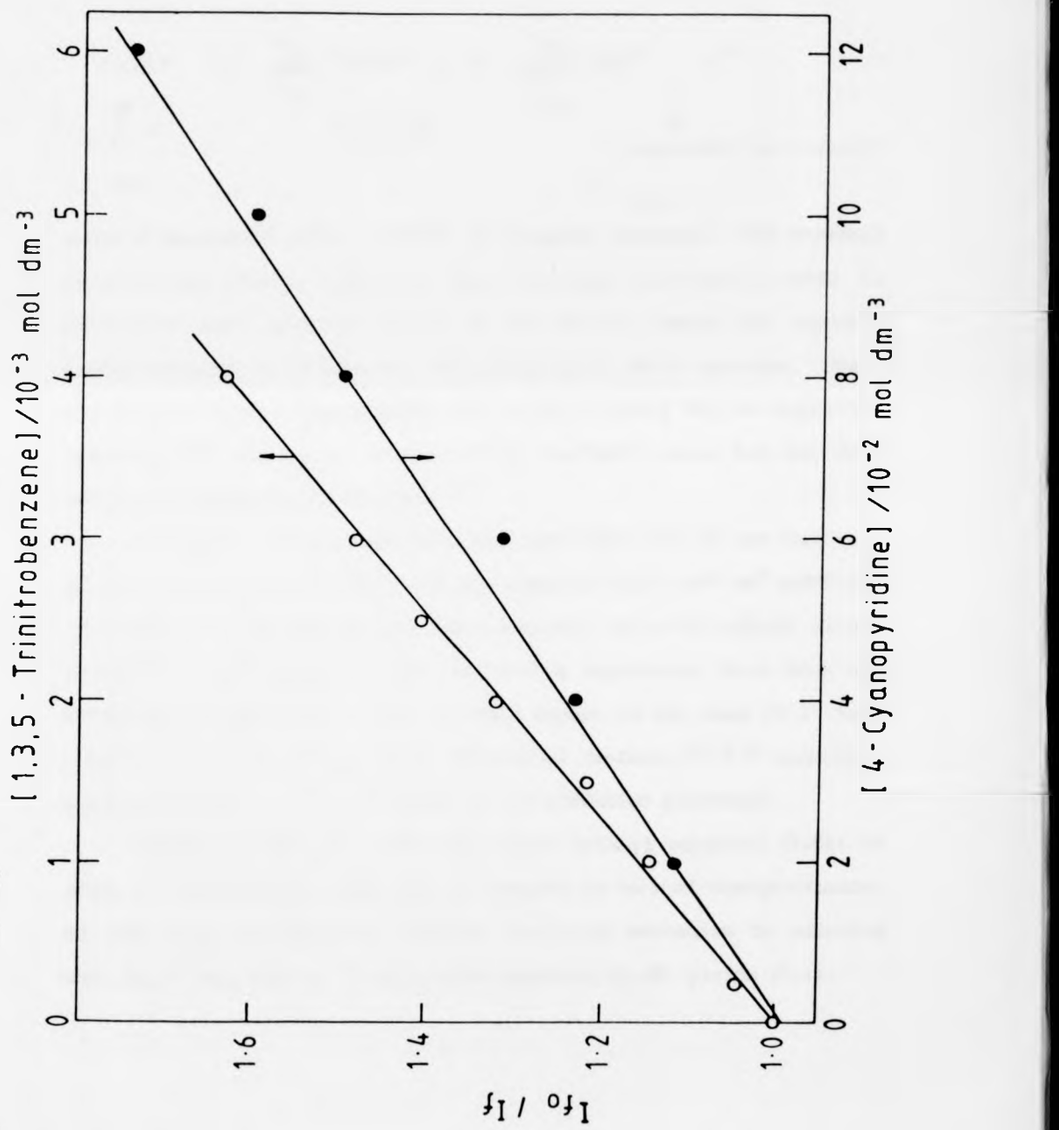

Figure (3.3) Typical Stern-Volmer plots for the fluorescence quenching of 9,10-dicyanoanthracene by organic electron-acceptors in methanol.

The kinetic scheme of fluorescence quenching by one electron-transfer mechanism in polar solvents which was developed by Rehm and Weller[15,16] is as follows:

$$^1(DCA)^* + Q \underset{k_{21}}{\overset{k_{12}}{\rightleftharpoons}} {}^1(DCA)^* \ldots Q \underset{k_{32}}{\overset{k_{23}}{\rightleftharpoons}} DCA^{\pm\cdot} \ldots Q^{\mp\cdot} \downarrow \text{separated ion-radical}$$

$$^1/\tau_o \downarrow\uparrow h\nu$$

DCA

encounter complex

or

DCA + Q

where Q represents either a donor or acceptor quencher. The standard free energy change ΔG^o_{23} for the electron transfer process is calculated from equation (1.56) in (kJ mol^{-1}), using the reported electrochemical potentials for DCA measured in MeCN solution. They are $E_{A^{\cdot-}/A}$ = -0.98 V vs.SCE using 0.2 mol dm^{-3} $N(Bu)_4^+ PF_6^-$ as supporting electrolyte[50] and $E_{D/D^{+\cdot}}$ = 1.43 V vs. $Ag/AgNO_3$ using 0.5 mol dm^{-3} $NaClO_4$ as supporting electrolyte.[138]

In Figure 3.4 are shown the data from Table 3.2 in the form of a plot of log k_q against ΔG^o_{23}, with k_{12} taken as 8.0 x 10^9 dm^3 mol^{-1} s^{-1} (a figure more appropriate for this solvent) and with $\Delta G^{\ddagger}_{23}(0)$ as 6.5 kJ mol^{-1}. The agreement with the curve calculated from Rehm and Weller equations (1.52) (1.57) is good except in the case of F^- ion, which has shown exceptional behaviour before,[57,139] possibly originating in the reported value of its oxidation potential.

Various groups have used the linear polanyi equation (1.61) in order to explain their experimental results in term of charge-transfer or even full one-electron transfer quenching mechanism by assuming that $k_{30} >> k_{32}$ and $k_{21} >> k_{23}$, thus equation (1.48) yields (3.1).

$$k_q = k_{12}\, k_{23}/k_{21} \qquad (3.1)$$

This may be rewritten as

$$k_q = k_{12}/k_{21}\ \kappa^{o} \exp(-\Delta G^{\ddagger}_{23}/RT) \qquad (3.2)$$

and simplified further to :

$$k_q = 1 \times 10^{10} \exp(-\Delta G^{\ddagger}_{23}/RT) \qquad (3.3)$$

A plot of $\Delta G^{\ddagger}_{23}$ (calculated from equation (1.61)) against ΔG^{o}_{23} is shown in Figure (3.5) with $\alpha = 0.487 \pm 0.068$ and $\beta = 5.805 \pm 0.483$ kJ mol^{-1}. The value of β is similar to that found for other aromatic hydrocarbons[77] ($\alpha = 0.138$ and $\beta = 6.56$ kJ mol^{-1}) but our value for α is much nearer the ideal value of 0.5. This particular group of experiments do not allow a clear distinction to be made between the Polanyi and Rehm-Weller equation; other free energy relationships have not been discussed since the Scandola-Balzani equation gives results similar to those of the Rehm-Weller equation, while no inverted region has been found experimentally (see introduction to section 1.5).

There have been few systematic investigations concerning electron donor/acceptor quenching in alkane or aromatic solvents. This introduces several complicating factors namely (i) the possible formation of exciplexes (both emissive and non-emissive), (ii) a much more significant Coulombic term in equation (1.56) and (iii) an absence of electrochemical data relating to the solvent medium. It becomes more appropriate therefore to use equation (3.4) to derive ΔG^{o}_{23}, and to plot log k_q against (I-A), where (I) refers to the

$$\Delta G^{o}_{23} = I - A - C \qquad (3.4)$$

ionisation energy of the donor, (A) to the electron affinity of the acceptor and C is the Coulombic term. In Figure (3.6) is shown such a plot for the results of Table 3.3; for I-A < 4.0 eV, k_q is about 10^{10} dm^3 mol^{-1} s^{-1} but in the narrow range 4.0 < (I-A) < 4.6 eV, k_q falls very sharply. In this range a plot $\Delta G^{\ddagger}_{23}$ versus (I-A) is linear, with slope α [equation (1.61)] of 0.24 ± 0.04 and β = -1.02 ± 0.19 eV, and the theoretical values based on these parameters are given as the broken (sloping) line in Figure (3.6). (The value of β is not strictly $\Delta G^{\ddagger}_{23}(0)$ because the ordinate is not ΔG^{o}_{23}).

The Rehm-Weller kinetic model has been simplified by setting k_{32} = 0 to yield equation (3.5).

$$k_q = \frac{k_{12}}{1 + k_{12}/k_{23}} \qquad (3.5)$$

Substitution into (3.5) with equation (3.4) and invoking the Polanyi equation (1.61) yields equation (3.6)

$$k_q = \frac{k_{12}}{1 + \exp[\alpha(I-A-C_o)/RT]} \qquad (3.6)$$

where C_o is an empirical parameter given by equation (3.7). A plot of $\ln[(2 \times 10^{10}/k_q) - 1]$ against (I-A),

$$C_o = C + \Delta G^{\ddagger}_{23}(0) + \left(\frac{RT}{\alpha}\right) \ln \frac{\kappa^o}{k_{12}} \qquad (3.7)$$

i.e. the linear form of equation (3.6), yields a straight line with α= 0.22 ± 0.03 and C_o = 4.03 ± 0.6 eV. The latter figures compare with those of Kuzmin et al.[80,81] of α = 0.14 ± 0.02 and C_o = 3.42 ± 0.5 eV in heptane for quenching both of exciplexes and ^{1}(DCA)*.

In Figure (3.7) are shown the results of Table 3.4 for quenching of ^{1}(DCA)* by <u>acceptor</u> molecules in MeOH solution. Optimum fitting to the Rehm-Weller equations (1.52) (1.57) was achieved with $k_{12} = 1.5 \times 10^{10}$ dm^3 mol^{-1} s^{-1} and $\Delta G^{\ddagger}_{23}(0) = 7.11$ kJ mol^{-1}, but even so the agreement in the endoergonic region is rather poor; the observed quenching rates usually exceed those calculated by a considerable factor, although the downward trend at higher ΔG^{o}_{23} is of the correct magnitude, implying the possibility of a small systematic error in a thermochemical datum, probably the oxidation potential of DCA. Interestingly, the fluorescence quenching of zinc octaethylporphyrin by electron donors both in MeCN and toluene solution also shows anomalously high k_q at $\Delta G^{o}_{23} > 0$.[141]

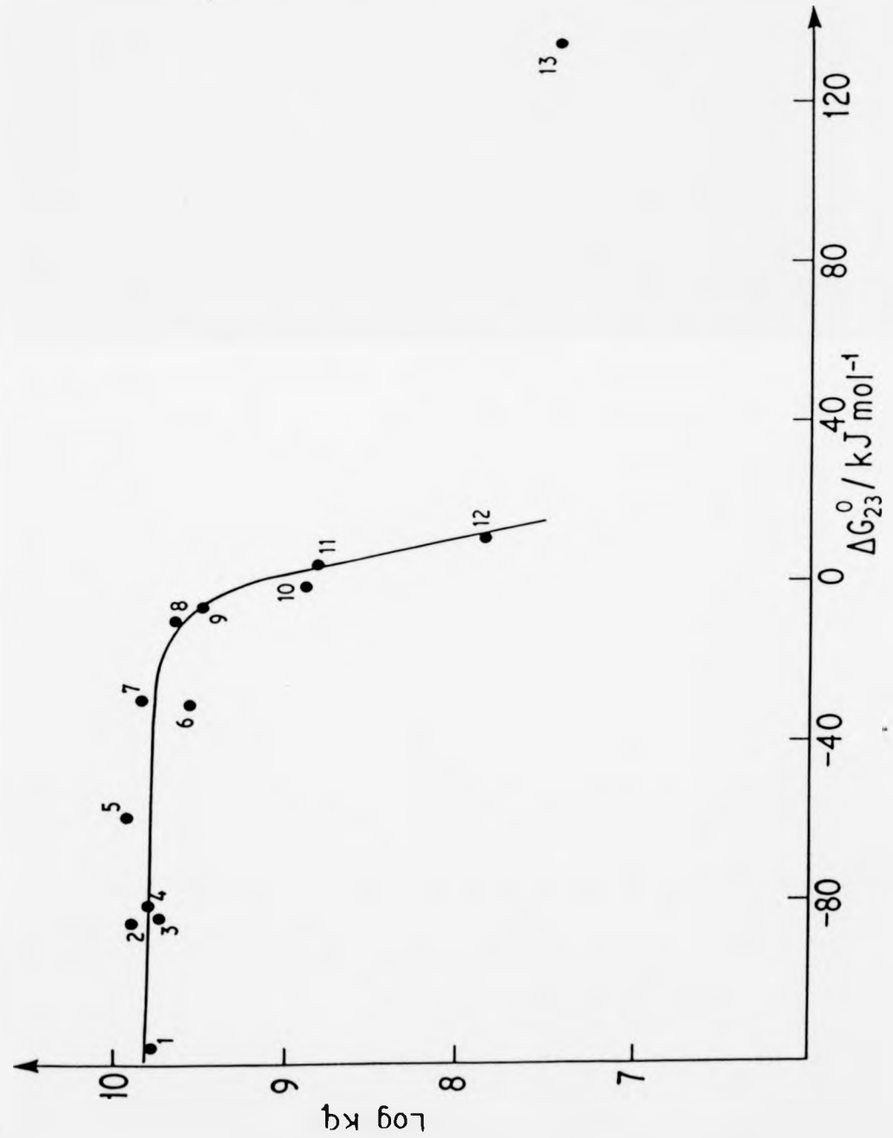

Figure (3.4) Log k_q against ΔG°_{23} for the reductive quenching of ^{1}(DCA)* by inorganic anions in MeOH-H_2O (1:1 v/v). Numbering of quenchers as in Table (3.2). Full line - theoretical values derived from Rehm-Weller treatment (for parameters see text).

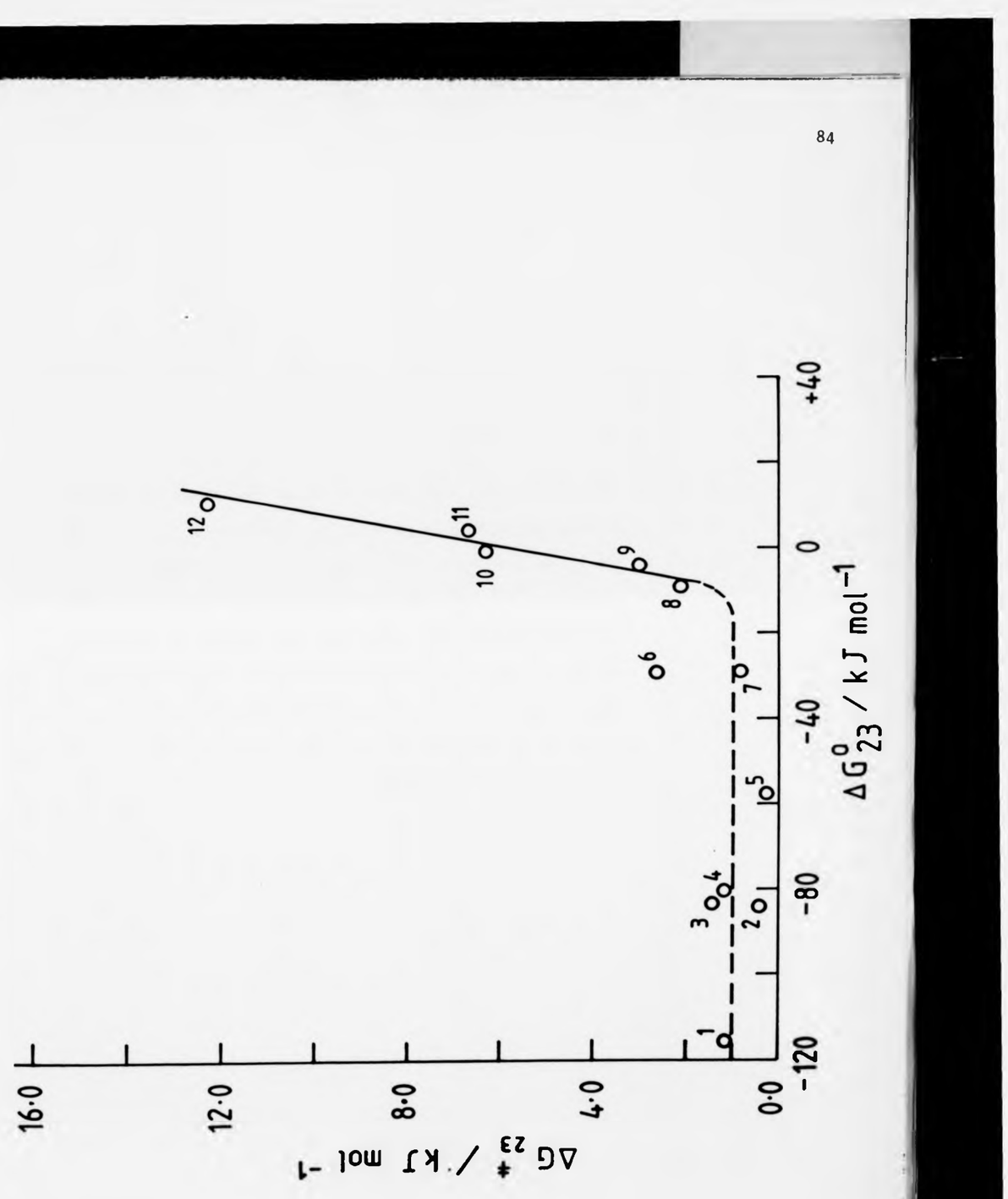

Figure (3.5) Plot of $\Delta G_{23}^{\ddagger}$ [where $k_q = 1 \times 10^{10} \exp(-\Delta G_{23}^{\ddagger}/RT)$] against ΔG_{23}^{o} in Table (3.2). Full line theoretical values from Polanyi equation (1.61) with an $\alpha = (0.487 \pm 0.068)$ and $\beta = (5.805 \pm 0.483)$ kJ mol^{-1}.

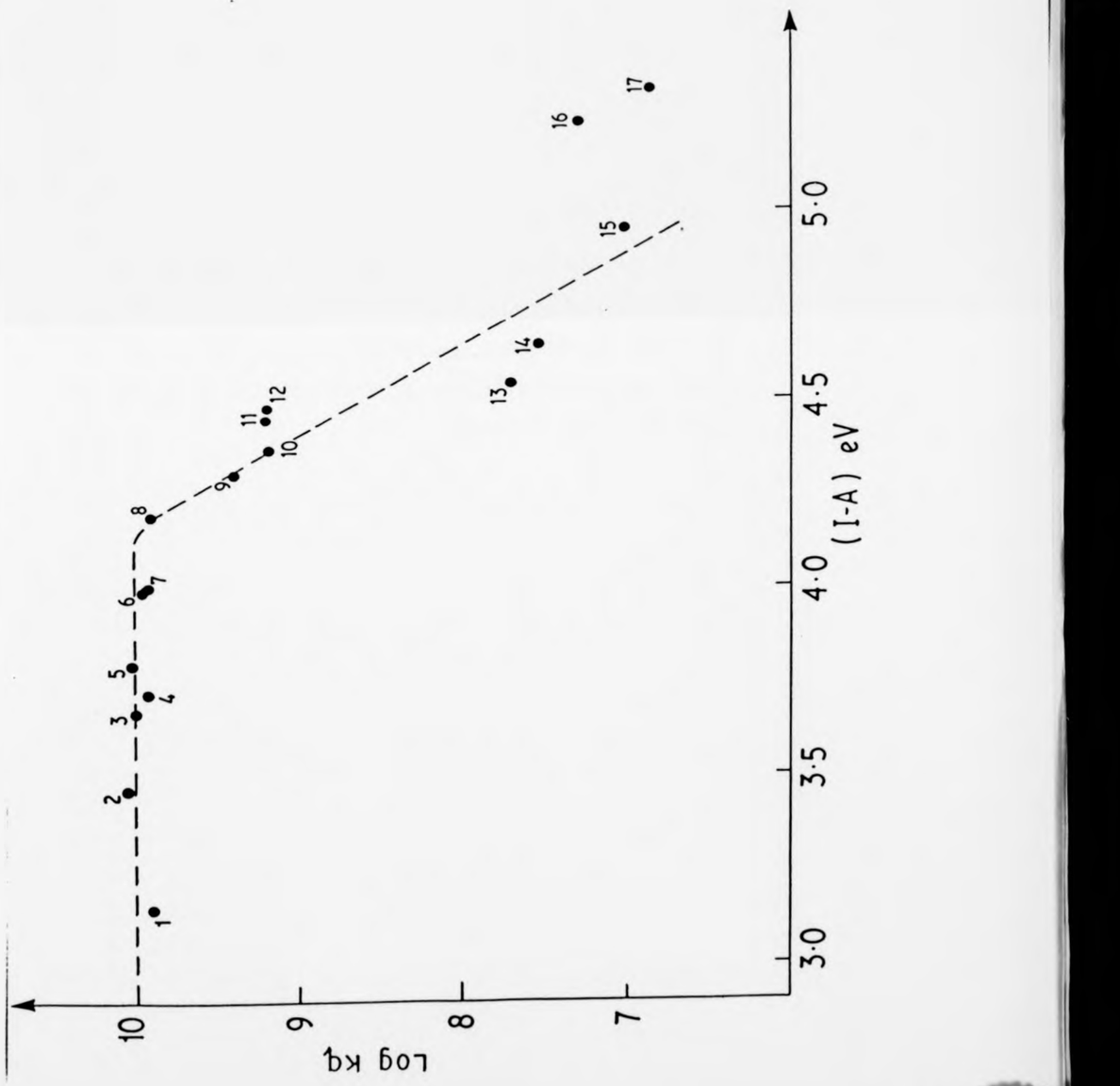

Figure (3.6) Log k_q against (I-A) for reductive quenching of ^{1}(DCA)* by organometallic compounds in cyclohexane. Numbering of quenchers as in Table (3.3). Broken line - theoretical values derived from Polanyi equation (1.61) (for parameters see text). (A) for ^{1}(DCA)* is estimated by us as 4.45 eV from E_i (DCA/DCA$\cdot^-$) = -0.98 V vs.SCE,[50] the correlation A = 2.49 + E_i (vs. SCE[140]) and $\Delta^1E_{0,0}$ = 2.945 eV in cyclohexane. Reference (81) gives A = 4.58 eV for ^{1}(DCA)* in heptane.

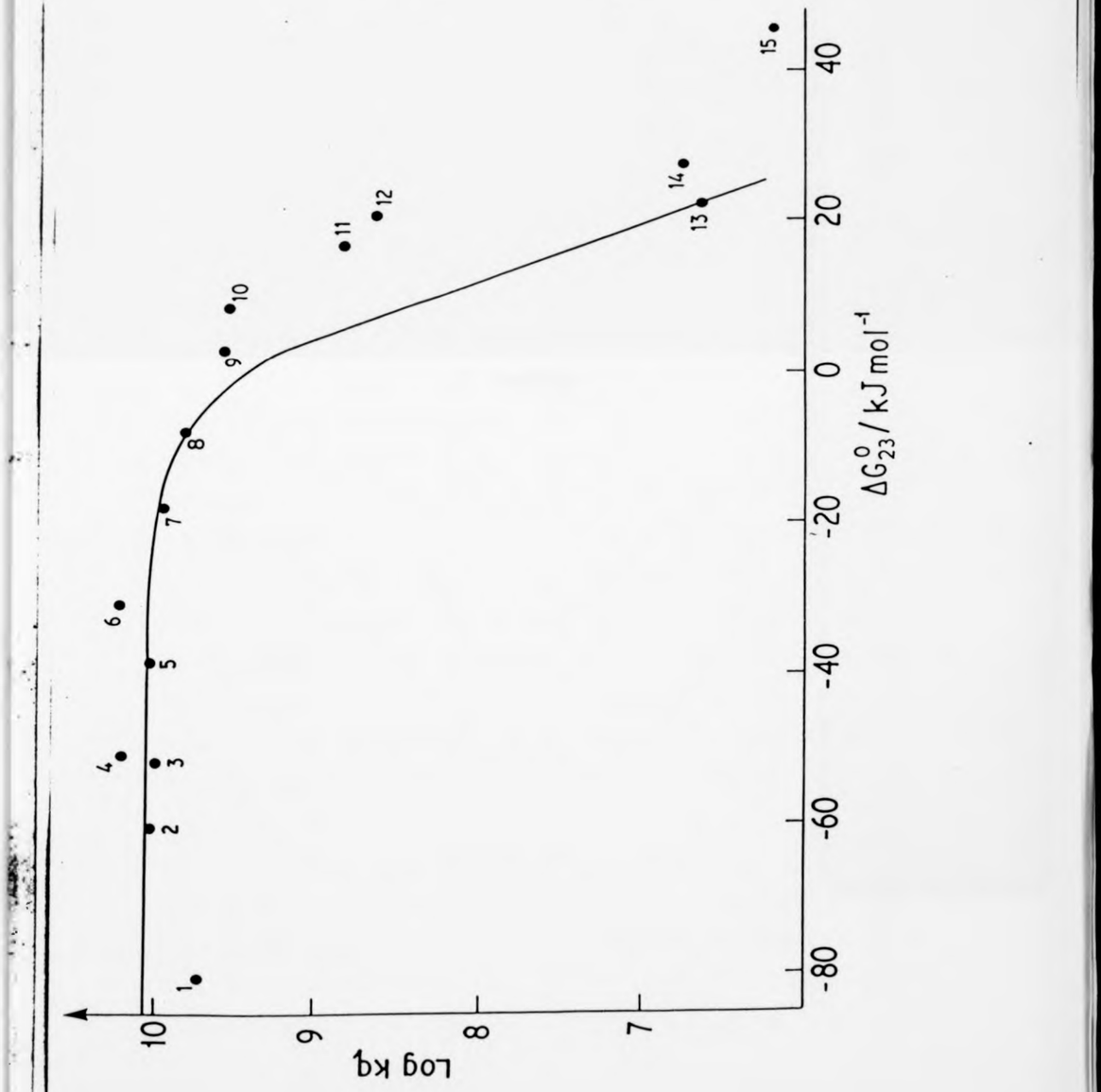

Figure (3.7) Log k_q versus ΔG^{o}_{23} for the oxidative quenching of ^{1}(DCA)* by organic electron-acceptors in MeOH. Numbering of quenchers as in Table (3.4). Full line - theoretical values derived from Rehm-Weller treatment (for parameters see text).

CHAPTER 4

4.1 Oxidative Quenching of the Fluorescence of 2-Aminoanthracene in Polar and Non-Polar Solvents: Results and Discussion

2-Aminoanthracene (2-AA) was selected for this study because it exhibits eminently suitable physical properties, namely it functions as a powerful electron donor in its ground state ($E_{\frac{1}{2}}$ = +0.44 V vs. SCE in acetronitrile[154]) and it exhibits an absorption peak in the visible region[160] (λ_{max} = 403 nm in EtOH), which means that troublesome inner-filter effects from quencher molecules can be minimised or eradicated.

Quenching of ^{1}(2-AA)* followed excellent Stern-Volmer kinetics, i.e. plots of I_{fo}/I_f versus quencher concentration are linear (with slope K^{SV}) with an intercept not less than 0.96 in the case of any quencher. K^{SV} is given by $k_q\tau_o$ where k_q is the bimolecular singlet quenching rate constant and τ_o is the lifetime of ^{1}(2-AA)*. In Table 4.1 are presented fluorescence spectral and lifetime data for ^{1}(2-AA)* in the solvents employed, together with the zero-zero excitation energy of the fluorophore, ($\Delta^1E_{o,o}$), estimated from the intersection of the absorption and fluorescence spectra of 2-AA in each solvent. Fluorescence from ^{1}(2-AA)* in deoxygenated solution at room temperature was quenched by a wide range of organic electron-acceptors in MeOH (Table 4.2) and in cyclohexane (Table 4.3). Diffusion quenching rate constants were found in both solvents when $E_{\frac{1}{2}}$ (acceptor) was more positive than -1.7 V vs. SCE. For quenchers with more negative potentials the quenching rate drops about 10^3 times at $E_{\frac{1}{2}}$ = -1.8 V vs. SCE, Figure (4.1). This quenching process cannot be attributed to ground state complexation, since the shape of the absorption spectrum is unchanged upon addition

of quenchers. No evidence for exciplex formation was apparent, although addition of large mole fraction of PhCN, causes a monotonic red-shift in the emission of ^{1}(2-AA)* in cyclohexane, and the same phenomenon has been observed in the case of excited N,N-dimethyl-2-aminoanthracene ^{1}(2-DMA)* with pyridine and quinoline in a nonpolar solvent (see Table 4.4).

In Figure (4.2) are shown the data from Table 4.2 in the form of a plot of log k_q versus ΔG°_{23}, with a computer-derived optimum fitting according to the Rehm-Weller equations (1.52) (1.57), with $k_{12} = 2 \times 10^{10}$ dm^3 mol^{-1} s^{-1} and $\Delta G^{\ddagger}_{23}(0) = 13.60$ kJ mol^{-1}. The experimental values of k_q coincides with the calculated figure in the highly exoergonic region (ΔG°_{23} more negative than -63.96 kJ mol^{-1}), but at more positive values of ΔG°_{23} a discrepancy between them is clear. However, a better agreement with a higher value of $\Delta G^{\ddagger}_{23}(0)$ could be obtained with the aid of the Polanyi equation (1.61), which shows a good fitting to these experimental results, Figure (4.2). The value for α and β are: $\alpha = 0.24 \pm 0.07$ and $\beta = 20.0 \pm 4.0$ kJ mol^{-1}; the parameter β fulfils a similar conceptual role as $\Delta G^{\ddagger}_{23}(0)$ but is not identical to it[70], while the value of α is usually between 0 and 1. The main contribution to $\Delta G^{\ddagger}_{23}(0)$ is a solvent reorganisation energy following electron removal from ^{1}(2-AA)*, although bond reorganisation energies may play some role as well since the expected[155,156] increases in polarisation of 2-AA upon excitation (rehybridisation of the amino nitrogen atom to an sp^2-type configuration), especially on the transition ^1L_b-^1L_A, implies a difference in geometry between 2-AA and ^{1}(2-AA)*, and this view is supported by a relatively large Stokes' shift (see section 6.1).

Table 4.1 Spectral and Lifetime Data for 2-Aminoanthracene

Solvent	τ_o/ns[a]	$\lambda_{exc.}$ /nm[b]	λ_F /nm[c]	$_{\Delta}{}^{1}E_{o,o}$/eV[d]
MeOH	30.38	420	493	2.743
Cyclohexane	25.67	400	437	3.084

a Ref. (160) gives 30.8 ns, 25.8 ns in EtOH and benzene respectively, ref.(161) gives 26.6 ns in cyclohexane.

b Excitation wavelength during quenching experiments.

c Fluorescence wavelength where the quenching is monitored.

d Obtained from intersection of absorption and fluorescence spectra. Ref. (155) gives 2.74 ± 0.013 eV in aqueous EtOH (1:1 v/v).

Table 4.2 Quenching of Singlet Excited 2-Aminoanthracene by Organic Acceptors in Methanol Solution

Acceptor	(number)	$E_{\frac{1}{2}}/V$ [a] vs. SCE	ΔG^{o}_{23} [b] /kJ mol^{-1}	k_q/dm^3 mol^{-1} s^{-1} (in Methanol)	k_q/dm^3 mol^{-1} s^{-1} (Calculated) [c]
Nifuroxime	(1)	-0.295 [d]	-199.52	(1.838 ± 0.03) x 10^{10}	1.472 x 10^{10}
Misondiazole	(2)	-0.395 [d]	-189.88	(1.407 ± 0.07) x 10^{10} [e]	1.460 x 10^{10}
1,4-Benzoquinone	(3)	-0.51	-178.78	(2.377 ± 0.19) x 10^{10}	1.451 x 10^{10}
2-Methyl-5-nitroimidazole	(4)	-0.545 [d]	-175.40	(1.45 ± 0.06) x 10^{10}	1.448 x 10^{10}
1,4-Dinitrobenzene	(5)	-0.70	-160.45	(2.209 ± 0.13) x 10^{10}	1.432 x 10^{10}
1,2-Dinitrobenzene	(6)	-0.83	-147.90	(2.405 ± 0.08) x 10^{10}	1.416 x 10^{10}
1,3-Dinitrobenzene	(7)	-0.91	-140.19	———	———
Methyl 3-nitrobenzoate	(8)	-1.045	-127.16	(1.751 ± 0.06) x 10^{10}	1.383 x 10^{10}
Nitrobenzene	(9)	-1.147	-117.32	(2.140 ± 0.04) x 10^{10}	1.362 x 10^{10}
4-Nitroanisole	(10)	-1.25	-107.38	(1.338 ± 0.05) x 10^{10}	1.338 x 10^{10}
Phthalic anhydride	(11)	-1.31	-101.60	(7.92 ± 0.6) x 10^{9}	1.321 x 10^{10}
2,3-Dimethylnitrobenzene	(12)	-1.318	-100.82	———	———
1,4-Dicyanobenzene	(13)	-1.39 [f]	-93.87	(1.440 ± 0.06) x 10^{10}	1.295 x 10^{10}
4-Cyanopyridine	(14)	-1.44 [f]	-89.05	(1.337 ± 0.05) x 10^{10}	1.276 x 10^{10}
Nitromesitylene	(15)	-1.442	-88.86	(1.640 ± 0.06) x 10^{10}	1.276 x 10^{10}
Nitromethane	(16)	-1.46 [g]	-87.12	(1.308 ± 0.08) x 10^{10}	1.269 x 10^{10}
2,4,6-Tri-tertbutylnitrobenzene	(17)	-1.50	-83.26	(1.042 ± 0.04) x 10^{10}	1.251 x 10^{10}

Acceptor	(number)	$E_{\frac{1}{2}}$/V vs. SCE	ΔG^{o}_{23} /kJ mol^{-1}	k_q/dm^3 mol^{-1}s^{-1} (in Methanol)	k_q/dm^3 mol^{-1}s^{-1} (Calculated)
1,2-Dicyanobenzene	(18)	-1.54[f]	-79.40	(1.569 ± 0.06) x 10^{10}	1.233 x 10^{10}
1,3-Dicyanobenzene	(19)	-1.59[f]	-74.58	(1.496 ± 0.05) x 10^{10}	1.206 x 10^{10}
2-Methyl-2-nitro-propane	(20)	-1.70	-63.96	(5.73 ± 0.2) x 10^{9}	1.134 x 10^{10}
Iodobenzene	(21)	-1.81	-53.35	(1.025 ± 0.02) x 10^{7}	1.035 x 10^{10}
Benzonitrile	(22)	-2.23[h]	-12.83	(5.040 ± 0.41) x 10^{6}	2.208 x 10^{9}
Bromobenzene	(23)	-2.49	+12.25	(3.870 ± 0.32) x 10^{6}	1.609 x 10^{7}

Footnote for Table 4.2

a Measured in MeCN or DMF vs. SCE using 0.1 mol dm^{-3} $R_4N^+ClO_4^-$ (R = Et or n-P_r) as supporting electrolyte; except where indicated otherwise, values are taken from ref. (152).

b Calculated using $E_{\frac{1}{2}}$ for 2-aminoanthracene equal + 0.44 V vs. SCE in MeCN using 2.0 mol dm^{-3} $NaClO_4$ as supporting electrolyte, taken from ref. (154).

c Calculated from the best fitting parameters (k_{12} = 2 x 10^{10} dm^3 mol^{-1} s^{-1} and $\Delta G^{\ddagger}_{23}(O)$ = 13.60 kJ mol^{-1}) to the experimental data.

d Measured in phosphate-buffered saline at pH = 7.2, from ref. (153).

e I_{fo}/I_f was corrected to the following equation,[162] where A_D, A_Q are the absorbances at 420 nm for 2-aminoanthracene and 1,4-benzoquinone, respectively

$$(I_{f_o}/I_f)_{corr.} = (I_{f_o}/I_f)_{app.} \left[\frac{1 - 10^{-(A_D + A_Q)}}{1 - 10^{-A_D}}\right]$$

f Calculated from electron affinities according to the following correlation taken from ref. (140),

Electron affinity = 2.49 + $E_{\frac{1}{2}}$(red.) (V vs.SCE)

g From ref. (161).

h From ref. (91).

Table 4.3 Quenching of Singlet Excited 2-Aminoanthracene by Organic Acceptors in Cyclohexane Solution

Acceptor (number)[a]		$E_{\frac{1}{2}}/V$[b] vs. SCE	k_q/dm^3 mol^{-1} s^{-1} (in cyclohexane)
1,3-Dinitrobenzene	(7)	-0.91	$(2.39 \pm 0.09) \times 10^{10}$
Methyl 3-nitrobenzoate	(8)	-1.045	$(9.56 \pm 0.23) \times 10^{9}$
Nitrobenzene	(9)	-1.147	$(2.37 \pm 0.05) \times 10^{10}$
4-Nitroanisole	(10)	-1.25	$(2.06 \pm 0.05) \times 10^{10}$
2,3-Dimethylnitrobenzene	(12)	-1.318	$(1.70 \pm 0.05) \times 10^{10}$
4-Cyanopyridine	(14)	-1.44	$(1.43 \pm 0.02) \times 10^{10}$
Nitromethane	(16)	-1.46	$(1.56 \pm 0.04) \times 10^{10}$
2,4,6-Tri-tertbutylnitrobenzene	(17)	-1.50	$(1.29 \pm 0.03) \times 10^{10}$
2-Methyl-2-nitropropane	(20)	-1.70	$(1.34 \pm 0.04) \times 10^{10}$
Iodobenzene	(21)	-1.81	$(2.32 \pm 0.06) \times 10^{7}$
Benzonitrile	(22)	-2.23	Causes red-shift in the fluorescence maximum

a The same numbering as in Table 4.2. Two factors limited the test of other acceptors namely, solubility and inner-filter effect since $\lambda_{exc.} = 400$ nm was applied in this solvent.

b Data sources given as footnotes to Table 4.2.

Table 4.4 Fluorescence Quenching of 2-Aminoanthracene and N,N-Dimethyl-2-aminoanthracene by Heterocyclic Compounds in Methanol and Cyclohexane Solution

		2-AA		2-DMA[a,b]	
Quencher	E_1/V vs.SCE	k_q/dm^{3}mol^{-1}s^{-1} (in MeOH)	k_q/dm^{3}mol^{-1}s^{-1} (in cyclohexane)	k_q/dm^{3}mol^{-1}s^{-1} (in MeOH)	k_q/dm^{3}mol^{-1}s^{-1} (in cyclohexane)
4-Cyanopyridine	-1.44[c]	$(1.34 \pm 0.05) \times 10^{10}$	$(1.43 \pm 0.03) \times 10^{10}$	$(1.33 \pm 0.02) \times 10^{10}$	$(4.55 \pm 0.05) \times 10^{8}$
Quinoline	-2.133[d]	$(8.95 \pm 0.03) \times 10^{9}$	$(1.26 \pm 0.05) \times 10^{10}$	$(1.00 \pm 0.03) \times 10^{10}$	causes red-shift in the fluorescence maximum
Pyridine	-2.718[d]	$(3.87 \pm 0.31) \times 10^{6}$	$(3.98 \pm 0.19) \times 10^{9}$	$(1.88 \pm 0.25) \times 10^{6}$	

a τ_o = 28.6 ns in methanol and 24.5 ns in cyclohexane.

b $\lambda_{exc.}$ = 420 nm was used in both solvents, while λ_F was monitored at λ 494 nm (methanol) and 458 nm (cyclohexane).

c See footnote of Table 4.2 .

d From ref.(163) after correction for change of reference electrode from Ag/AgCl to SCE by addition of 0.042 V.

Figure (4.1) Correlation of log k_q against$(-E_{\frac{1}{2}})$(V vs. SCE) for the oxidative quenching of $^1(2\text{-AA})^*$ by organic electron-acceptors in methanol (●) and cyclohexane (O). Numbering of quenchers as in Tables(4.2) and (4.3).

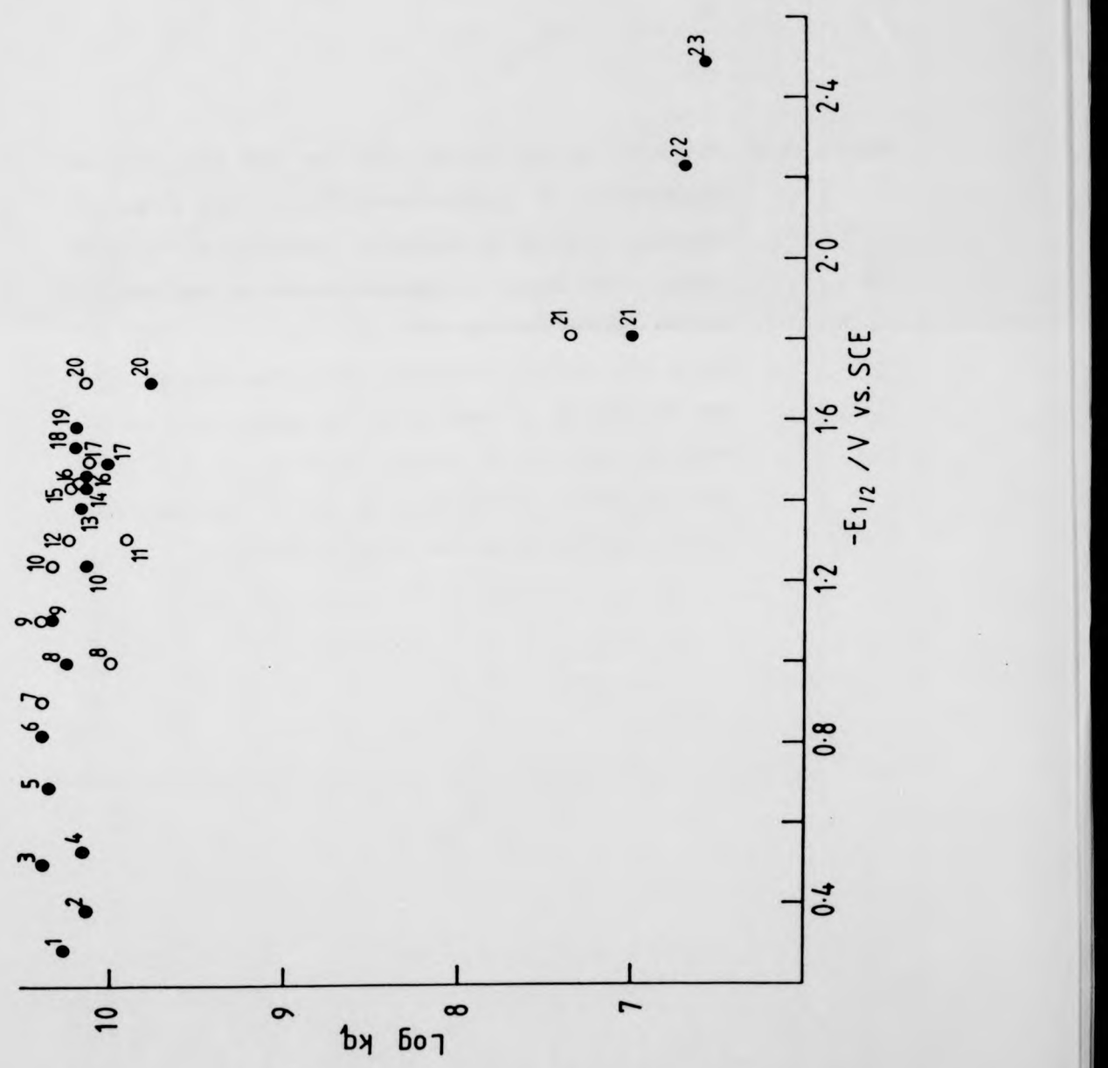

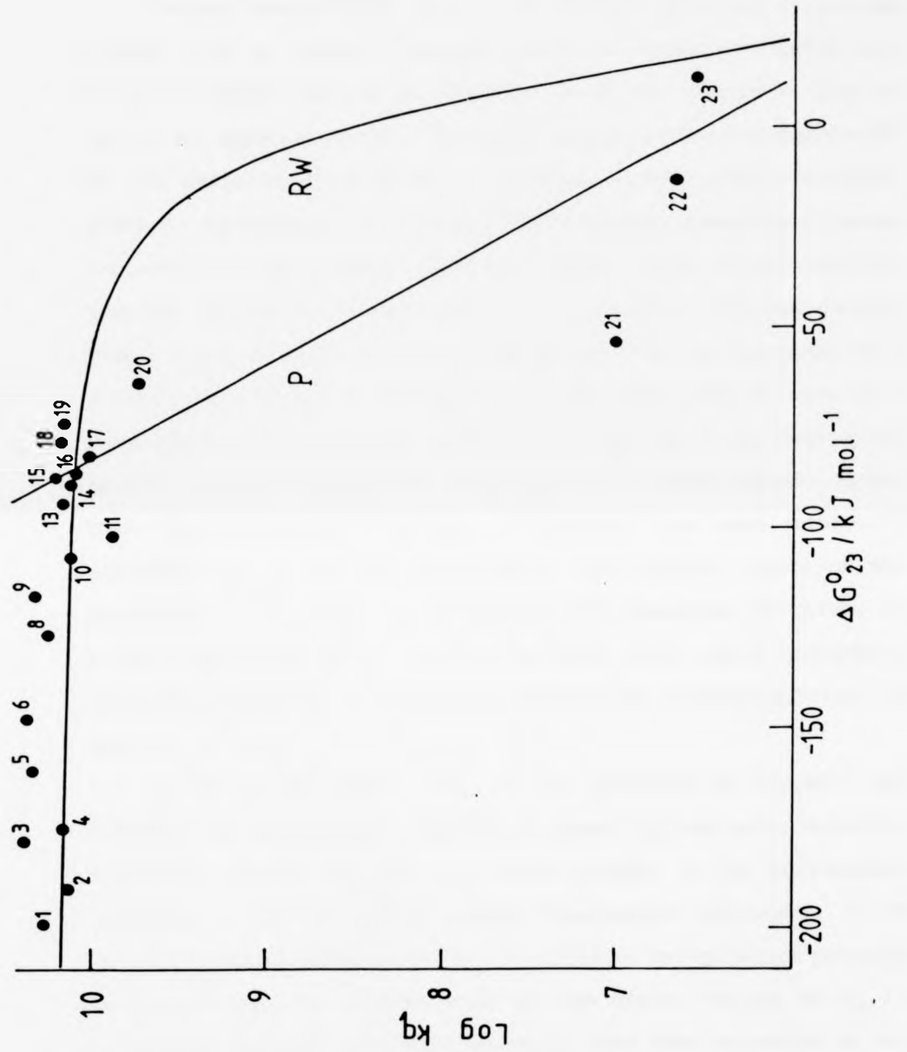

Figure (4.2) Plots of log k_q versus ΔG^{o}_{23} for the fluorescence quenching of 2-aminoanthracene by organic electron-acceptors in methanol. Numbering as in Table (4.2). Full curve: a computer-derived optimum fitting to the Rehm-Weller equation (RW): $k_{12} = 2 \times 10^{10}$ dm^3 mol^{-1} s^{-1}, $\Delta G^{\ddagger}_{23}(0) = 13.6$ kJ mol^{-1}. The straight line (P) corresponds to theoretical treatments based on the Polanyi equation (1.61) and [$k_q = 1 \times 10^{10}$ exp($-\Delta G^{\ddagger}_{23}/RT$)]; for values of ($\alpha$) and ($\beta$) see text. (The analysis depends on points 18 to 23 inclusive).

Recent studies[91,92] on the fluorescence quenching of certain radical ions by organic electron donors and acceptors require high values of $\Delta G^{\ddagger}_{23}(0)$ (41.8 to 64 kJ mol^{-1}) to fit the results in terms of the Marcus equation (1.60). The large energy barrier is explained[92] on the basis of large geometric changes in the electron-transfer process. In another recent study,[157] fluorescence quenching of pyrene and naphthalene by aromatic nitriles in ethanol shows deviant behaviour from the Rehm-Weller curve. The rate of quenching decreases rapidly from 7 x 10^9 dm^3 mol^{-1} s^{-1} to 2 x 10^7 dm^3 mol^{-1} s^{-1} in the range $-35.7 < \Delta G^{\circ}_{23} < -5.9$ kJ mol^{-1}. Such behaviour was interpreted in terms of a competition between the rate constants k_{23} and k_{21} in the Rehm-Weller scheme, and the mechanism is considered to be charge transfer rather than full one-electron transfer. Moreover, the same authors[157] confirmed that k_q is very sensitive to the chemical nature of the quenchers on the basis of the fluorescence quenching of pyrene by 1,2,4-trimethoxybenzene in EtOH and MeCN, which shows consistency with the Rehm-Weller curve, while quenching by aromatic nitriles is not.

A short comparative study on the quenching of ^{1}(2-AA)* and ^{1}(2-DMA)* by heterocyclic compounds in polar and non-polar solvents, Table 4.4, reveals the role of H-atom transfer in the fluorescence quenching of 2-AA by hydrogen-bonded heterocyclic compounds. If we consider that quenching of ^{1}(2-AA)* by pyridine and quinoline proceeds by H-atom transfer on the basis of the higher values of k_q in cyclohexane compared with polar solvents, then this mechanism is not operative for 4-cyanopyridine (whose k_q is virtually independent of solvent) since the latter has a more positive reduction potential; consequently the mechanism for quenching of ^{1}(2-AA)* and ^{1}(2-DMA)*

by 4-cyanopyridine is charge-transfer in both MeOH and cyclohexane. A picosecond study by Mataga et al.[158] confirmed that the mechanism of fluorescence quenching of 2-aminonaphthalene by pyridine in both hexane and MeCN is charge-transfer from excited 2-aminonaphthalene to hydrogen-bonded pyridine on the basis of the observation of 2-aminonaphthalene cation radical at 540 nm.

In spite of a lack of definite evidence for exciplex formation, addition of either pyridine or quinoline induces a red-shift in the fluorescence of ^{1}(2-DMA)* in cyclohexane; the only similar case we have observed is the system ^{1}(2-DMA)*/ dimethyl phthalate in cyclohexane, Figure (4.3). However ^{1}(2-AA)* does not exhibit similar behaviour and instead normal quenching was observed with $k_q = 7 \times 10^9$ $dm^3\ mol^{-1}\ s^{-1}$. The failure to observe any exciplex in the case of ^{1}(2-AA)* is probably due to electron-transfer followed by proton-transfer from the amino group to give neutral radicals. A similar observation has been reported[159] for N,N-dimethyl-2-aminonaphthalene (and not 2-aminonaphthalene) with dimethyl isophthalate in cyclohexane.

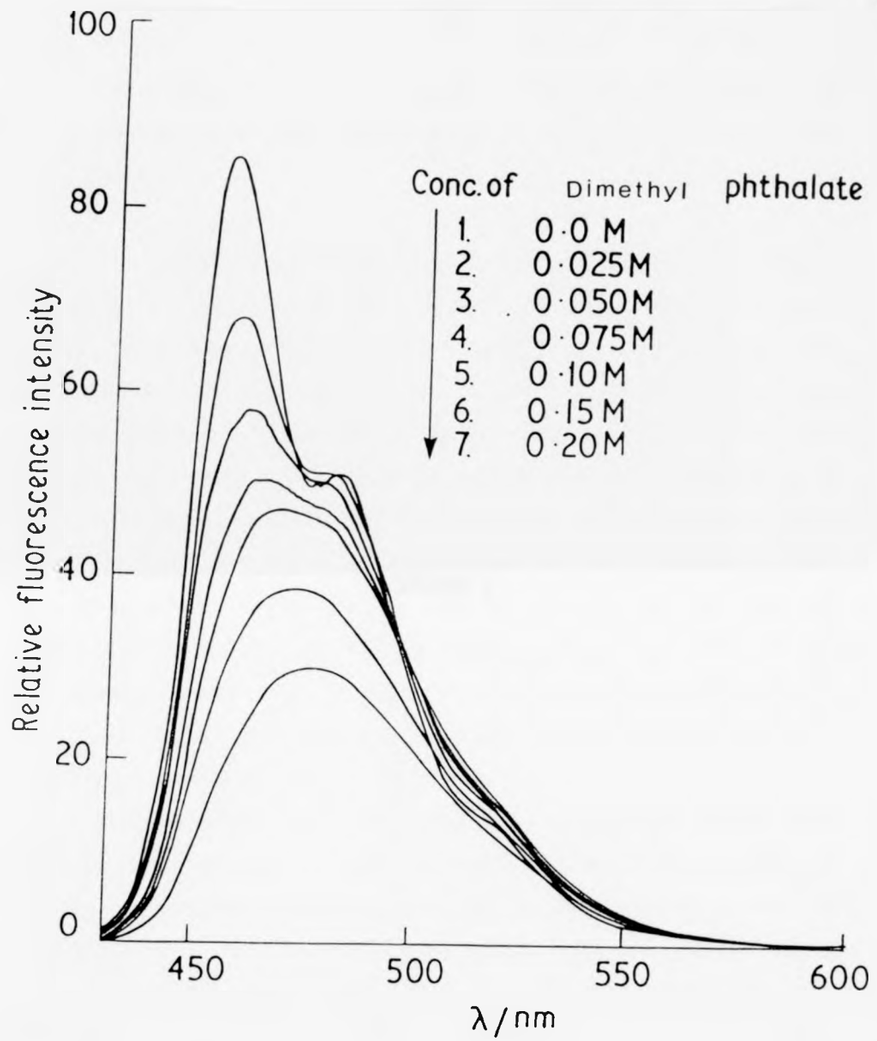

Figure (4.3) Fluorescence spectra of N,N-dimethyl-2-aminoanthracene (2×10^{-5} mol dm^{-3}) in cyclohexane at room temperature varying concentrations of dimthyl phthalate.

CHAPTER 5

5.1 Quenching of Excited State Xanthone and Thioxanthone by Inorganic Anions in the MeCN-H_2O Mixture: Results and Discussion

The transient absorption spectra of the triplet states of xanthone and thioxanthone after deoxygenation in MeCN-H_2O (3:2 v/v) mixtures are shown in Figure (5.1), and their first-order decays were monitored at the λ_{max} values of 610 ± 5 and 605 ± 5 nm, respectively. The first-order triplet state decay rate constants (k_1) of the two xanthones increased with increasing concentrations of added anions to give pseudo-first order rate constants (k_{obs}). This type of quenching is not caused by the countercation as there was no differential effect of using sodium or potassium salts.[77-79,164] The second-order quenching rates of the two triplet xanthones (^3k_q) were obtained from the slopes of the plots of equation (2.4), i.e. by plotting (k_{obs}) versus anion concentration [Q], as shown in Figures (5.2) and (5.3) for xanthone and thioxanthone respectively.

It is known[169] that the triplet lifetime (k_1^{-1}) of the xanthones depends on their concentration, indicating self-quenching and for this reason the same concentration of ketone was kept throughout all the experiments. Rate constants (^1k_q) for singlet quenching of fluorescence of thioxanthone by anions were obtained from conventional Stern-Volmer plots, typified by Figure (5.4), of I_{fo}/I_f versus [Q] to give a Stern-Volmer constant K^{SV} which was factorised using the relation $K^{SV} = {}^1k_q \tau_o$, where τ_o is the fluorescence lifetime of thioxanthone in the absence of quencher.

In all cases there was no evidence for any new emitting species such as an exciplex on addition of anions. In general we were unable to detect the presence of the semi-oxidised inorganic ion in absorption following the laser pulse; however, in the case of SCN^- ion, a weak absorption maximising at 500 ± 5 nm was found in MeCN-H_2O (3:2 v/v) following flash photolysis of either xanthone or thioxanthone, as shown in Figures (5.5) and (5.6) respectively. This absorption is similar to that of $(SCN)^-_2$, previously reported in aqueous solution,[57] acetone[139] and MeCN.[58] The yields of such semi-oxidised species are usually particularly small in water as compared with pure MeOH or MeCN.[165,166]

In Table 5.1 are presented spectral and physical constants for photosensitisers utilised in this study. Values of the quenching constants of the singlet and triplet xanthones at room temperature are summarised in Table 5.2.

It is known that flash photolysis of aromatic carbonyl compounds in aqueous solution produces two distinct transients, namely the short-lived triplet state absorption and the much longer-lived absorption due to ketyl radicals or radical-anions (depending on pH). The transient produced upon laser flash photolysis of xanthone in MeCN-H_2O with λ_{max} 610 ± 5 nm, Figure (5.1), has been observed both in water and 95% ethanol by other workers,[125,167,168] and it has been assigned[125] to the triplet-triplet absorption on the basis of energy transfer data (rather than to a ketyl radical). Kinetic quenching of the transient due to triplet thioxanthone in MeCN-H_2O was monitored at 605 ± 5 nm, a wavelength resembling that observed at 625 ± 5 nm in pure MeCN by Yip et al.[169] and very recently by Schuster et al.[170] in MeCN at 620 nm. Our value for λ_{max} in pure MeCN is 630 ± 10 nm (see section 6.2).

Table 5.1 Spectral and Physical Data for Ketones in Medium $MeCN/H_2O$ (3:2 v/v)

Molecule	τ_o/ns	$\Delta^1E_{o,o}$ /eV	$\Delta^3E_{o,o}$ [a] /eV	$E_{\frac{1}{2}}^T$ [b]/V vs. NHE
Thioanthone	4.9 [c]	3.069 [d]	2.84	-1.37 [e]
Xanthone	——	——	3.21	-1.40 [f]
Biacetyl	——	——	2.48	-0.78 [g]

a From ref.(176).

b After correction for change of reference electrode from SCE to NHE by addition of 0.25 V.

c Monitored at λ_F = 432 nm (maximum emission).

d Obtained from intersection of absorption and fluorescence spectrum (see Fig.5.7); ref.(173) gives 3.278 eV in hexane.

e From ref.(177) (measured in DMF and n-Bu_4NClO_4 as supporting electrolyte).

f From ref.(178) (measured in DMF and n-Bu_4NI as supporting electrolyte).

g From ref.(179) (measured in 50% aqueous ethanol at pH 12.65; a figure of -1.21 V vs. NHE is given in ref.(180)).

Table 5.2a Fluorescence Quenching Rate Constants of Thioxanthone by Inorganic Anions in MeCN/H_2O (3:2 v/v)

Inorganic anion (number)	$E(D^{+\cdot}/D)$[a]/V vs. NHE	ΔG^{o}_{23} /kJ mol^{-1}	$^{1}k_q$ /10^9 dm^3 mol^{-1} s^{-1}
$[Fe(CN)_6]^{4-}$ (1)	0.356[b]		See text
$[IrCl_6]^{3-}$ (2)	0.892 ± 0.009[c]		See text
NO_2^- (3)	1.0 ± 0.1[d]	-73.25	9.27 ± 0.05
$SeCN^-$ (4)	1.27[e]	-47.20	9.23 ± 0.19
I^- (5)	1.33±0.03[f], 1.4±0.05[d]	-41.41	9.38 ± 0.23
$S_2O_3^{2-}$ (6)	1.34[g], 1.35[h]	-40.44	2.78 ± 0.05
N_3^- (7)	1.37 ± 0.02[h] 1.87[k]	-37.55	4.60 ± 0.06
SCN^- (8)	1.601[g], 1.50[k], 1.66[f]	-15.26	8.58 ± 0.10
Br^- (9)	1.904[g], 2.0 ± 0.1[k,d]	+13.97	2.54 ± 0.07

a The first figure listed was utilised in calculating ΔG^{o}_{23}.

b From ref.(181).

c From ref.(182).

d From ref.(142).

e Calculated using E(Ctts) = 5.27 eV from ref.(183) and E(Ctts) = 1.35 $E_{D^{+}\cdot/D}$ + 3.55 (in eV units) given in ref.(77-79).

f From ref.(143).

g From ref.(57).

h From ref.(144).

k From ref.(77-79).

Table 5.2b Triplet Quenching Rate Constants of Ketones by Inorganic Anions in MeCN/H_2O (3:2 v/v)

Inorganic anion (number)[a]	Thioxanthone		Xanthone		Biacetyl	
	ΔG^o_{23}/ kJ mol^{-1}	^3k_q /dm^3 mol^{-1} s^{-1}	ΔG^o_{23}/ kJ mol^{-1}	^3k_q /dm^3 mol^{-1} s^{-1}	ΔG^o_{23}/ kJ mol^{-1}	^3k_q[b] /dm^3 mol^{-1} s^{-1}
(1)	-113.31	$(5.02\pm0.13)\times10^9$	-146.08	$(5.14\pm0.22)\times10^9$		
(2)	-61.59	$(4.10\pm0.12)\times10^9$	-94.36	$(4.56\pm0.11)\times10^9$		
(3)	-51.17	$(4.02\pm0.17)\times10^9$	-83.94	$(5.37\pm0.17)\times10^9$		
(4)	-25.12	$(7.76\pm0.12)\times10^9$	-57.89	$(7.68\pm0.12)\times10^9$	-47.28	5.7×10^9
(5)	-19.33	$(6.60\pm0.18)\times10^9$	-52.10	$(7.13\pm0.12)\times10^9$	-41.49	5.5×10^9
(6)	-18.37	$(1.60\pm0.05)\times10^9$	-51.14	$(2.68\pm0.05)\times10^9$		
(7)	-15.47	$(3.78\pm0.03)\times10^9$	-48.24	$(4.88\pm0.13)\times10^9$		
(8)	+ 6.81	$(2.98\pm0.17)\times10^7$	-25.95	$(6.10\pm0.11)\times10^9$	-15.34	1.7×10^9
(9)	+36.05	$(1.14\pm0.10)\times10^6$	+ 3.28	$(1.42\pm0.04)\times10^9$	+13.89	5.6×10^7

a The same numbering as in Table 5.2a.

b From ref.(89), measured by phospherescence quenching in aqueous solution at room temperature.

Figure (5.1) Spectrum of the transient absorption obtained by laser flash photolysis of deaerated solutions of thioxanthone (O, 2 x 10^{-4} mol dm^{-3}) and xanthone (●, 2 x 10^{-4} mol dm^{-3}) in MeCN-H_2O (3:2 v/v) taken 10 μs after the laser pulse.

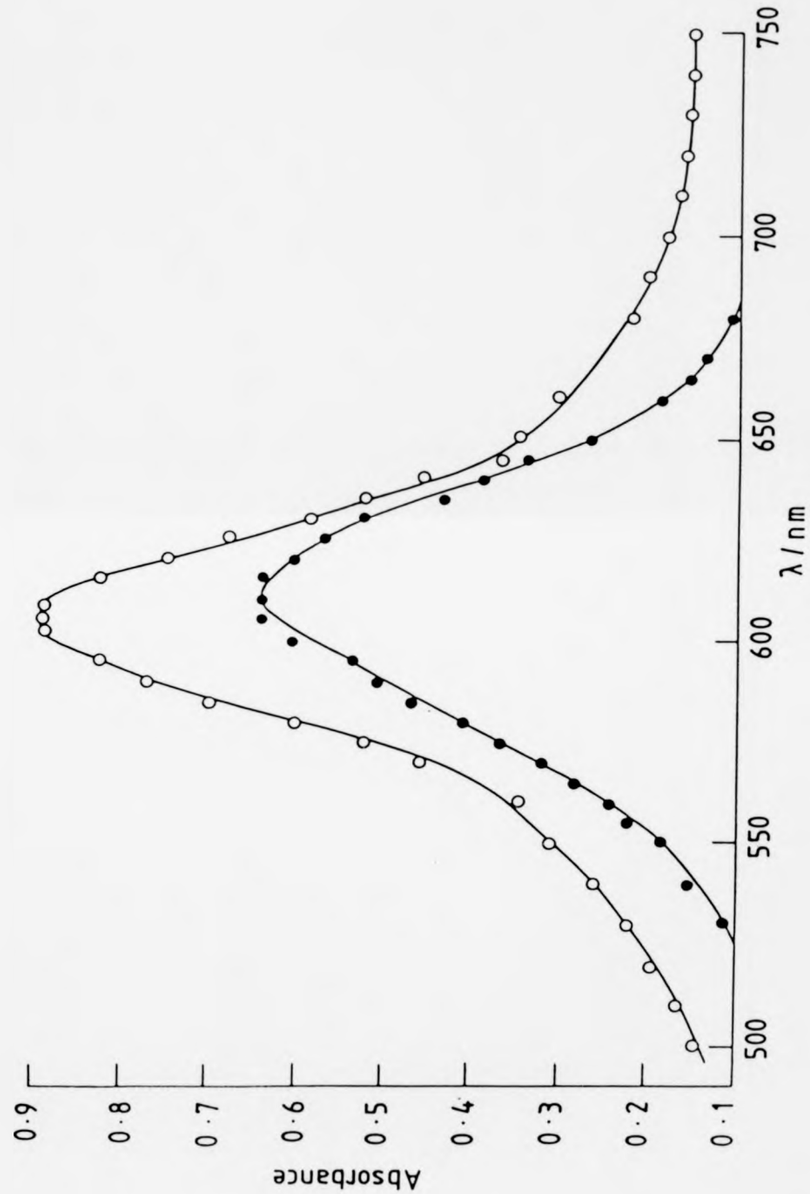

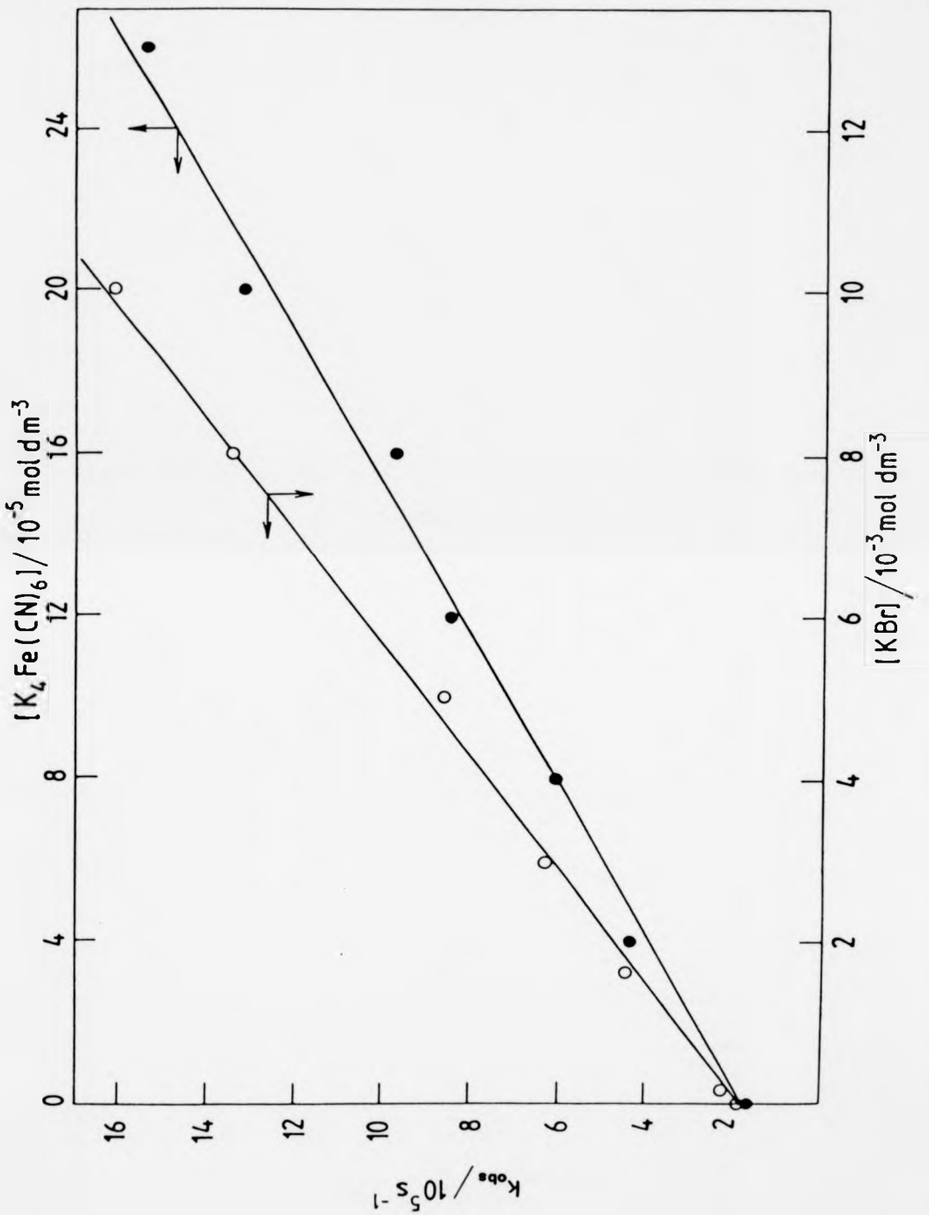

Figure (5.2) Triplet quenching of xanthone by electron-donors in MeCN-H_2O (3:2 v/v) mixture.

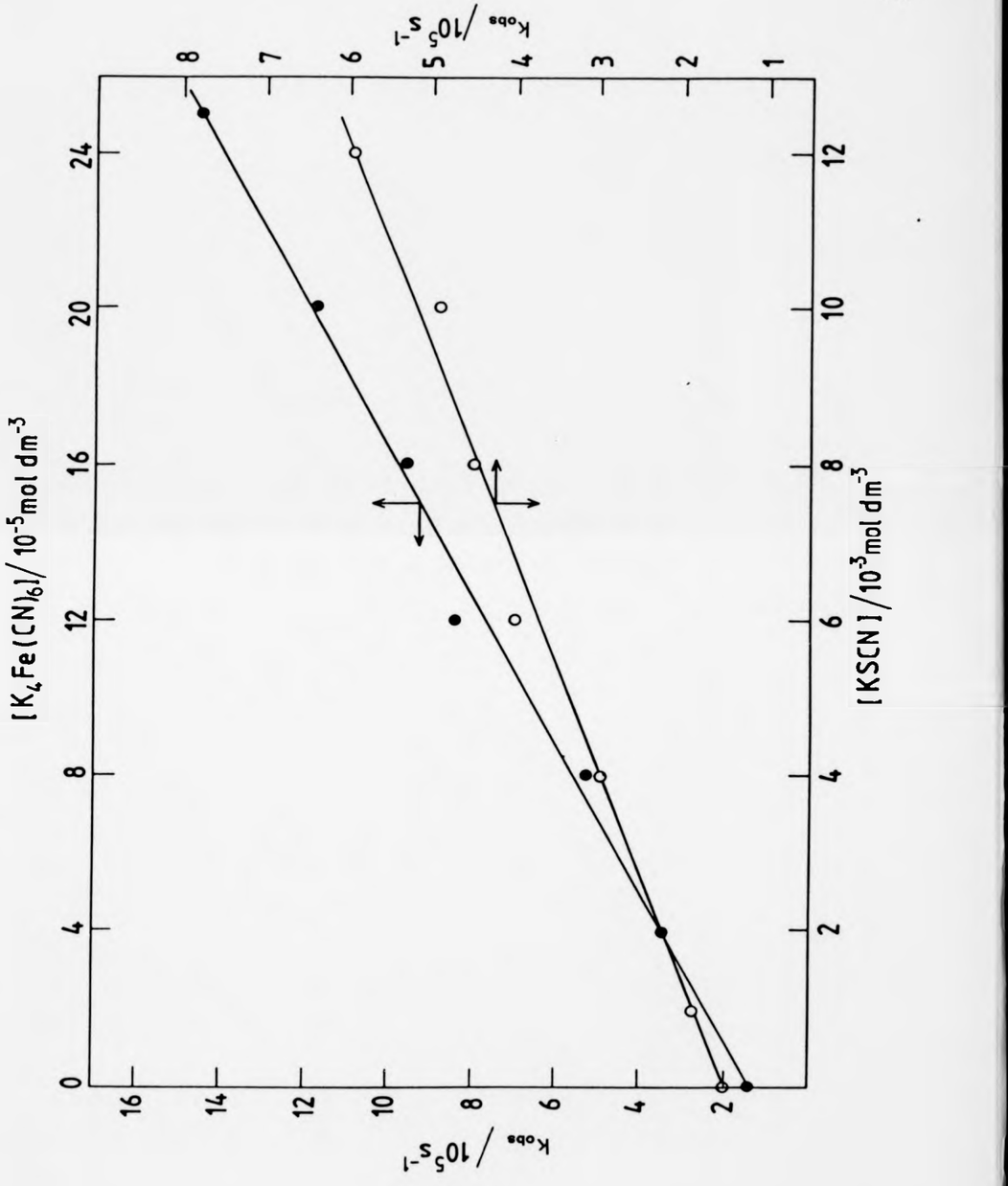

Figure (5.3) Triplet quenching of thioxanthone by electron-donors in MeCN-H_2O (3:2 v/v) mixture.

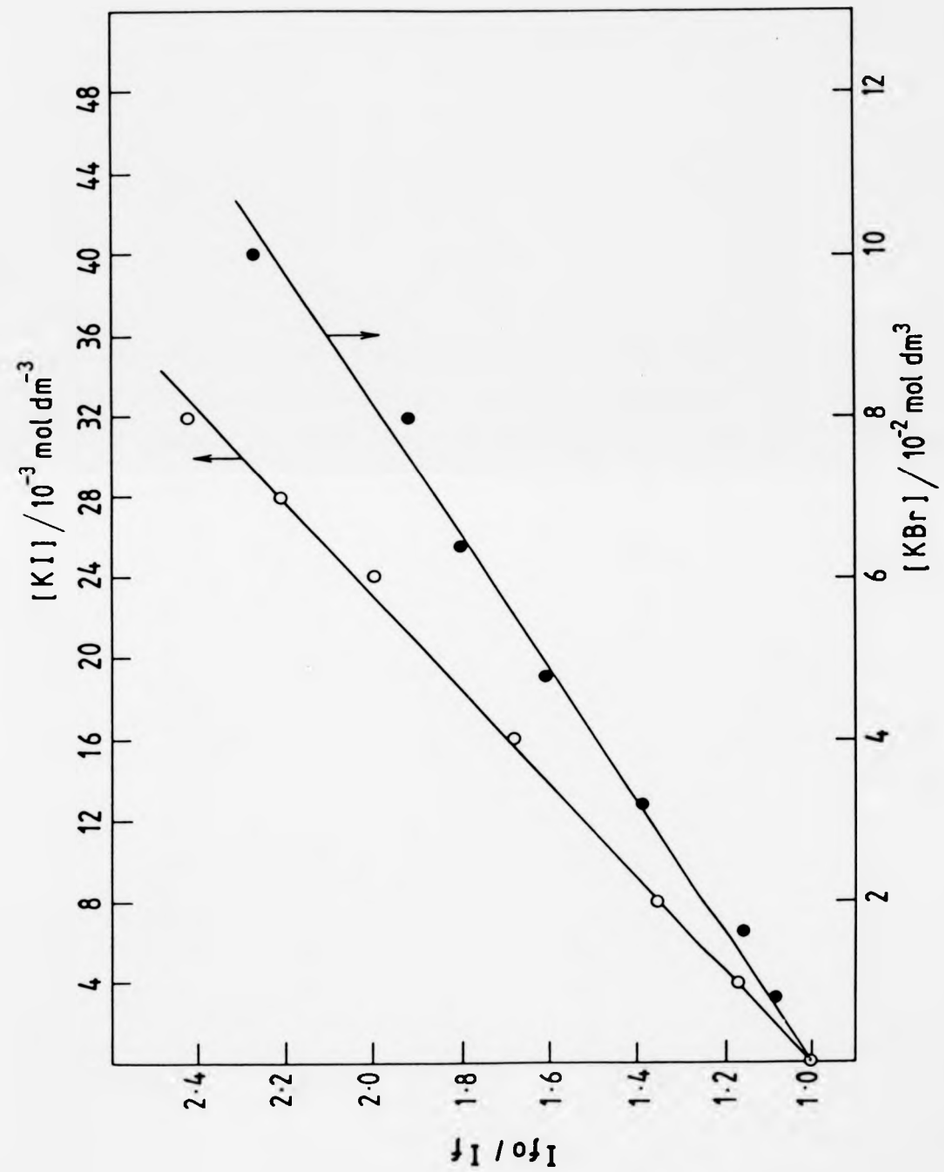

Figure (5.4) Typical Stern-Volmer plots for the quenching of singlet thioxanthone by inorganic anions in MeCN-H_2O (3:2 v/v) mixture; $\lambda_{exc.}$ = 380 nm, λ_F = 432 nm.

Figure (5.5) Spectrum of the transient obtained on laser flash photolysis of deaerated solution of xanthone (1×10^{-4} mol dm^{-3}) and KSCN (0.21 mol dm^{-3}) in MeCN-H_2O (3:2 v/v), as measured 5 μs after the end of the laser pulse.

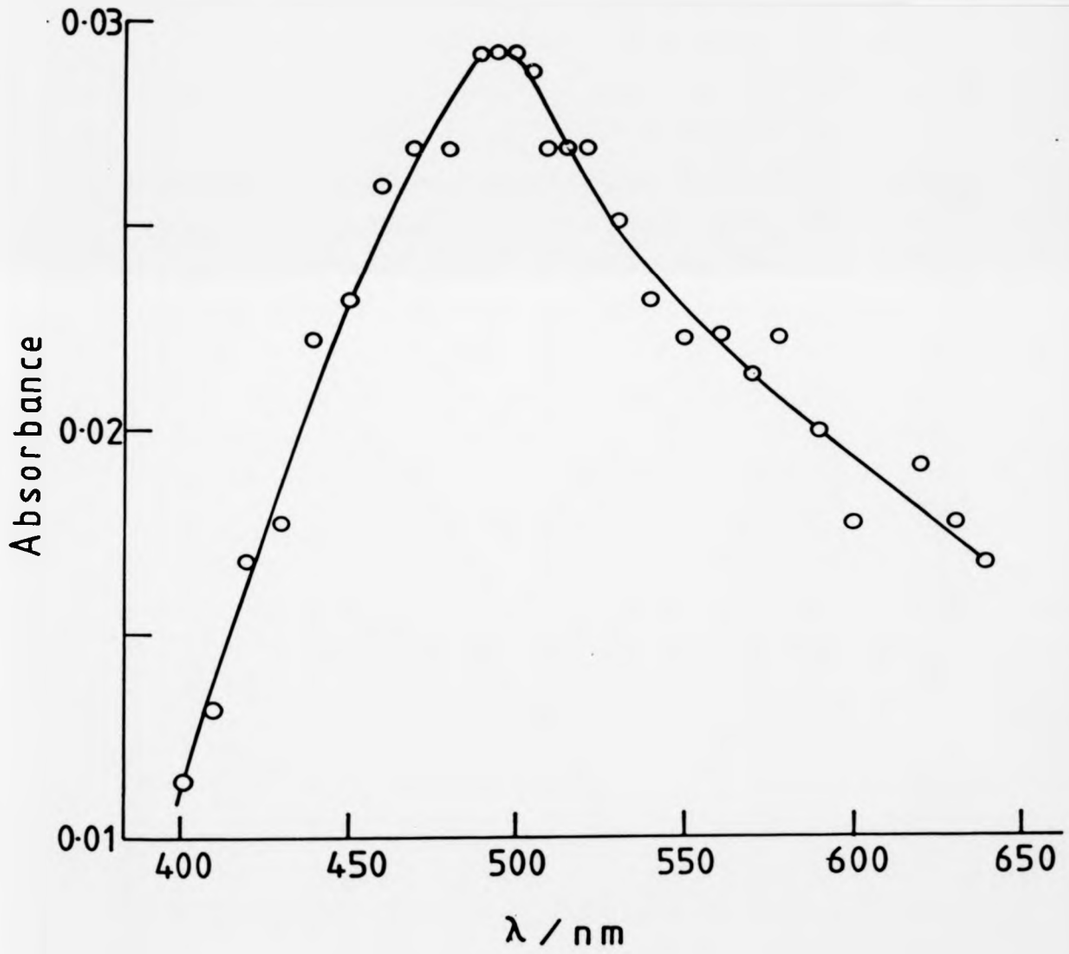

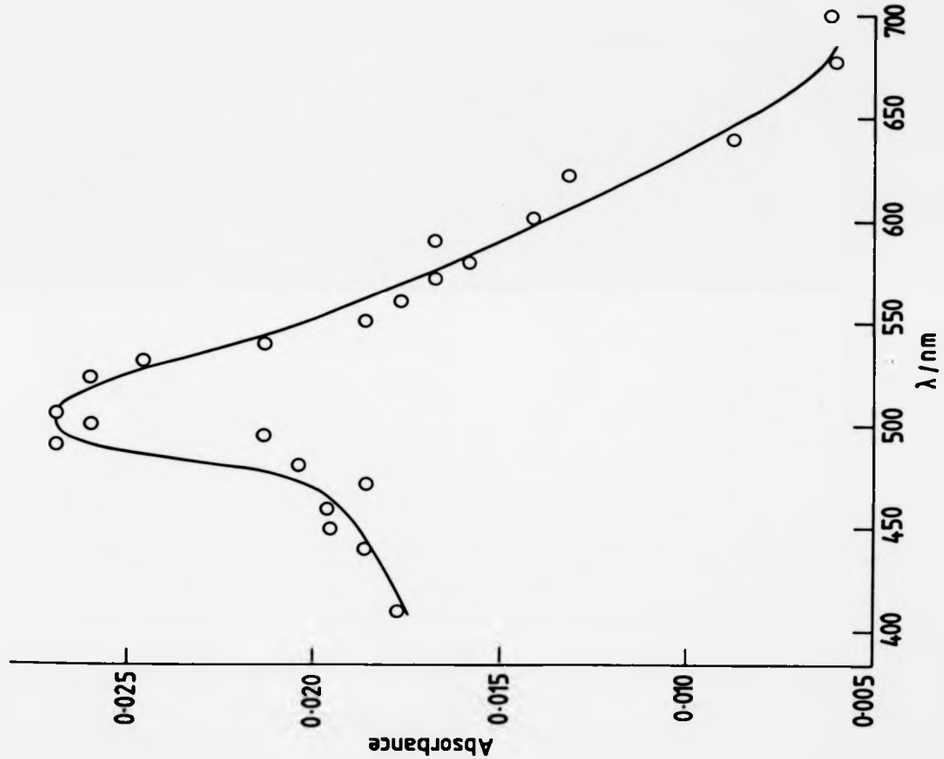

Figure (5.6) Spectrum of the transient obtained on laser flash photolysis of deaerated solution of thioxanthone (1 x 10^{-4} mol dm^{-3}) and KSCN (0.21 mol dm^{-3}) in MeCN-H_2O (3:2 v/v), as measured 2 μs after the end of the laser pulse.

The fluorescence of thioxanthone shows increases both in quantum yield and λ_F with solvent polarity.[171,172] One explanation[171] of this behaviour invokes a decrease in the rate of intersystem crossing, $S_1(\pi\pi^*) \rightarrow T_2(n\pi^*)$ with increasing solvent polarity as the energy-gap increases, but an alternative view[172] is that solvent influences the internal conversion $S_1(n\pi^*) \rightarrow S_o$ because of the proximity of the $S_1(\pi\pi^*)$ and $S_2(n\pi^*)$ levels which are subject to vibronic coupling.[172,173] Our fluorescence spectrum for thioxanthone, Figure (5.7), is in good agreement with that of Lai and Lim.[172]

Singlet state thioxanthone is quenched very effectively by anions covering a range of oxidation potentials of nearly 1.0 V, Table 5.2a. The short lifetime of 4.9 ns prevented examination by sparingly soluble materials such as $K_4[Fe(CN)_6]$ and $K_3[IrCl_6]$. With the notable exception of $S_2O_3^{2-}$ ion, quenching is near the diffusion-controlled rate throughout the exoergonic region, which suggests that heavy-atom induced spin-orbit effects in promoting intersystem crossing make an insignificant contribution to the quenching process. The deviance of $S_2O_3^{2-}$ may be associated with the problem of accuracy of associated thermodynamic data: electrochemical potentials for such inorganic radical systems are inherently more imprecise than for reversible systems. Triplet state quenching for both ketones (Table 5.2b) can be accounted for by the electron-transfer mechanism developed by Rehm and Weller[15,16] and modified by others for triplet state quenching.[53,54,79,174,175] This modified kinetic scheme also can be simplified by setting $k_{21} > k_{23}$; the additional assumption that $k_{30} > k_{32}$, leads to equation (5.1), which is similar to equation (3.3), previously derived in detail in Chapter 3.

$$^{3}k_q \simeq 1 \times 10^{10} \exp(-\Delta G^{\ddagger}_{23}/RT) \qquad (5.1)$$

Taking the Polanyi linear equation (1.61) in conjunction with equation (5.1), a plot of Log $^{3}k_q$ versus ΔG^{o}_{23} should be linear with slope α and intercept (at ΔG^{o}_{23} equal zero) of β. Figure (5.8) illustrates both the Polanyi and Rehm-Weller plots for all our data: a slightly better agreement is given by the Polanyi equation (1.61) compared with the Rehm-Weller treatment as is found to be the case with anion quenching both of triplet states of benzophenone and similar ketones[79] and of singlet excited aromatic hydrocarbons.[77,78] Our values for α and β are: $\alpha = 0.367 \pm 0.027$, and $\beta = 9.83 \pm 0.57$ kJ mol^{-1} which are compared with others obtained recently in Table (5.3); the value of β is similar to that found for other triplet ketones but that of α is much nearer the 'ideal' value of 0.5 in our case. Otherwise our Polanyi plot resembles that of Shizuka and Obuchi[79] and it includes literature data for quenching of triplet biacetyl by anions in the weakly exoergonic and endoergonic regions.[89] One explanation for adherence to the Polanyi equation outside its limits of validity ($\Delta G^{\ddagger}_{23} \geqslant \Delta G^{o}_{23}$ and $\Delta G^{\ddagger}_{23} > 0$) may be found in the participation of a weak charge-transfer state, i.e. not corresponding to complete electron-transfer in the first stage.[79]

Finally, comparison of Table 5.2a and 5.2b reveals that singlet thioxanthone is quenched at rates exceeding 2.5×10^{9} dm^{3} mol^{-1} s^{-1} in all cases, whereas triplet thioxanthone is quenched 10^{2}-fold more slowly by SCN^{-} and Br^{-} ions; this accords with the general observation of relatively higher reactivity of singlet states in electron-transfer quenching,[53,54] which may be understood both in terms of a higher value for ΔG^{o}_{23} for the same acceptor in singlet and triplet states, and also the relatively higher polarisability of singlet states.[88,89]

Table 5.3 Values of the Polanyi Coefficients α and β for Excited State Electron-Transfer Quenching

	System	α	β/kJ mol^{-1}	Reference
$[^3Ar_2CO]$	- inorganic anions	0.207	10.3	79
$[^1ArH]^*$	- inorganic anions	0.138	6.56	77
$[UO_2^{2+}]^*$	- organosulphur compounds	0.046±0.004	8.46±0.4	83
$[UO_2^{2+}]^*$	- organometallic compounds	0.120±0.003	26.01±0.4	83
$[UO_2^{2+}]^*$	- halogenoalkanes	0.110±0.004	9.69±0.2	83
$[^3ArH]$	- quinones	1.0	4.824±0.482	75
$[^1DCA]^*$	- inorganic anions[a]	0.487±0.068	5.805±0.483	b
$[2\text{-}^1AA]^*$	-organic electron acceptors[a]	0.24 ±0.07	20.0 ±4.0	c

a DCA = 9,10-dicyanoanthracene; 2-AA = 2-aminoanthracene.

b See chapter 3.

c See chapter 4.

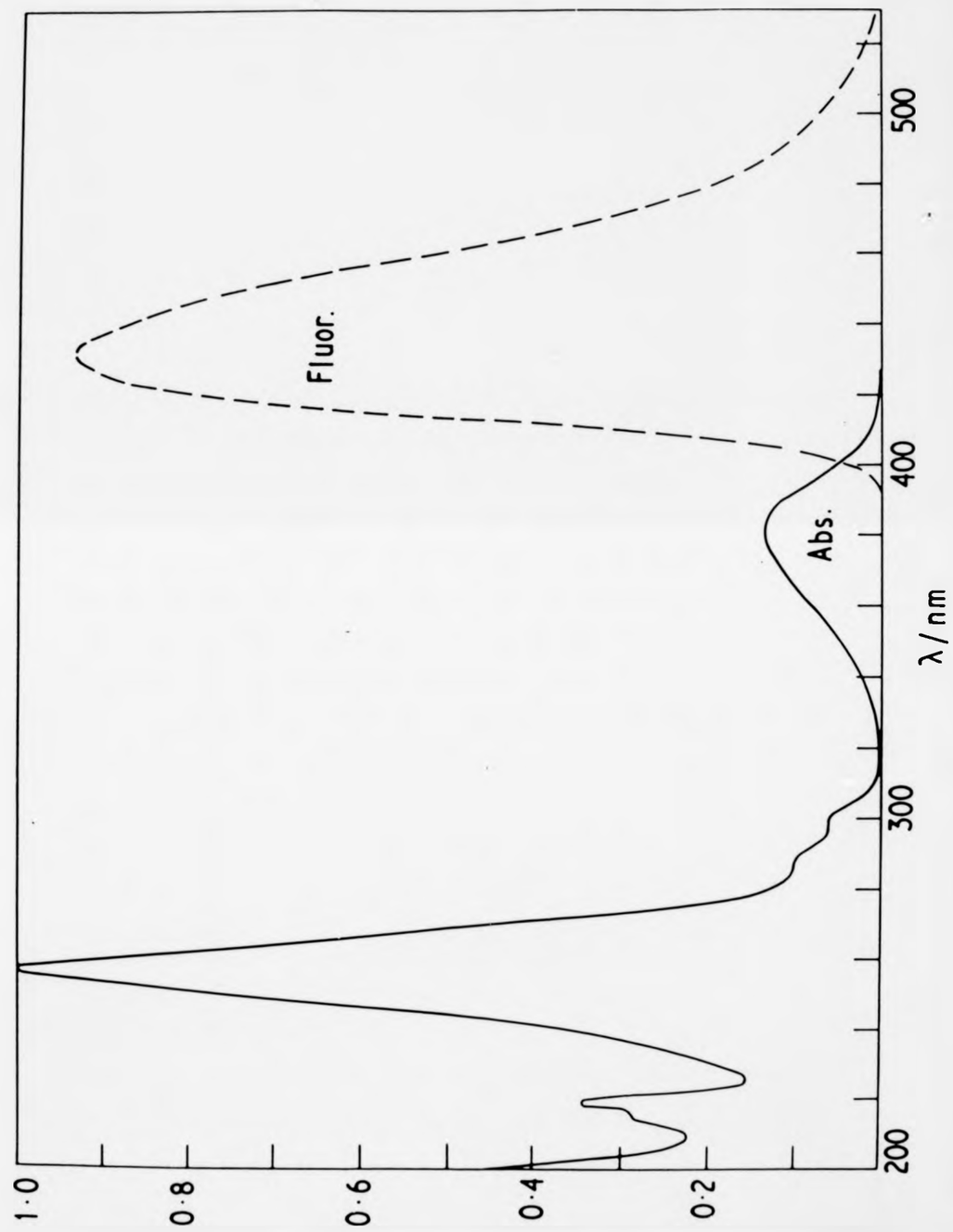

Figure (5.7) Absorption and fluorescence spectra of thioxanthone (2 x 10^{-5} mol dm^{-3}) in MeCN-H_2O (3:2 v/v) mixture; $\lambda_{exc.}$ = 380 nm, λ_F = 432 nm.

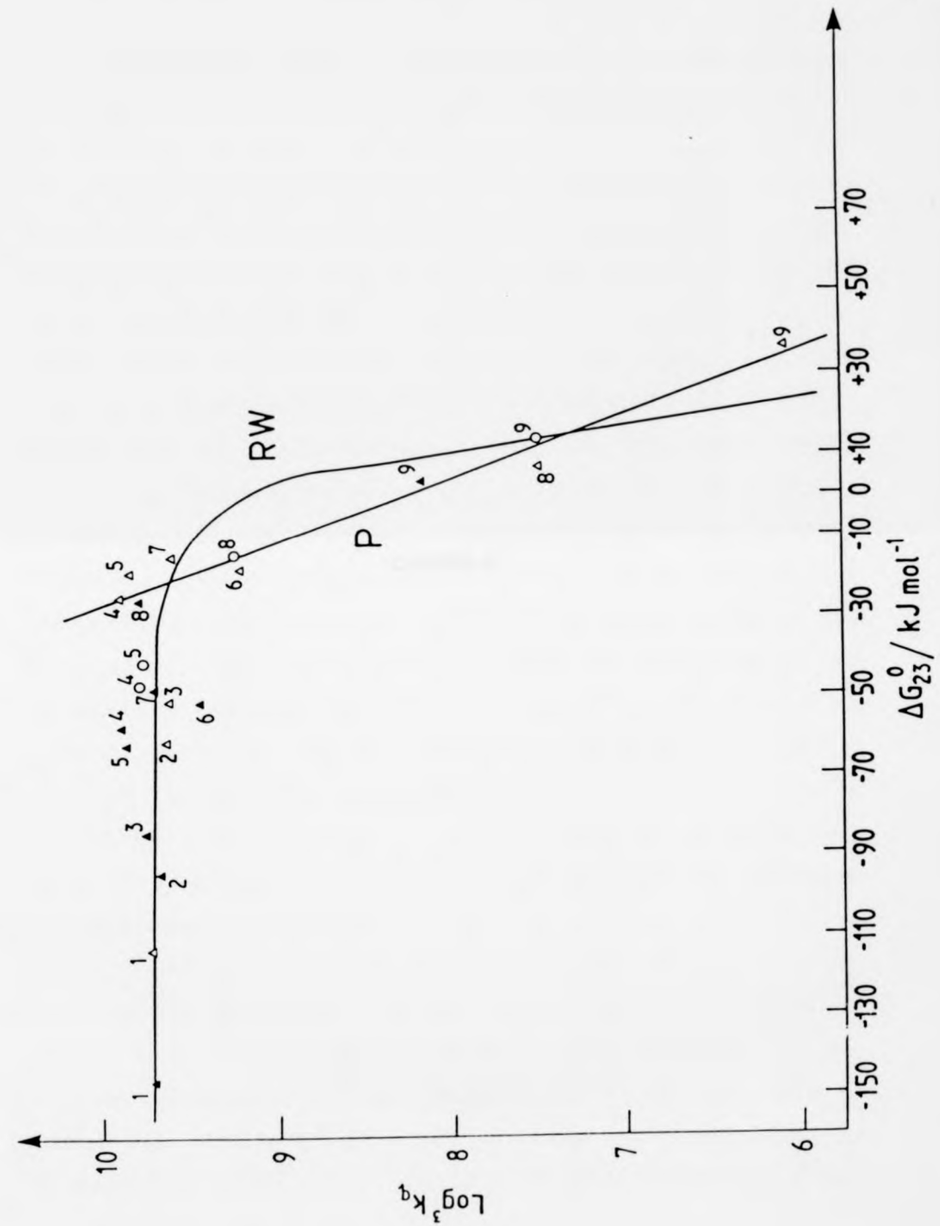

Figure (5.8) Plots of log ^3k_q versus ΔG°_{23} for the quenching by anions of triplet thioxanthone (Δ), triplet xanthone (▲) and triplet biacetyl (O). Lines drawn corresponding to theoretical treatments based on Polanyi equation (P) and Rehm-Weller treatment (RW). For key to numbering of quenching ions see Table (5.2a). Best-fit parameters for the Rehm-Weller plot: $k_{12} = 6.5 \times 10^9$ dm^3 mol^{-1} s^{-1}, $\Delta G^\ddagger_{23}(O) = 6.7$ kJ mol^{-1}. For values of (α) and (β) parameters see text.

CHAPTER 6

6.1 Solvatochromic Effects in the Fluorescence of 2-Aminoanthracene and N,N-Dimethyl-2-aminoanthracene: Results and Discussion

Absorption and fluorescence data for 2-aminoanthracence (2-AA) and N,N-dimethyl-2-aminoanthracene (2-DMA) in nineteen solvents are presented in Table 6.1 There is no discernible effect (more than few nm) of solvent polarity upon the absorption of maxima $\bar{\nu}_A$, whereas the emission maxima $\bar{\nu}_F$, and hence the Stokes' shift $\Delta\bar{\nu}_{SS}$ (i.e. $\bar{\nu}_A - \bar{\nu}_F$) are strongly solvent dependent, being positively correlated with solvent polarity in a general sense. The Bilot and Kawski[94] equation (1.68) which correlates $\Delta\bar{\nu}_{SS}$ with polarisability function through $(\mu_e-\mu_g)$, i.e. the difference between the dipole moments of the excited and ground states, is often employed to analyse the solvatochromic effects of 2-AA and 2-DMA. The solute cavity radius, taken as 5.5Å for both 2-AA[184] and 2-DMA, and the values of the polarisability function, designated B-K in equation (1.68), are listed in Table 6.1, while $\Delta\bar{\nu}_{SS}$ is plottedagainst B-K in Figures (6.1) and (6.2) for 2-AA and 2-DMA, respectively.

From Figure (6.1) it is clear that solvents 1 - 11 and 13 give an excellent correlation according to equation (1.68), the regression line being given by equation (6.1).

$$\Delta\bar{\nu}_{SS}/cm^{-1} = (2898 \pm 148) + (1126 \pm 304)\ B\text{-}K \qquad (6.1)$$

From equation (6.1), $(\mu_e - \mu_g)$ can be estimated as 6.1 D, which is similar to values given previously of 6.1 D[184] and 5.4 D.[155] The solvents deviating strongly and positively from the regression line in Figure (6.1) are all hydroxylic solvents, while all those adhering to it are non-hydroxylic. If the deviation is due to the specific effect

of hydrogen-bonding in the ground state between proton-accepting 2-AA and proton-donor solvents,[184] which is completely lost on excitation to highly acidic $^1(2\text{-AA})^*$ then much reduced deviation should be present for 2-DMA by virtue of steric inhibition of its acceptor function. Figure (6.2) indicates that an excellent correlation is achieved for the non-hydroxylic solvents for 2-DMA, according to equation (6.2),

$$\bar{\nu}_{SS}/cm^{-1} = (2786 \pm 132) + (1330 \pm 271)\ B\text{-}K \qquad (6.2)$$

while the hydroxylic solvents show a consistent, small negative deviation from this equation. From equation (6.2), a value for $(\mu_e - \mu_g)$ of 6.63 D is obtained for 2-DMA, consonant with the expected development of additional positive charge at the N-atom on excitation relative to 2-AA. A very recent study reports strong positive deviation for butan-1-ol and water from plots of the related Bakhshiev[95] equation (1.69) for both 1-aminonapthalene and N,N-dimethyl-1-aminonapthalene for values of the polarisibility function exceeding 1.0.[111]

The second comparative analysis correlates $\Delta\bar{\nu}_{SS}$ with the Dimroth parameter $E_T(30)$, as given in Figures (6.3) and (6.4) for 2-AA and 2-DMA, respectively. Since $E_T(30)$ includes a contribution from hydrogen-bonding, the good correlation found for 2-AA is not unexpected, while the absence of these contributions in the case of 2-DMA results in the separate correlations found for hydroxylic and non-hydroxylic solvents in Figure (6.4). (All the data for 2-AA, and those for 2-DMA in non-hydroxylic solvents, lie on a single line). Such separate correlations with $E_T(30)$ are a feature of a recent study[113] and have been observed before.[122]

Dioxan–water mixture afford a wide range of values of $E_T(30)$ while restricting other solvent-variable parameters to just two solvents, and have attracted interest as a probe for specific effects on fluorescence.[108,109,123] A short investigation of the dependence of the fluorescence maximum $\Delta\bar{\nu}_F$ upon solvent composition was carried out for 2-AA and 2-DMA and the results are presented in Table 6.2 and Figures 6.5 and 6.6. In this case, remarkably parallel behaviour is shown by both molecules in that $\Delta\bar{\nu}_F$ decreases linearly with increase in $E_T(30)$ until an inflection is reached at 40% H_2O (2-AA) or 50% H_2O (2-DMA) after which the further red-shift with increase of $E_T(30)$ is halved in effect. This type of effect has been reported[108,111,123] before and is attributable to increasing solvation of the S_1 state by water molecules, which impart an enhanced solvent-structuring effect,[122] although in one case a change in geometry of the emitting species is proposed.[108,109] This effect would be expected to be rather small for aminoanthracenes, although a recent study on aminonapthalenes would take an opposite view.[111]

Table 6.1 Solvent Effects on Stokes' Shift of 2-AA and 2-DMA

				2-AA			2-DMA		
Solvent	No.	$E_T(30)$[a] /kJ mol^{-1}	B-K[b]	λA /nm	λF /nm	$\Delta\bar{\nu}_{SS}$ /cm^{-1}	λA /nm	λF /nm	$\Delta\bar{\nu}_{SS}$ /cm^{-1}
Cyclohexane	(1)	130.540	-0.001	396	437	2369	414	458	2320
Toluene	(2)	138.908	0.031	401	447	3056	420	478	2889
Benzene	(3)	144.150	0.008	402	457	2994	421	481	2962
Dioxan	(4)	150.624	0.043	406	471	3399	419	485	3248
Tetrahydrofuran	(5)	156.481	0.550	401	476	3929	419	493	3583
Chlorobenzene	(6)	156.900	0.399	402	458	3041	423	483	2937
Bromobenzene	(7)	156.900	0.361	403	459	3027	424	487	3051
Chloroform	(8)	163.594	0.372	398	461	3424	420	496	3648
Pyridine	(9)	168.196	0.639	416	496	3877	425	502	3609
Dichloromethane	(10)	171.962	0.586	400	462	3355	421	492	3427
Acetone	(11)	176.564	0.793	409	483	3746	419	500	3866
2-Methyl-2-propanol	(12)	183.677	0.673	403	496	4652	412	485	3653
Acetonitrile	(13)	192.464	0.864	410	485	3772	419	505	4065
2-Butanol	(14)	197.066	0.734	404	495	4550	414	487	3621
2-Propanol	(15)	203.342	0.766	403	493	4530	414	489	3705
1-Butanol	(16)	210.036	0.754	404	492	4427	416	488	3547
Ethanol	(17)	217.150	0.812	403	490	4405	415	490	3688
Methanol	(18)	232.212	0.858	401	493	4654	415	494	3854
Ethanediol	(19)	236.814	—	403	496	4652	420	506	4047

a From ref.(115).

b Calculated from data in ref.(132) according to the Bilot-Kawski equation (see text); values of ε and n refer to 293 K.

Table 6.2 Effect of Solvent Polarity (dioxan : water mixture) on $\bar{\nu}_F$ of 2-AA and 2-DMA

	Dioxan:Water mixture	Solvent polarity parameter	2-AA	2-DMA
No.	Volume Percentage	$E_T(30)$[a] $/10^3 cm^{-1}$	$\bar{\nu}_F/10^2 cm^{-1}$ (nm)	$\bar{\nu}_F /10^2 cm^{-1}$ (nm)
1	100 : 0	12.589	212.31 (471)	206.18 (485)
2	98 : 2	14.477	210.08 (476)	204.91 (488)
3	96 : 4	15.002	209.20 (478)	203.25 (492)
4	94 : 6	15.561	207.46 (482)	202.83 (493)
5	90 : 10	16.331	206.61 (484)	202.42 (494)
6	85 : 15	16.785	205.76 (486)	201.20 (497)
7	80 : 20	17.135	204.91 (488)	200.40 (499)
8	70 : 30	17.800	204.29 (489)	199.60 (501)
9	60 : 40	18.290	203.66 (491)	198.41 (504)
10	50 : 50	18.744	203.25 (492)	197.62 (506)
11	40 : 60	19.443	202.83 (493)	197.23 (507)
12	30 : 70	20.002	202.42 (494)	196.85 (508)
13	20 : 80	20.492	202.02 (495)	196.85 (508)

a From ref.(114).

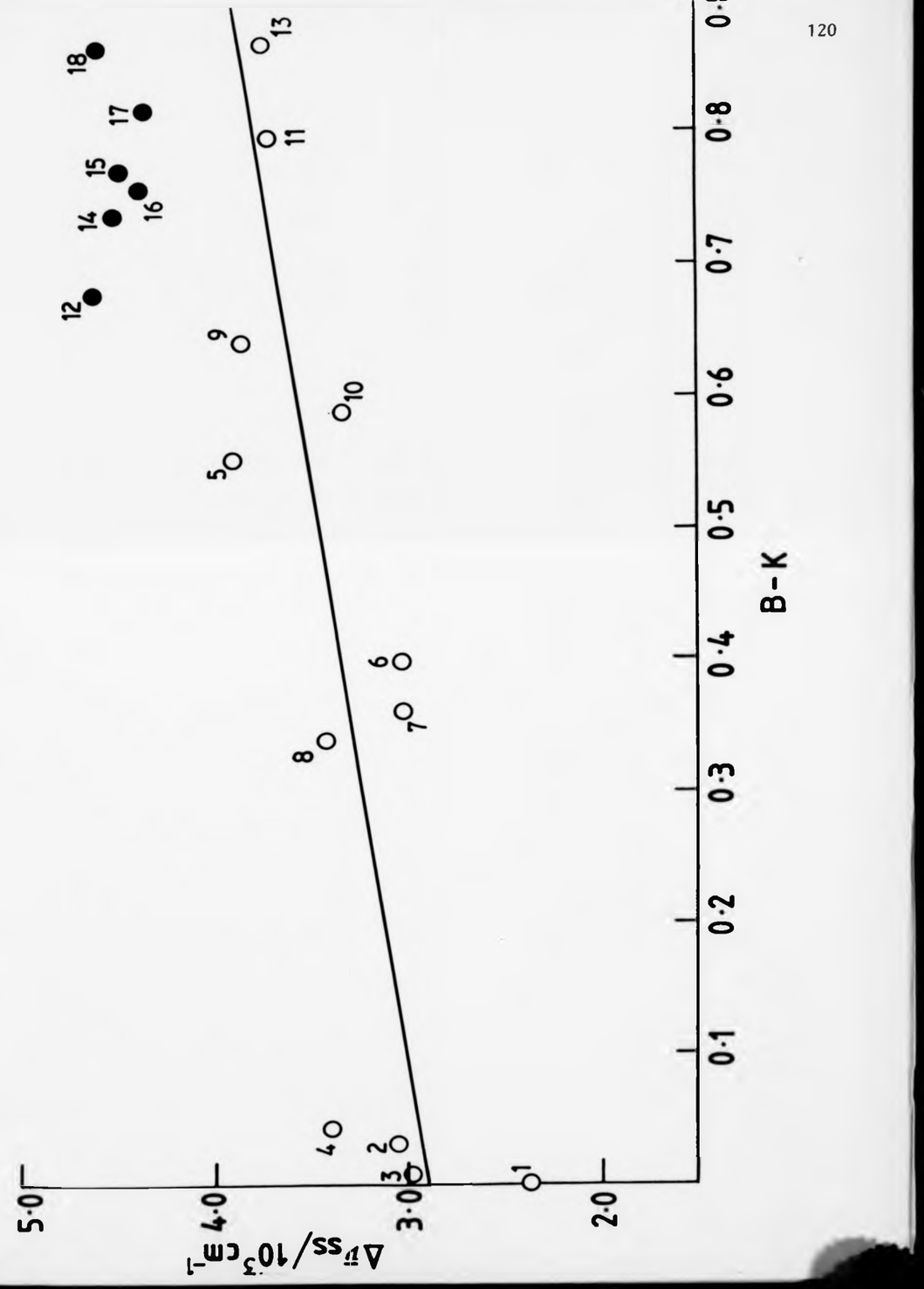

Figure (6.1) Correlation of the Stokes' shift $\Delta\bar{\nu}_{SS}$ of 2-AA with the value of B-K (see equation (6.1)). Filled circles refer to alcoholic solvents (which are excluded from the regression analysis). Numbering of solvents as in Table (6.1).

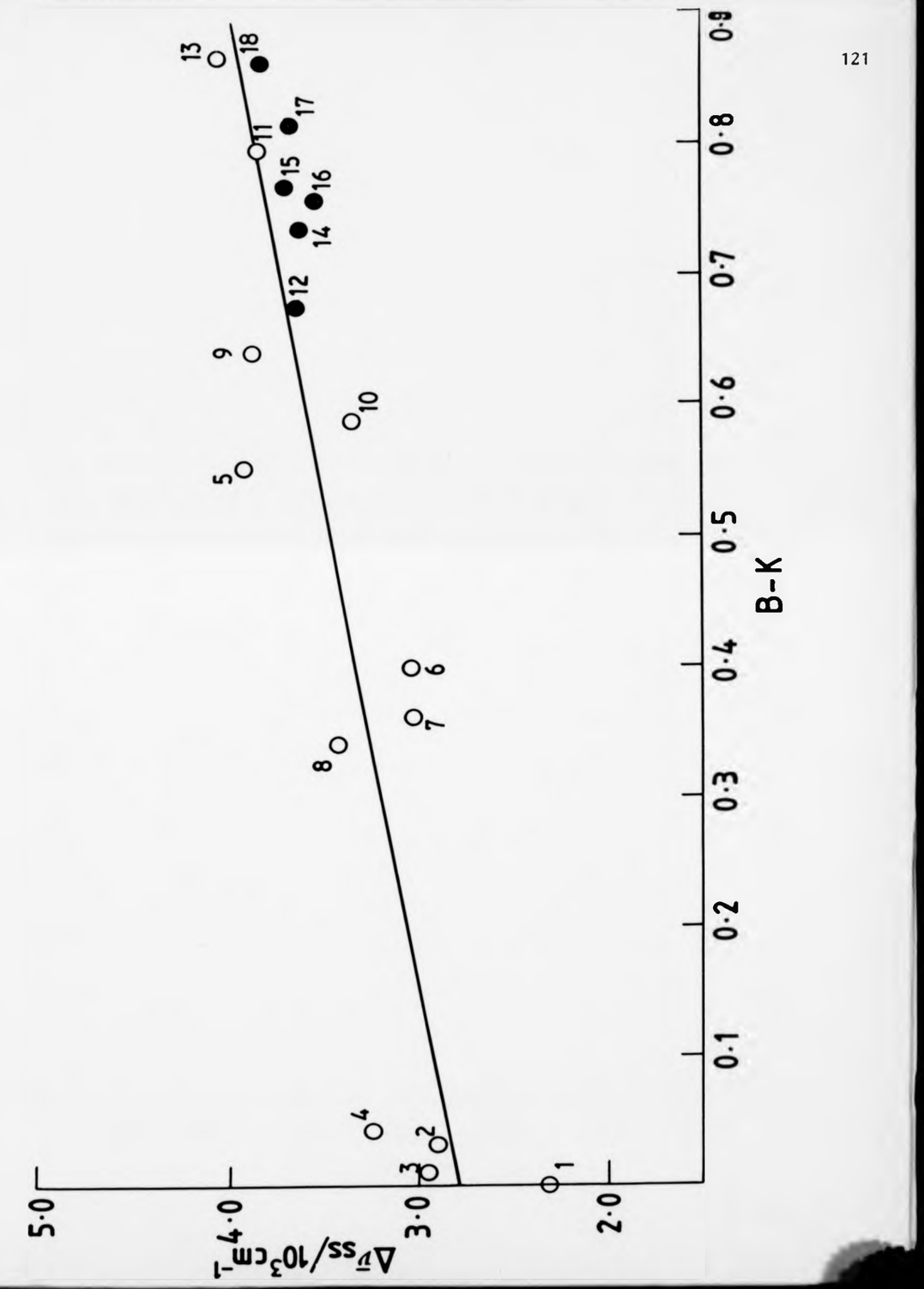

Figure (6.2) Correlation of the Stokes' shift $\Delta\bar{\nu}_{SS}$ of 2-DMA with the value of B-K (see equation (6.2)). Filled circles refer to alcoholic solvents (which are excluded from the regression analysis). Numbering of solvents as in Table (6.1).

Figure (6.3) Correlation of the Stokes' shift $\Delta\bar{\nu}_{SS}$ of 2-AA with the Dimroth solvent polarity parameter , $E_T(30)$. Numbering of solvents as in Table (6.1).

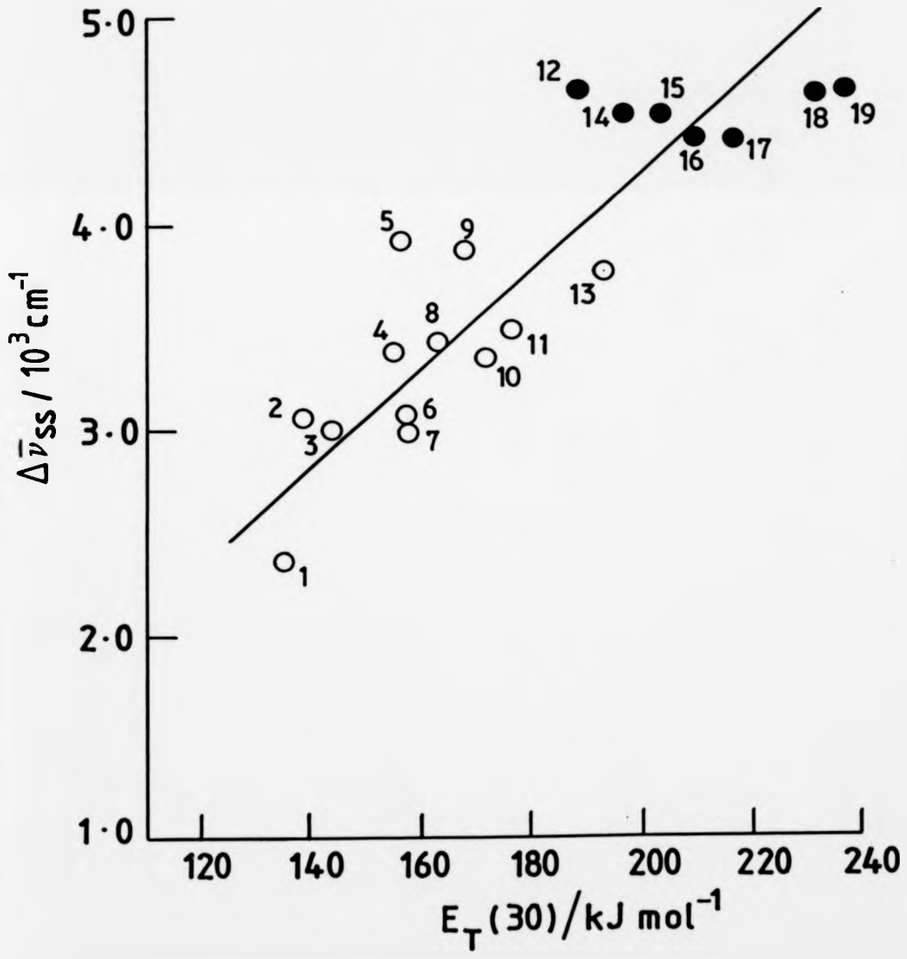

Figure (6.4) Correlation of the Stokes' shift $\Delta\bar{\nu}_{SS}$ of 2-DMA with the Dimroth solvent polarity parameter, $E_T(30)$. Numbering of solvents as in Table (6.1).

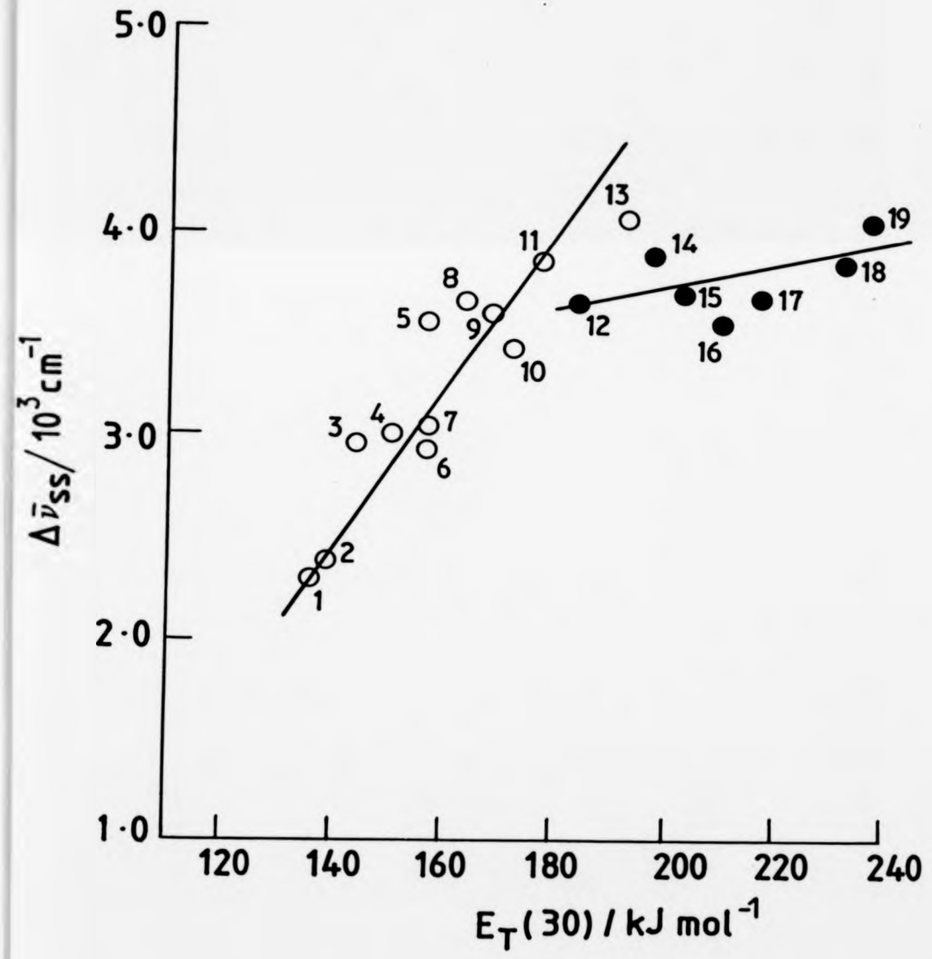

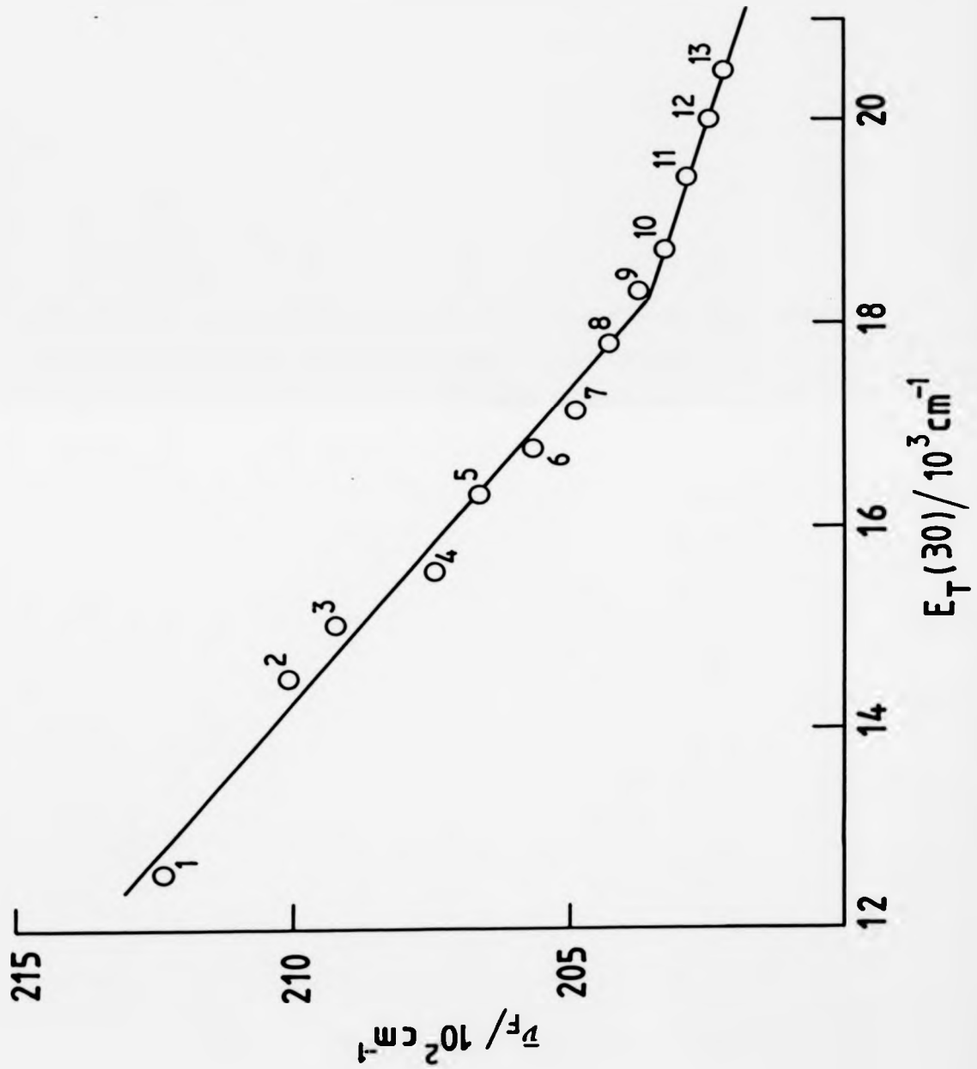

Figure (6.5) Correlation of the fluorescence energy $\bar{\nu}_F$ of 2-AA with $E_T(30)$ for dioxan/water mixtures. Numbering of mixtures as in Table (6.2).

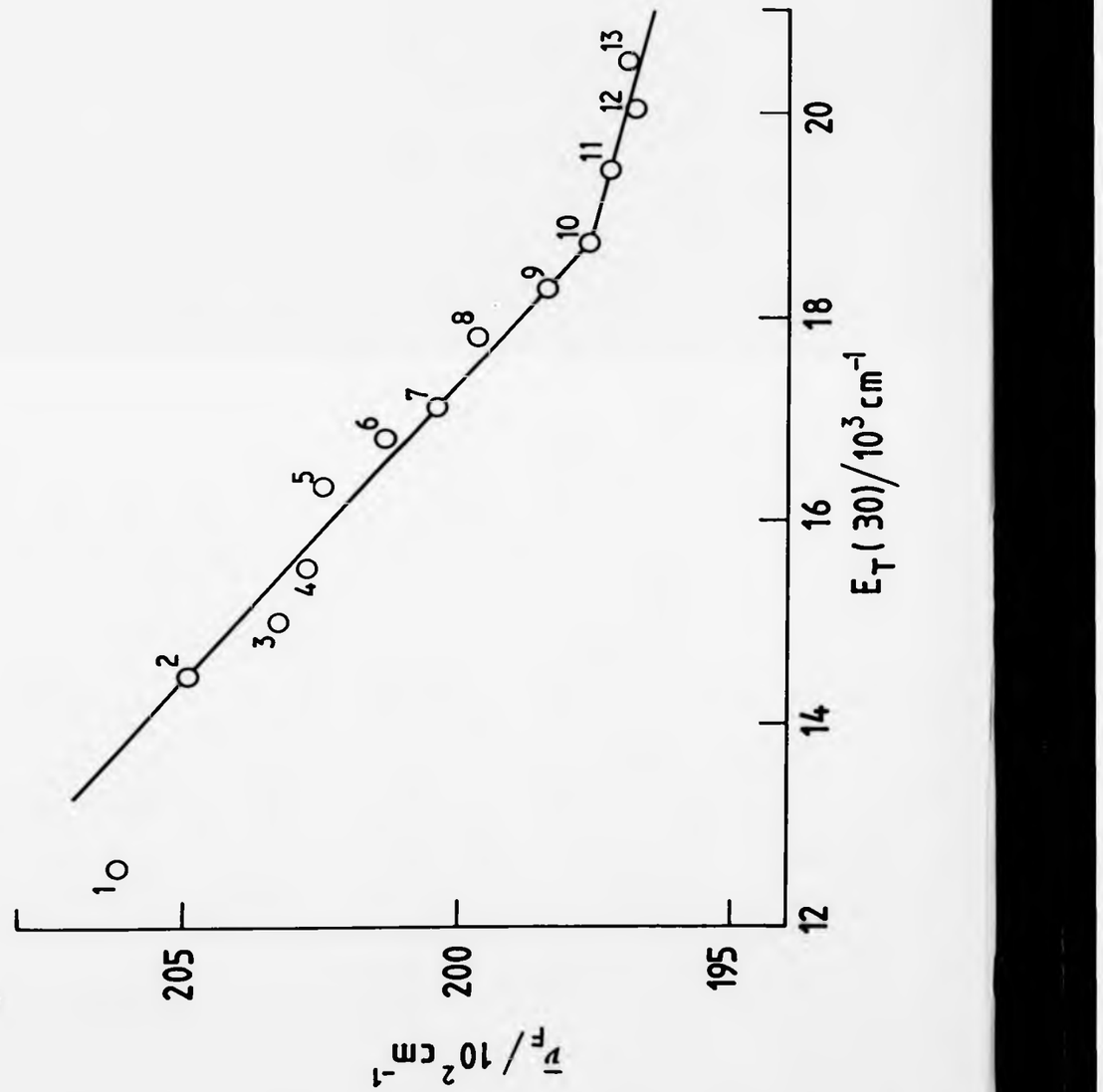

Figure (6.6) Correlation of the fluorescence energy $\bar{\nu}_F$ of 2-DMA with $E_T(30)$ for dioxan/water mixtures. Numbering of mixtures as in Table (6.2).

6.2 Solvatochromic Effects in the Fluorescence and Triplet-Triplet Absorption spectra of Xanthone, Thioxanthone and N-methylacridone: Results and Discussion

Absorption and fluorescence data for xanthone and thioxanthone in different solvents are given in Tables 6.3 and 6.4, respectively. It is evident from Tables 6.3 and 6.4 that the fluorescence maximum wavelength λ_F, and more particularly the Stokes' shift, $\Delta\bar{\nu}_{SS}$, are positively correlated with the polarisability function of Bilot and Kawski equation (1.68) through $(\mu_{S_1} - \mu_{S_o})$; i.e. the difference between the dipole moments of the first singlet excited and ground states. Equation (1.68) is utilised in graphical form to estimate the values of μ_{S_1} of xanthone and thioxanthone as shown in Figures (6.7) and (6.8), respectively. The solute cavity radius was taken as 3.6 Å for both xanthone and thioxanthone, (the figure originally reported[102] for the N-methylacridone molecule). The regression lines of xanthone (Figure 6.7) and thioxanthone (Figure 6.8) are given respectively by equations (6.3) and (6.4).

$$\Delta\bar{\nu}_{SS}/cm^{-1} = (3011 \pm 262) + (435 \pm 512)\ B\text{-}K \qquad (6.3)$$

$$\Delta\bar{\nu}_{SS}/cm^{-1} = (1313 \pm 137) + (543 \pm 267)\ B\text{-}K \qquad (6.4)$$

From the coefficients of equations (6.3) and (6.4), the values of $\mu_{S_1} - \mu_{S_o}$ for the transition $S_1 \rightarrow S_o$ can be derived; using the literature values for the dipole moments of the S_o states, S_1 can be estimated as 5.1 D for xanthone and 7.64 D for thioxanthone, i.e. the red-shifts in the fluorescence maxima are explained on the

basis of increases of the dipole moment of the S_1 state over that of S_0. The red-shift in the absorption spectrum of N-methylacridone as the polarity of the solvent is increased has been analysed recently[102] by several different types of solvatochromic equation and is attributed to the increase of the dipole moment of the first excited state (see Table 6.6).

The marked solvatochromic effects upon the $T_1 \rightarrow T_n$ absorption spectra of xanthone, thioxanthone and N-methylacridone are collected in Table 6.5, from which we can see the unusual feature of a strong blue-shift on increasing solvent polarity (clearly demonstrated in Figures 6.9, 6.10 and 6.11). From this observed shift in the absorption maxima, the change of dipole moment $\Delta\mu\,(T_1 \rightarrow T_n)$ accompanying the transition T_1–T_n can be calculated according to the Suppan[98,99] equation (6.5), making the simplification that the dipole moment

$$\bar{\nu}_S = \bar{\nu}_V + \frac{\mu_{T_1}\,(\mu_{T_1} - \mu_{T_n})}{hca^3}\,\Delta f(\varepsilon) \qquad (6.5)$$

of the S_1 state approximates to that of the state T_1 (following Capellos and Porter[124]). Here $\bar{\nu}_S$ represents the absorption band, expressed in energy units (cm^{-1}) in a solvent of dielectric constant (ε), while $\bar{\nu}_V$ represents the absorption band in vacuo. The cavity radius (a) has been taken as 3.6 Å for the three molecules and μ_{T_1} is the dipole moment of the T_1 state. $\Delta f(\varepsilon)$ is equal to $2(\varepsilon-1)/(2\varepsilon+1)$ while other symbols have their usual meaning. The plots of $\bar{\nu}_S$ versus $\Delta f(\varepsilon)$ show good correlations for these heterocyclic ketone molecules, see Figures (6.12) and (6.13), and the corresponding regression lines are given by equations (6.6), (6.7) and (6.8) for xanthone, thioxanthone and N-methylacridone, respectively.

$$\bar{\nu}_S = (14888.6 \pm 288) + (880.4 \pm 370.2)\ f(\varepsilon) \qquad (6.6)$$

$$\bar{\nu}_S = (14898.4 \pm 178) + (826.2 \pm 256.8)\ f(\varepsilon) \qquad (6.7)$$

$$\bar{\nu}_S = (15249.6 \pm 191.2) + (1125.4 \pm 273.3)\ f(\varepsilon) \qquad (6.8)$$

The deviation of the hydroxylic solvents from the regression line may be attributed to specific donor and acceptor-hydrogen bonding and hence they are excluded from the regression analysis. The estimated changes in dipole moment for the $T_1 \rightarrow T_n$ and $S_1 \rightarrow S_0$ transitions for the three molecules are summarised in Table 6.6, i.e. the observed blue-shift in the $T_1 \rightarrow T_n$ transition maxima is explained by a decrease of the dipole moment of T_n over that of T_1 for all three molecules. While blue shifts in absorption spectra are well-known, e.g. for the $n \rightarrow \pi^*$ transition in simple carbonyl compounds, the shifts obtained in our T-T spectra are much larger than the ca. 10 nm found for $S_0 \rightarrow S_1$ transitions of carbonyl compounds. Interestingly, the (0,0) band of the transition $T_1 \rightarrow S_0$ (phosphorescence) of xanthone[186] experiences a red-shift of ca. 1100 cm^{-1} on going from non-polar solvent (3-methylpentane) to polar solvent EPA (ethanol-isopentane-ether, 5:2:2) at 77 K implying a larger dipole moment for the T_1 than for the S_0 state, although an alternative explanation[187] favours solvent effects on the relative positions of proximate $n \rightarrow \pi^*$ and $\pi \rightarrow \pi^*$ states.

Table 6.3 Solvent Effects on the Stokes' Shift in the Fluorescence of Xanthone

Solvent	No.	B-K[a]	$^{\lambda}A$/nm	$^{\lambda}F$/nm	$\Delta\bar{\nu}SS$/cm^{-1}
n-Hexane	(1)	0.002	337	375	3007
Benzene	(2)	0.008	339	380	3183
Carbon tetrachloride	(3)	0.023	337	389	3967
Dioxan	(4)	0.043	333	367	2782
Bromobenzene	(5)	0.361	336	366	2439
Diethyl ether	(6)	0.365	336	375	3095
Chlorobenzene	(7)	0.399	334	366	2618
Tetrahydrofuran	(8)	0.55	333	371	3076
Dichloromethane	(9)	0.586	340	380	3096
2-Methyl-2-propanol	(10)	0.673	335	376	2603
2-Propanol	(11)	0.766	335	373	3041
Acetone	(12)	0.793	337	391	4098
Ethanol	(13)	0.812	336	373	2952
Dimethylformamide	(14)	0.836	334	369	2840
Methanol	(15)	0.858	335	382	3673
Acetonitrile	(16)	0.864	337	390	4033

a Calculated from data in ref.(132) according to the Bilot-Kawski equation (see section 1.6); values of ε and n refer to 293 K.

Table 6.4 Solvent Effects on the Stokes' Shift in the Fluorescence of Thioxanthone[a]

Solvent	No.	B-K[b]	λ_A/nm[a]	λ_F/nm	$\Delta\bar{\nu}_{SS}$[d]/cm^{-1}
n-Hexane	(1)	0.002	378	395	1139
Benzene	(2)	0.008	380	405	1624
Carbon tetrachoride	(3)	0.023	—	400	1316
Diethyl ether	(4)	0.365	--	398	1190
Dichloromethane	(5)	0.586	—	409	1866
Acetone	(6)	0.793	--	405	1624
Acetonitrile	(7)	0.864	380[c]	409	1866
2-Methyl-2-propanol	(8)	0.673	--	418	2392
2-Propanol	(9)	0.766	—	423	2675
Ethanol	(10)	0.812	380[c]	428	2951
Methanol	(11)	0.858	--	431	3114

a Data source for λ_A and λ_F are from ref.(171).

b Calculated from data in ref.(132) according to the Bilot-Kawski equation (see section 1.6); values of ϵ and n refer to 293 K.

c From ref.(172).

d λ_A is taken to equal 380 nm.

Table 6.5 Solvent Dependence of the Triplet-Triplet Absorption Spectral Maxima of Xanthone and Related Molecules at Room Temperature

			Thioxanthone		Xanthone		N-methylacridone	
Solvent	No.	f(ε)[a]	λ/nm	$\bar{\nu}_S$(cm^{-1})	λ/nm	$\bar{\nu}_S$(cm^{-1})	λ/nm	$\bar{\nu}_S$(cm^{-1})
Cyclohexane	(1)	0.405	650	(15385)	---	---	640	(15625)
Carbon tetrachloride[b]	(2)	0.452	662±5	(15105)	---	---	---	---
Benzene[b]	(3)	0.461	660±5[c]	(15159)	655±5[d]	(15270)	640	(15625)
Dioxan	(4)	0.446	650	(15385)	---	---	625	(16000)
Chloroform[b]	(5)	0.758	640±5	(15625)	637±3	(15700)	623±2	(16050)
Dichloromethane	(6)	0.843	645±5	(15505)	645±5	(15505)	---	---
Acetone[b]	(7)	0.929	645±5	(15505)	---	---	615±5	(16260)
Acetonitrile	(8)	0.961	630±10[c]	(15875)	635±5[e]	(15750)	610±5	(16390)
2-Propanol	(9)	0.931	620±20	(16130)	---	---	---	---
Ethanol	(10)	0.940	610±5	(16390)	610±5	(16390)	---	---
Methanol	(11)	0.956	608±8	(16450)	610±5	(16390)	582±3	(17182)
2,2,2-Trifluoroethanol	(12)	-	580±5	(17240)	---	---	---	---

a $\Delta f(\varepsilon) = 2(\varepsilon-1)/(2\varepsilon+1)$ where ε is the dielectric constant of the solvent at 239 K taken from ref.(132).

b Results using a ruby laser because the transmittances of the indicated solvents are higher at 347 nm (an excimer laser [249 nm] was used for other solvents).

c Ref.(170) gives 650 nm in benzene and 620 nm in MeCN.

d Ref.(125) gives 610 nm in benzene.

e Ref.(168) gives 620 nm in MeCN.

Table 6.6 Dipole Moments of Heterocyclic Ketones in Different Electronic States

Molecule	μ_{S_0}/D	μ_{S_1}/D	μ_{T_n}/D
Xanthone	3.1[a]	5.10	3.51
Thioxanthone	5.4[a]	7.64	6.64
N-methylacridone	5.39[b,c]	7.287[b]	5.85

a From ref.(185).

b From ref.(102); 1 D = 3.336 x 10^{-30} C m.

c Ref.(185) gives μ_{S_0} = 3.5 D.

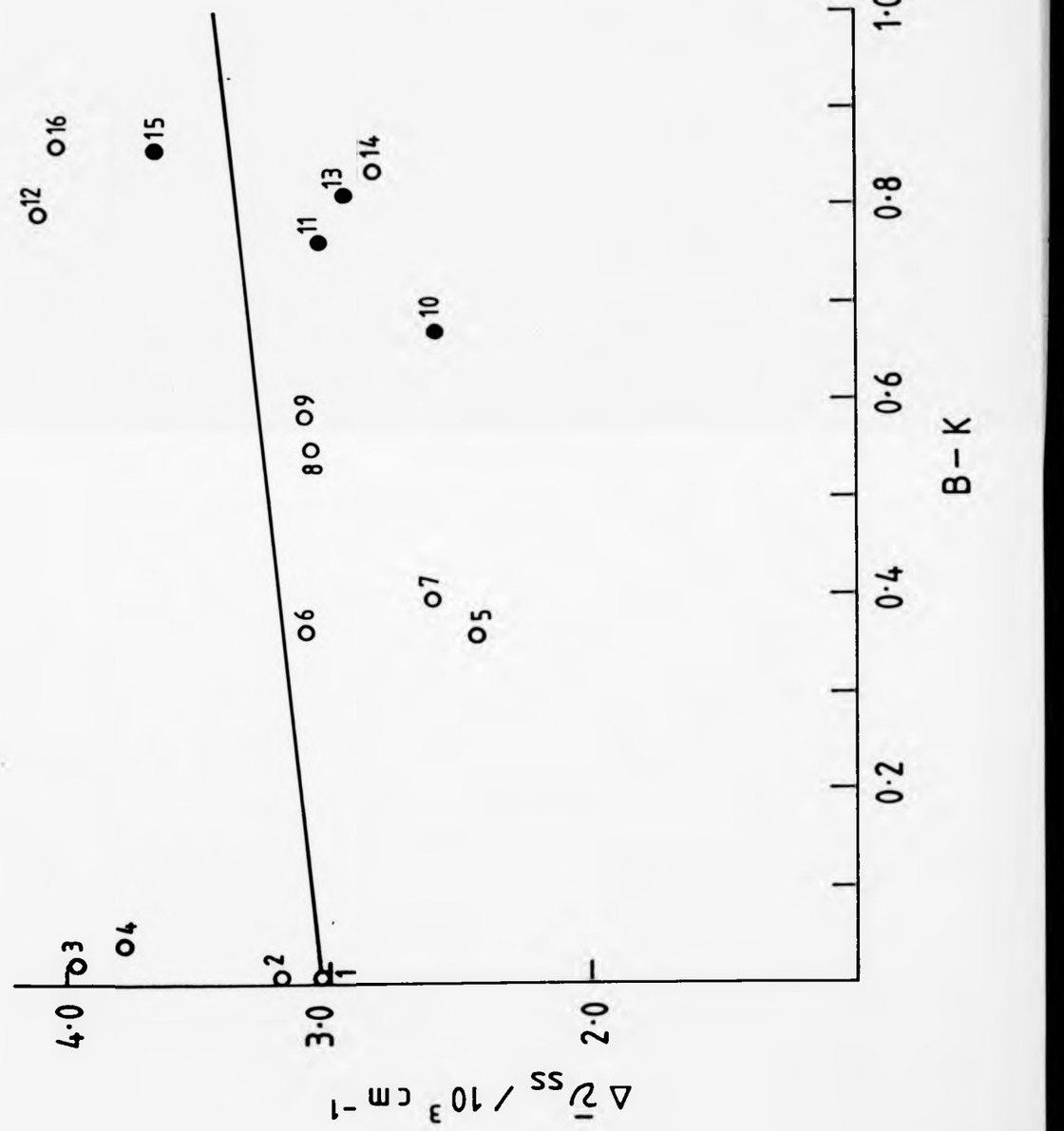

Figure (6.7) Correlation of the Stokes' shift $\Delta\bar{\nu}_{SS}$ of xanthone with value of B-K (see equation (6.3)). Filled circles refer to alcoholic solvents (which are excluded from the regression analysis). Numbering of solvents as in Table (6.3).

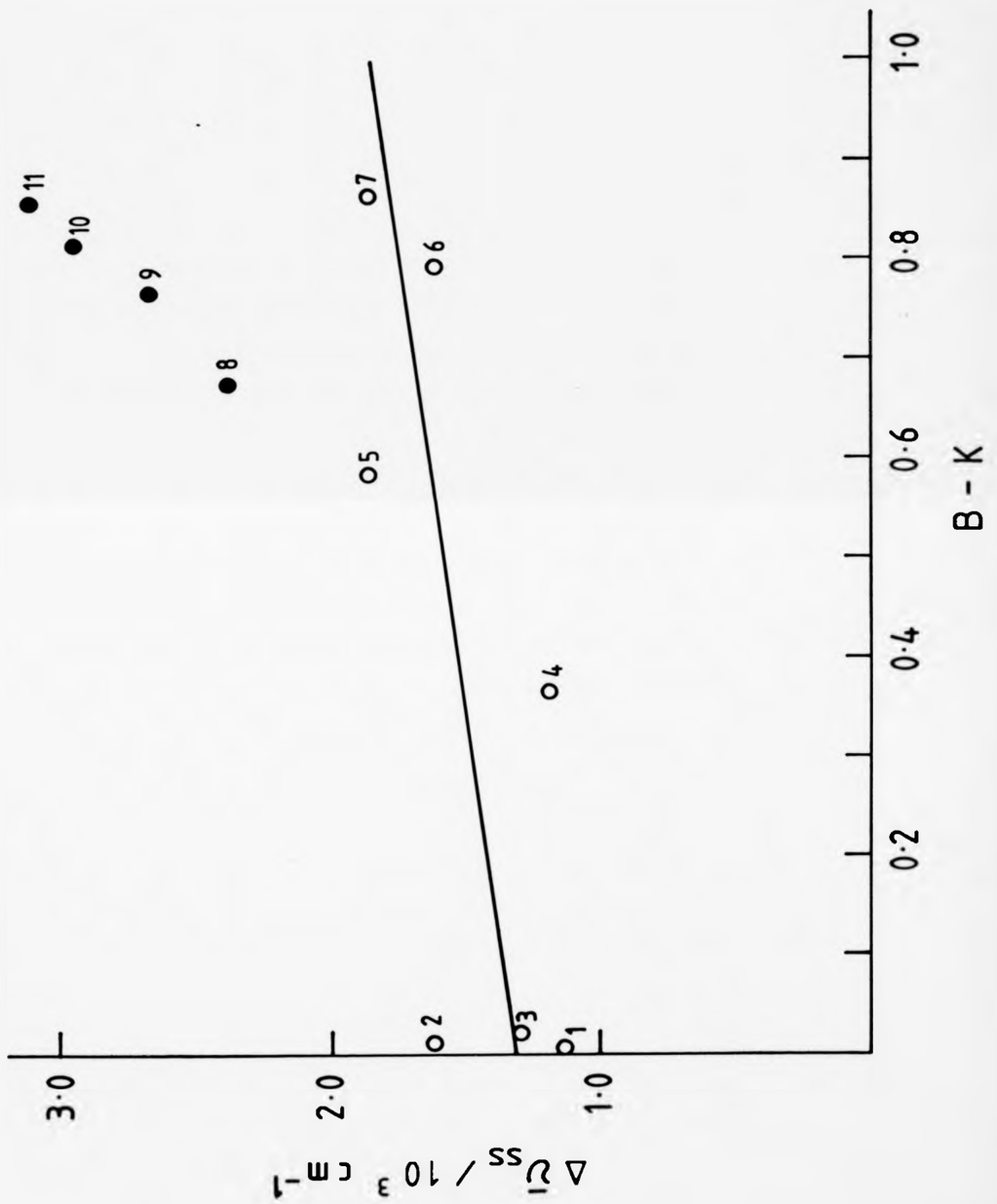

Figure (6.8) Correlation of the Stokes' shift $\Delta\bar{\nu}_{SS}$ of thioxanthone with the value of B-K (see equation (6.4)). Filled circles refer to alcoholic solvents (which are excluded from the regression analysis). Data source of λ_F taken from reference (171). Numbering of solvents as in Table (6.4).

Figure (6.9) Triplet-triplet absorption spectra of xanthone (ca. 2 x 10^{-4} mol dm^{-3}) obtained on laser flash photolysis of deaerated solutionsin the following solvents:

Acetonitrile (●) as measured 2μs after the end of the excimer laser pluse.

Methanol (O) as measured 2μs after the end of the excimer laser pluse.

Benzene (▲) as measured 200 ns after the end of the ruby laser pluse.

Dichloromethane (Δ) as measured 1μs after the end of the excimer laser pluse.

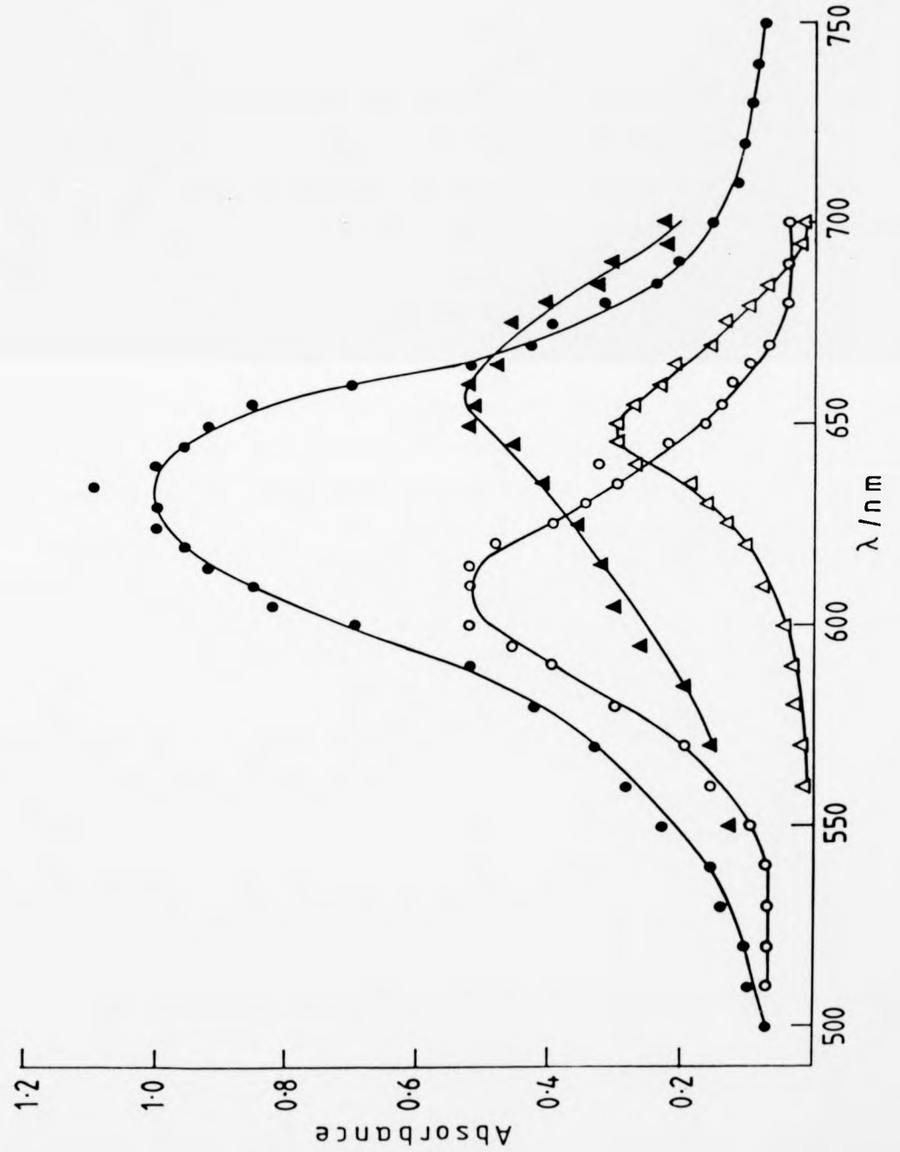

Figure (6.10) Triplet-triplet absorption spectra of thioxanthone (ca. 2×10^{-4} mol dm^{-3}) obtained on laser flash photolysis of deaerated solutionsin the following solvents:

Acetonitrile (△) as measured 5μs after the end of the excimer laser pulse.

Ethanol (O) as measured 2μs after the end of the ruby laser pluse.

2,2,2-Trifluoroethanol (●) as measured 2μs after the end of the ruby laser pulse.

Cyclohexane (▲) as measured 500ns after the end of the excimer laser pulse.

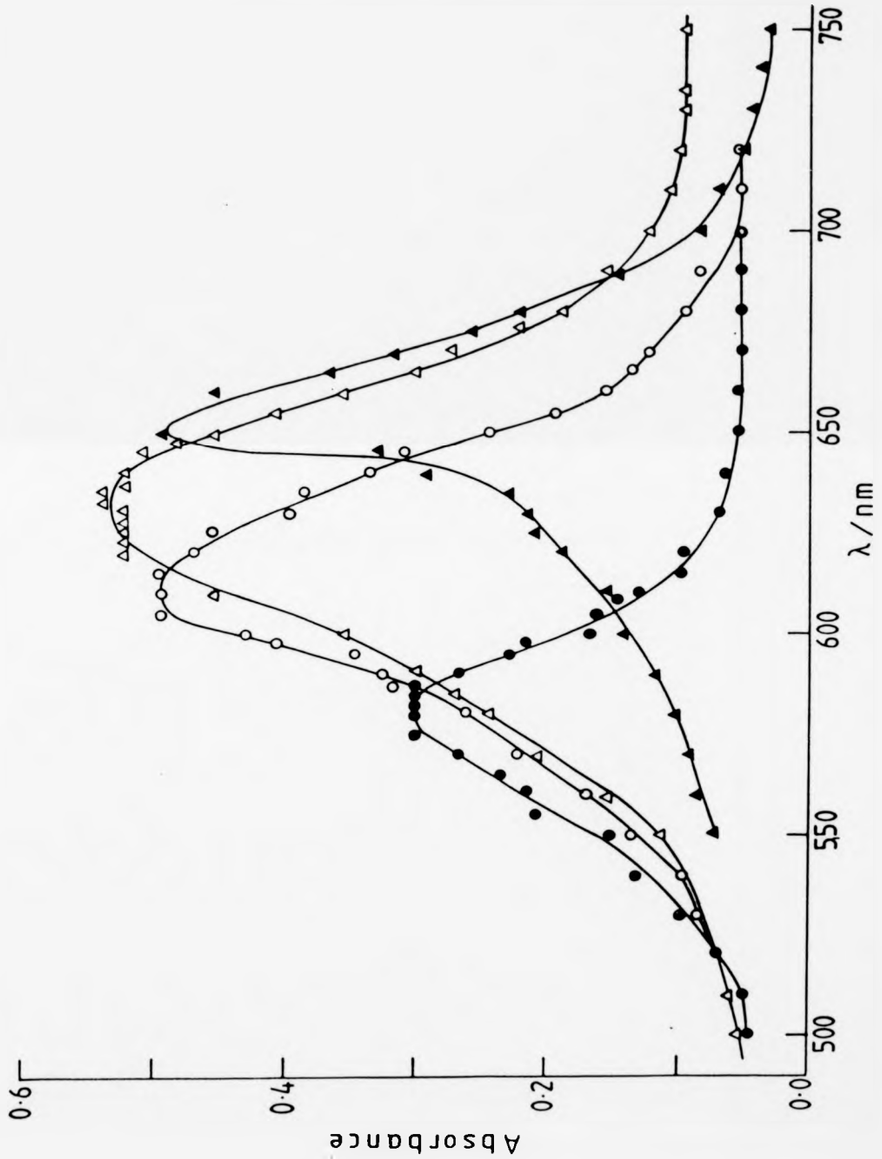

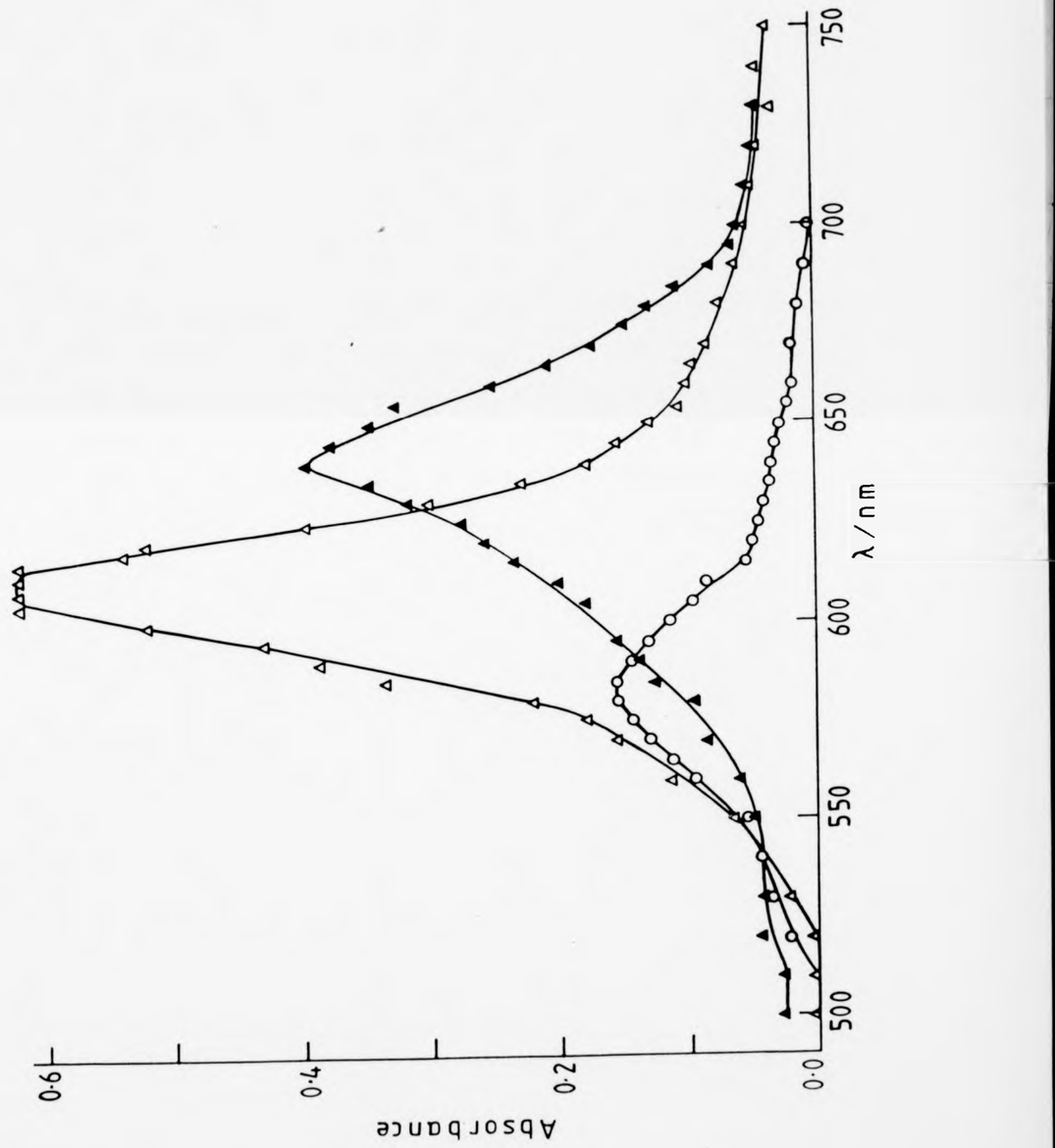

Figure (6.11) Triplet-triplet absorption spectra of N-methylacridone (ca. 1 x 10^{-4} mol dm^{-3}) obtained on laser flash photolysis of deaerated solutions in the following solvents:

Acetonitrile (△) as measured 10μs after the end of the excimer laser pulse.

Methanol (○) as measured 10μs after the end of the excimer laser pulse.

Benzene (▲) as measured 2μs after the end of the ruby laser pulse.

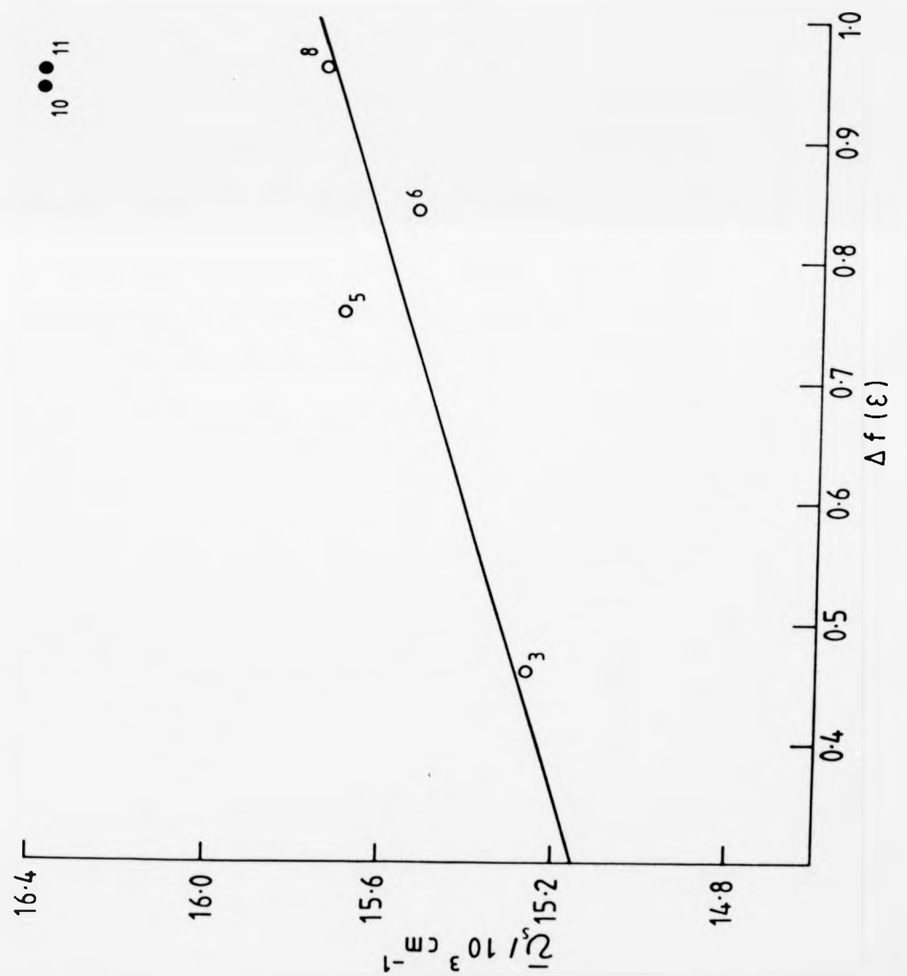

Figure (6.12) Correlation of the energy maxima $\bar{\nu}_S$ of xanthone with the polarisability function, $\Delta f(\varepsilon) = 2(\varepsilon-1)/(2\varepsilon+1)$, (see equation (6.6)). Filled circles refer to alcoholic solvents (which are excluded from the regression analysis). For key to numbering solvents see Table (6.5).

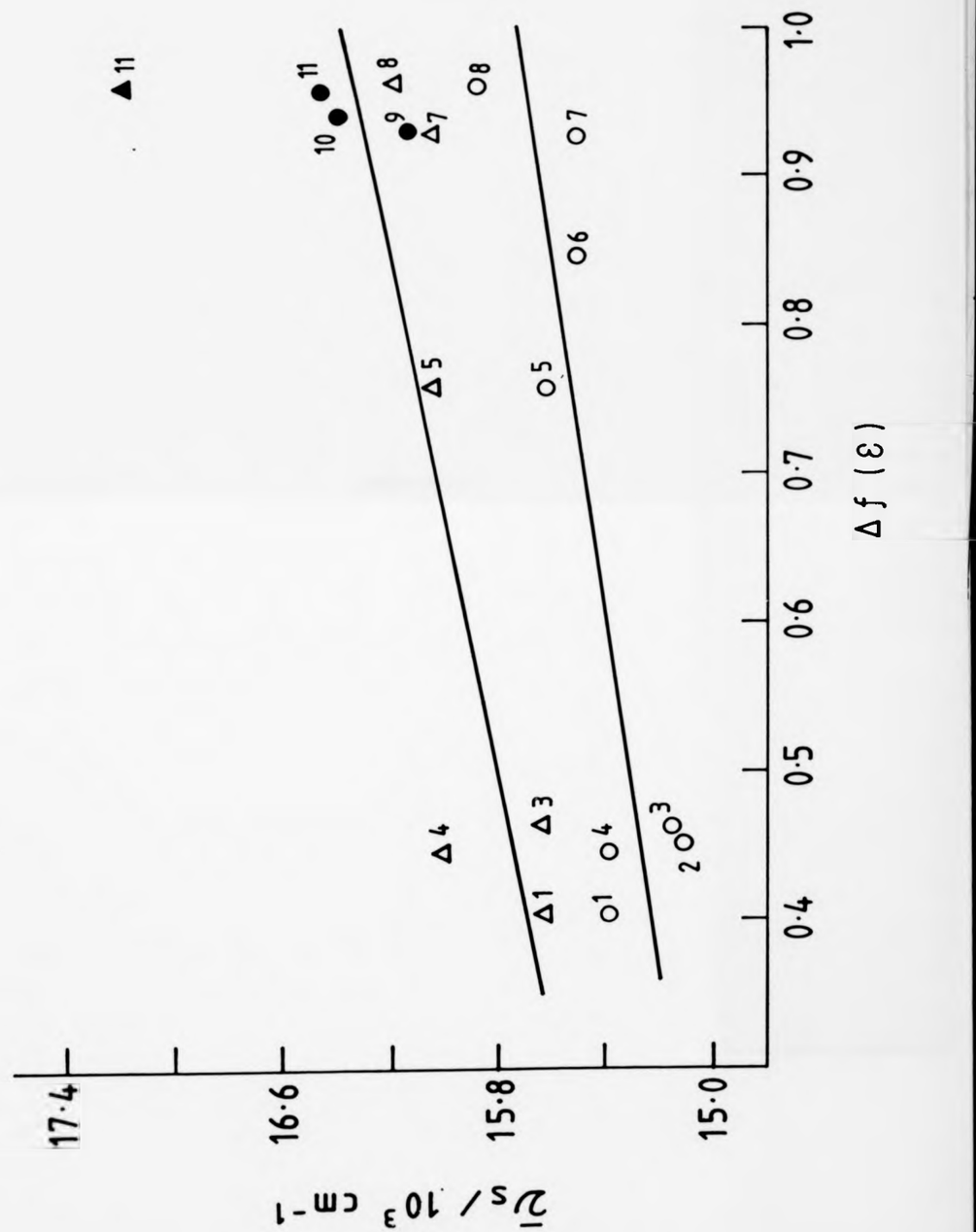

Figure (6.13) Correlation of the energy maxima $\bar{\nu}_S$ of thioxanthone (O) and N-methylacridone (Δ) with the polarisability function, $\Delta f(\varepsilon) = 2(\varepsilon-1)/(2\varepsilon+1)$, (see equations (6.7) and (6.8) for thioxanthone and N-methylacridone, respectively). Filled circles or triangles refer to alcoholic solvents (which are excluded from the regression analysis). For key to numbering solvents see Table (6.5).

APPENDICES

APPENDIX I

The computer program WELLERCHANGE enables the computation of the best fitting parameters to the experimental results expressed in the form of the Rehm-Weller plot. The variation in the range of the diffusion-controlled rate constant (k_{12}) is taken from 6×10^9 to 20×10^9 $dm^3\ mol^{-1}\ s^{-1}$ and the variation in the intrinsic barrier, $\Delta G^{\ddagger}_{23}(0)$, is from zero to 9 kcal mol^{-1}. In order to run this program, firstly specify the number of data points and then insert the data points in the following sequence: ΔG^{o}_{23} (in kcal mol^{-1}), k_q. The output $\Delta G^{\ddagger}_{23}(0)$ will be in units of kcal mol^{-1} and the corresponding value of k_q calculated for each point inserted. The program is written in FORTRAN, and is presented below.

```
 $RESET FREE
C       DATA IS READ FROM FILE "DATA/WELLER" WHICH HAS No. OF DATA
C       POINTS FIRST THEN DATA AS DELTA G23,kq
FILE  4(KIND=DISK,TITLE="DATA/WELLER.",FILETYPE=7)
        DIMENSIONDATA1(2,100)
        READ(4,/)N
         SSKQ=1.0E35
        DO 50 ICOUNT=1,N
        READ(4,/)DATA1(1,ICOUNT),DATA1(2,ICOUNT)
   50   CONTINUE
    5   WRITE(6,10)
   10   FORMAT(1X,'DO YOU WISH TO FIX kdiff (1=YES,2=NO)')
        READ(5,/)QD
        IF(QD.NE.1.AND.QD.NE.2)GOTO 5
        IF(QD.EQ.2)GOTO 16
        WRITE(6,12)
   12   FORMAT(1X,'ENTER kdiff ; ')
        READ(5,/)ALDIFF
        AHDIFF=ALDIFF
        GOTO 28
   16   AHDIFF=1.0E10
        ALDIFF=6.0E9
   28   WRITE(6,31)
   31   FORMAT(1X,'DO YOU WISH TO FIX G0 (1=YES,2=N0)')
        READ(5,/)QG
        IF(QG.NE.1.AND.QG.NE.2)GOTO 28
        IF(QG.EQ.1)GOTO 41
        ALG0=1
        AHG0=9.5
        GOTO80
   41   WRITE(6,42)
   42   FORMAT(1X,' ENTER G0 ; ')
        READ(5,/)ALG0
        AHG0=ALG0
   80    DO 88 DIFF=ALDIFF,AHDIFF,5E8
        WRITE(6,91)DIFF
    91    FORMAT( ' DIFF= ',E16.8)
          DO 100 G0=ALG0,AHG0,0.05
          SDKQ=0
       DO 75 ICOUNT=1,N
       X=DATA1(1,ICOUNT)
       CG23=X/2+SQRT(((X/2)*(X/2))+(G0*G0))
        KQ=DIFF/(1+(.25*(EXP(X/.593)+EXP(CG23/.593))))
       DKQ=(DATA1(2,ICOUNT)-KQ)*(DATA1(2,ICOUNT)-KQ)
       SDKQ=SDKQ+DKQ
   75  CONTINUE
       IF(SDKQ.GT.SSKQ)GO TO 100
       FOUNG0=G0
         SSKQ=SDKQ
         FDIFF=DIFF
         WRITE(6,92)FDIFF,SSKQ
   92    FORMAT( ' FDIFF=',2E16.9)
  100  CONTINUE
   88    CONTINUE
   90    CONTINUE
       WRITE(6,150)FOUNG0
  150  FORMAT(/// ' THE BEST G0 FOUND WAS',F15.3)
        ABSDKQ=0
        SDATAKQ=0
        DO 200 ICOUNT=1,N
        X=DATA1(1,ICOUNT)
         CG23=X/2+SQRT(((X/2)*(X/2))+(FOUNG0*FOUNG0))
         KQ=FDIFF/(1+(.25*(EXP(X/.593)+EXP(CG23/.593))))
        WRITE(6,190)ICOUNT,DATA1(2,ICOUNT),KQ
  190   FORMAT( ' Kq ', I4, '  Exp=' ,E10.5, '  Calcd=', E10.5)
       ABSDKQ=ABS(KQ-DATA1(2,ICOUNT))+ABSDKQ
```

```
      SDATAKQ=DATA1(2,ICOUNT)+SDATAKQ
200   CONTINUE
      R=100*ABSDKQ/SDATAKQ
       WRITE(6,250)R
250   FORMAT( ' GOODNESS OF FIT FACTOR=    ',F10.7,' %')
       WRITE(6,300)FDIFF
  300  FORMAT( ' DIFFUSION RATE ESTIMATE= ',E16.8)
      STOP
      END
```

APPENDIX II

Fluorescence decay curves were obtained by the time-correlated single-photon technique from the following deaerated solutions, in which the emissions from these fluorophores (λ_F) were monitored at the wavelengths specified. The residual and autocorrelation functions (on the back of each figure) were calculated on the basis of a single exponential decay of the fluorophore luminescence utilising a non-linear least square fitting computer program.

Fluorophore	Solvent	λ/nm
9,10-DCA	MeOH	436
9,10-DCA	MeOH/H_2O (1:1 v/v)	442
9,10-DCA	Cyclohexane	448
2-AA	MeOH	493
2-AA	Cyclohexane	437
2-DMA	MeOH	495
2-DMA	Cyclohexane	458
Thioxanthone	MeCN/H_2O (3:2 v/v)	432

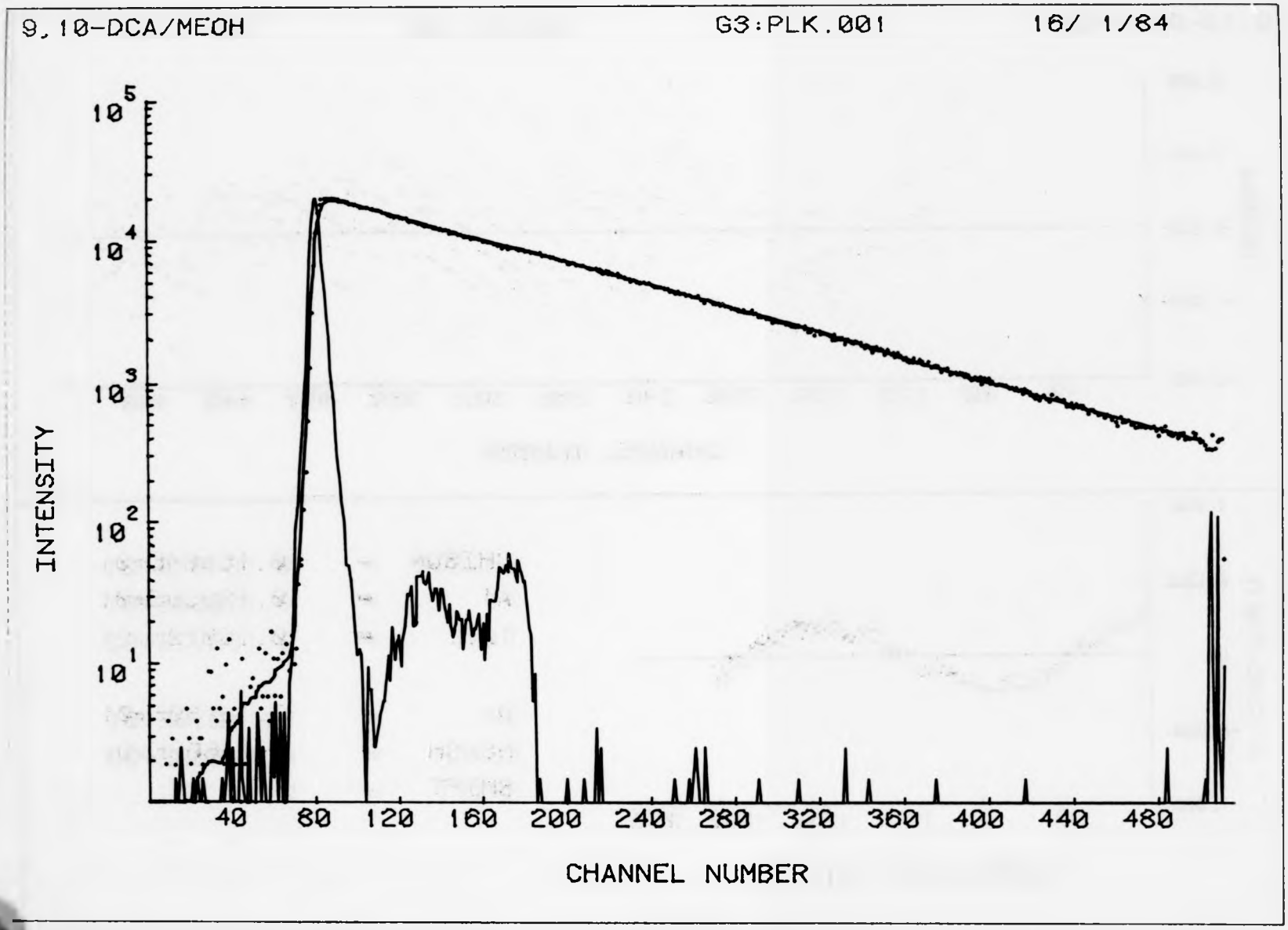
9,10-DCA/MEOH
G3:PLK.001
16/ 1/84
INTENSITY
10^5
10^4
10^3
10^2
10^1
40
80
120
160
200
240
280
320
360
400
440
480
CHANNEL NUMBER

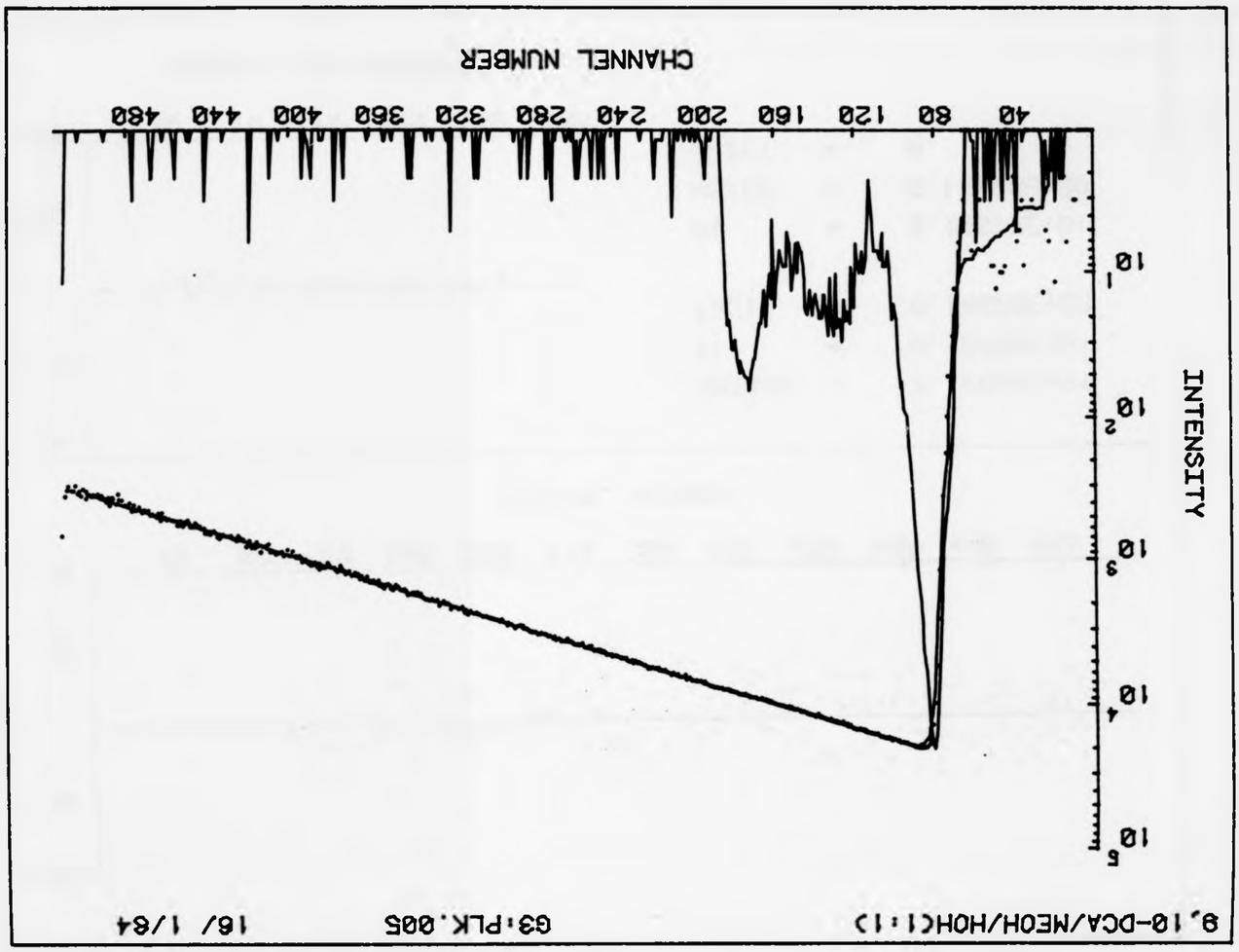
9,10-DCA/MEOH/HOHC1:13
G3:PLK.005
16/ 1/84
INTENSITY
CHANNEL NUMBER

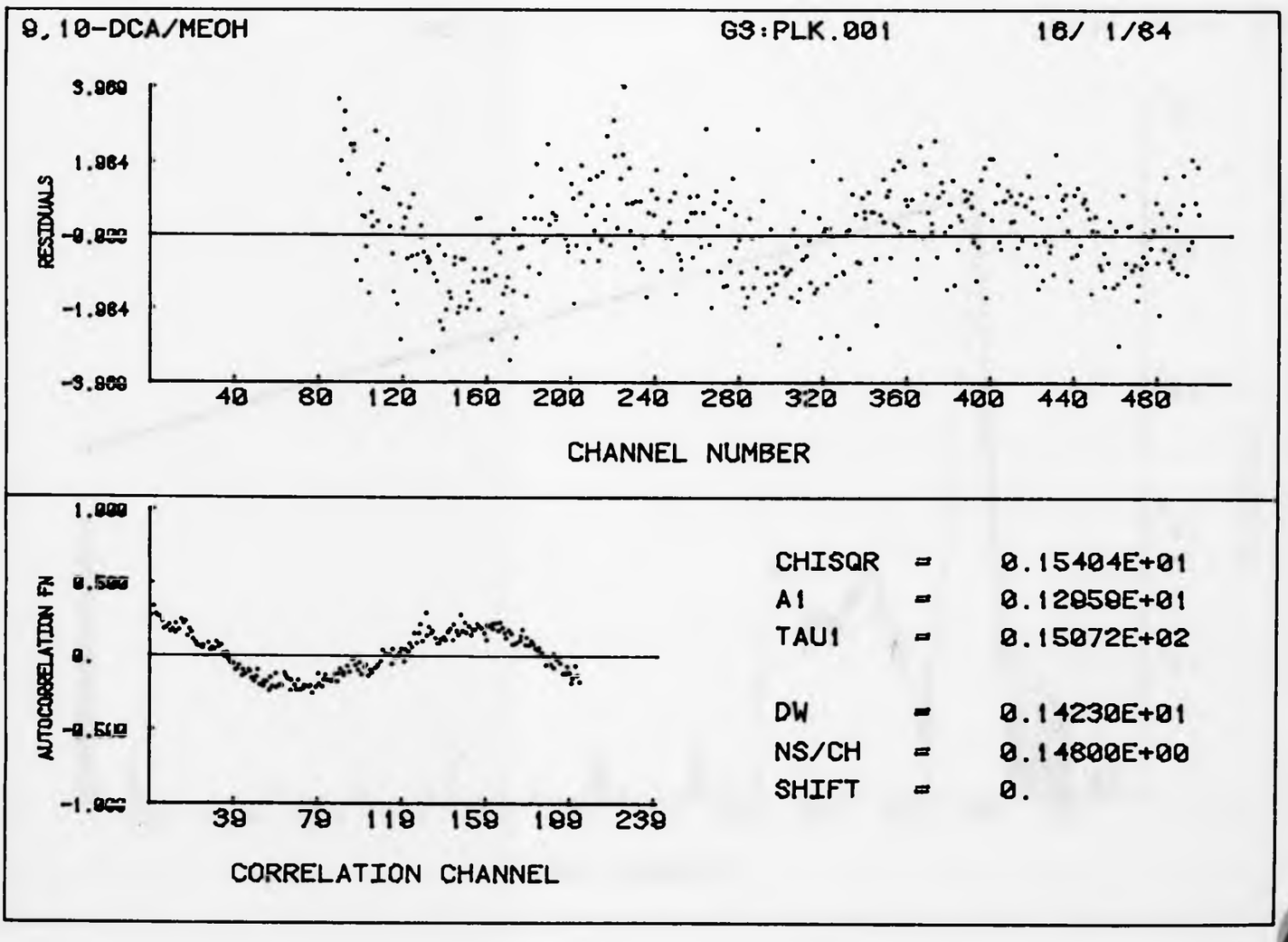
9,10-DCA/MEOH
G3:PLK.001
16/ 1/84
RESIDUALS
CHANNEL NUMBER
AUTOCORRELATION FN
CORRELATION CHANNEL
CHISQR = 0.15404E+01
A1 = 0.12858E+01
TAU1 = 0.15072E+02
DW = 0.14230E+01
NS/CH = 0.14800E+00
SHIFT = 0.

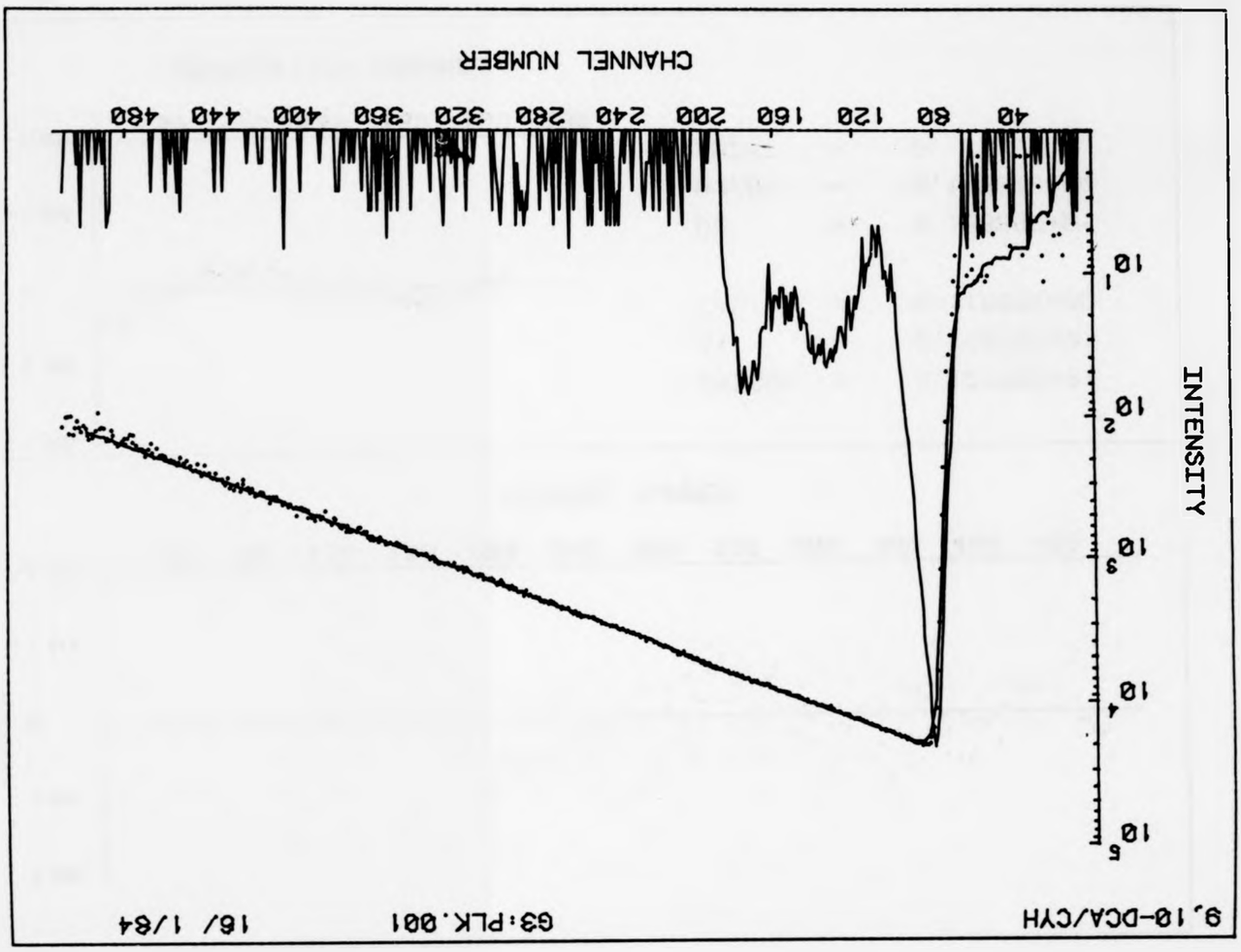
CHANNEL NUMBER
40 80 120 160 200 240 280 320 360 400 440 480
INTENSITY
10^1 10^2 10^3 10^4 10^5
9.10-DCA/CYH
G3:PLK.001
16/ 1/84

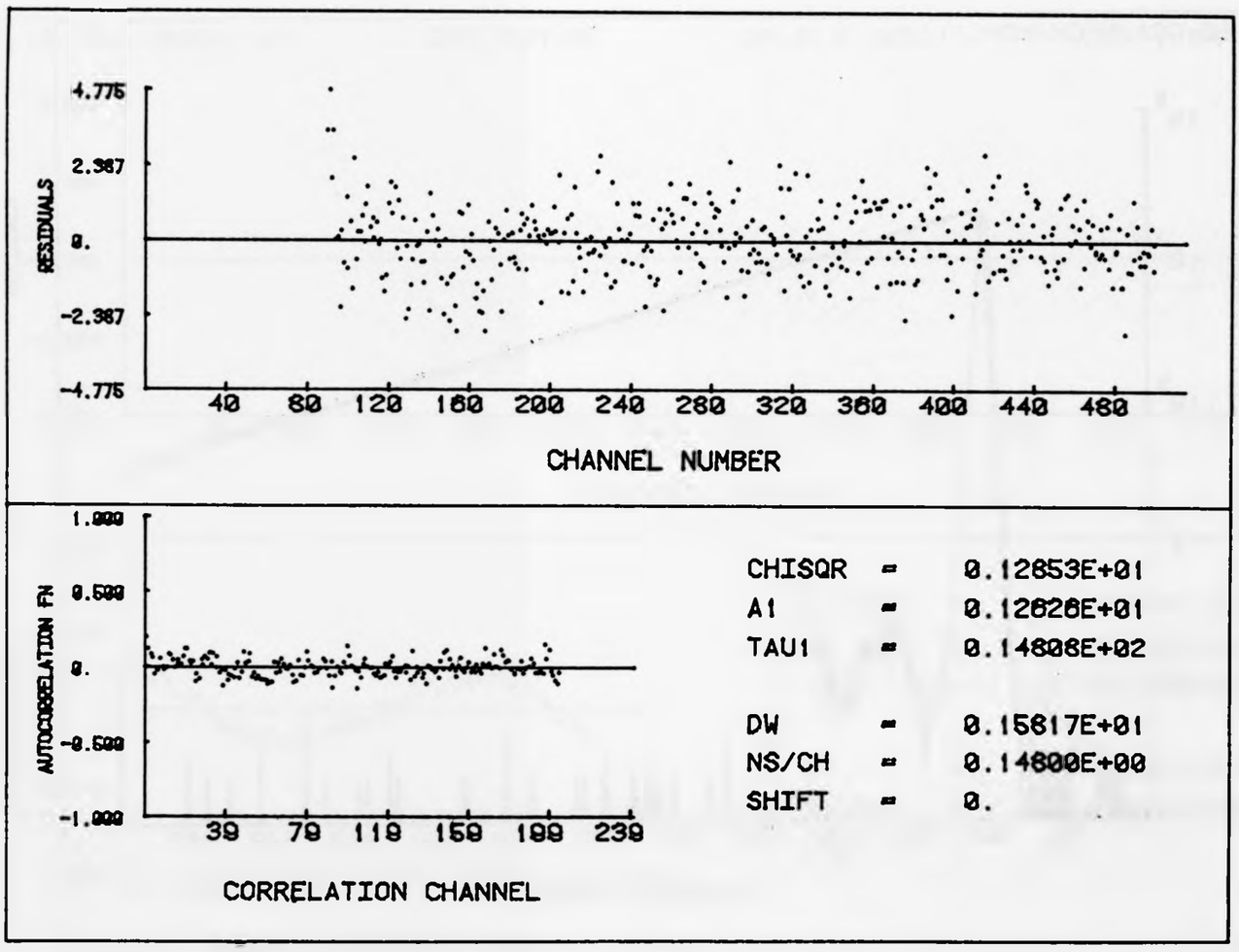
RESIDUALS
4.775
2.387
0.
-2.387
-4.775
40 80 120 160 200 240 280 320 360 400 440 480
CHANNEL NUMBER
AUTOCORRELATION FN
1.000
0.500
0.
-0.500
-1.000
39 79 119 159 199 239
CORRELATION CHANNEL
CHISQR = 0.12853E+01
A1 = 0.12626E+01
TAU1 = 0.14806E+02
DW = 0.15817E+01
NS/CH = 0.14800E+00
SHIFT = 0.

CHISQR = 0.12788E+01
A1 = 0.12875E+01
TAU1 = 0.11863E+02

DW = 0.13638E+01
NS/CH = 0.14800E+00
SHIFT = 0.

CHISQR	=	0.13593E+01
A1	=	0.17128E+01
TAU1	=	0.30388E+02
DW	=	0.20408E+01
NS/CH	=	0.82000E-01
SHIFT	=	0.

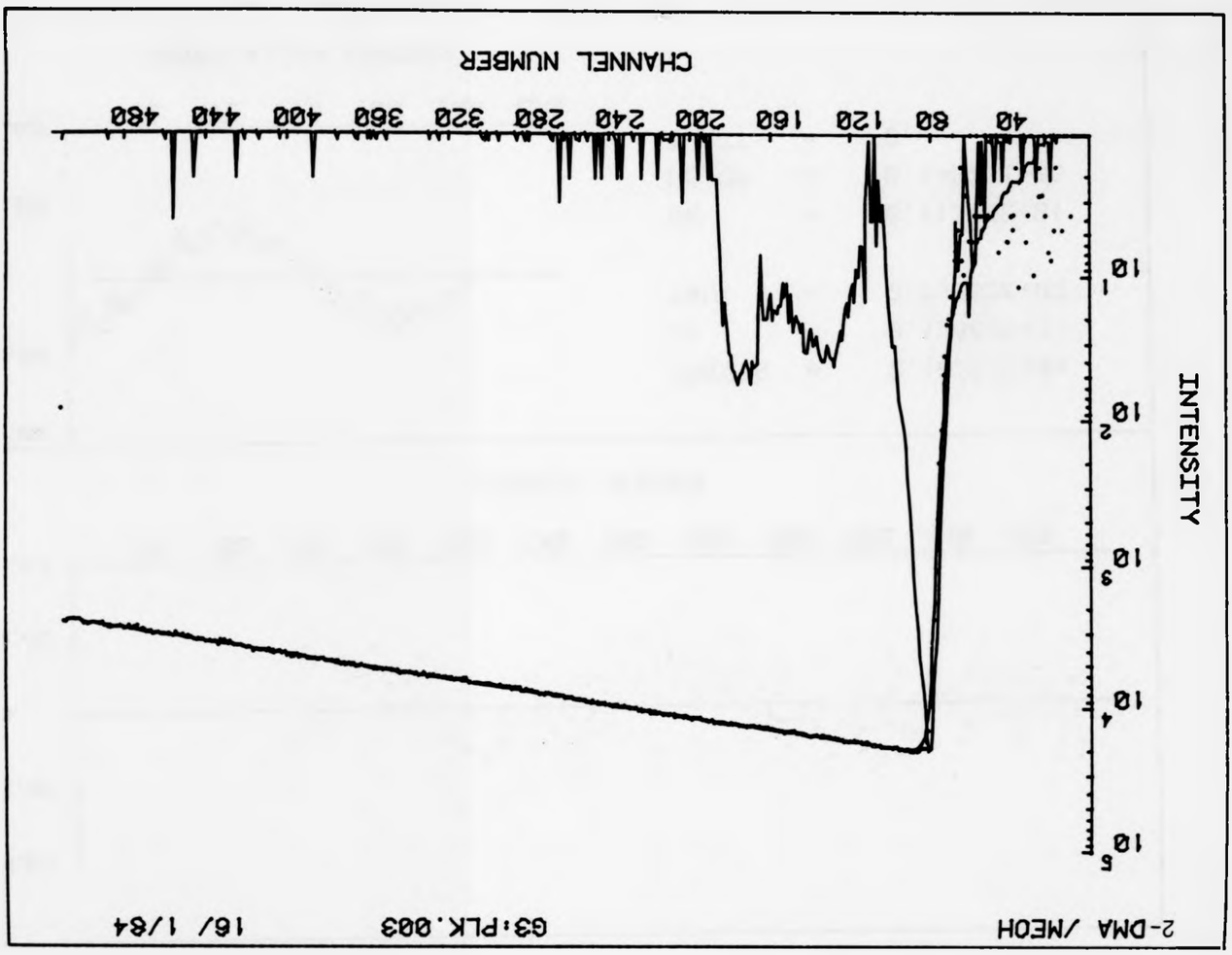
CHANNEL NUMBER
40 80 120 160 200 240 280 320 360 400 440 480
INTENSITY
10^1
10^2
10^3
10^4
10^5
2-DMA /MEOH
G3:PLK.003
16/ 1/84

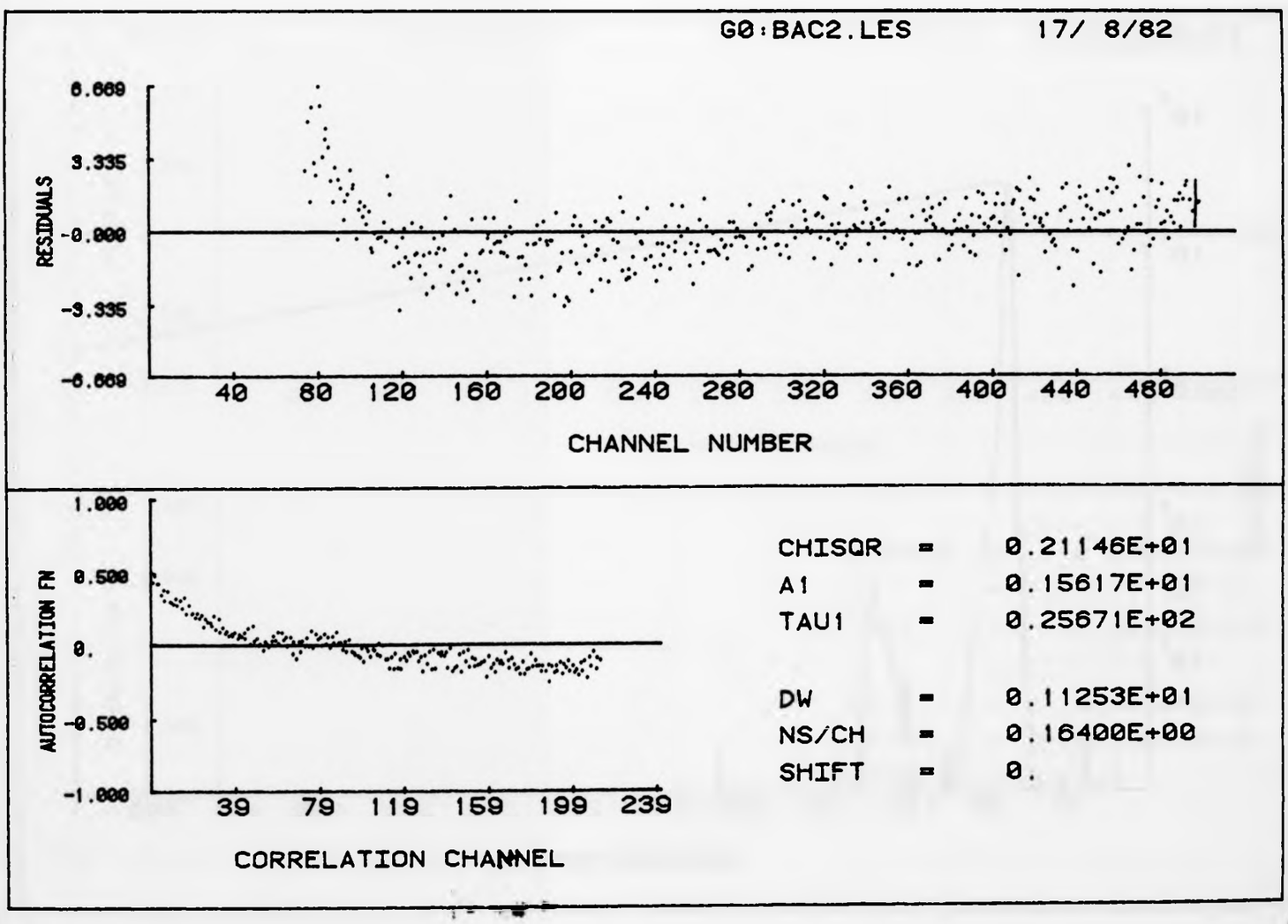
G0:BAC2.LES
17/ 8/82
RESIDUALS
6.669
3.335
-0.000
-3.335
-6.669
40 80 120 160 200 240 280 320 360 400 440 480
CHANNEL NUMBER
AUTOCORRELATION FN
1.000
0.500
0.
-0.500
-1.000
39 79 119 159 199 239
CORRELATION CHANNEL
CHISQR = 0.21146E+01
A1 = 0.15617E+01
TAU1 = 0.25671E+02
DW = 0.11253E+01
NS/CH = 0.16400E+00
SHIFT = 0.

CHISQR	=	0.19251E+01
A1	=	0.12883E+01
TAU1	=	0.28632E+02
DW	=	0.11369E+01
NS/CH	=	0.14800E+00
SHIFT	=	0.

G3:PLK.006
18/ 1/84
THIOXANTHONE IN MECN/HOH(3:2)
INTENSITY
CHANNEL NUMBER

RESIDUALS
CHANNEL NUMBER
AUTOCORRELATION FN
CORRELATION CHANNEL
CHISQR = 0.18845E+01
A1 = 0.12208E+01
TAU1 = 0.24518E+02
DW = 0.11180E+01
NS/CH = 0.14800E+00
SHIFT = 0.

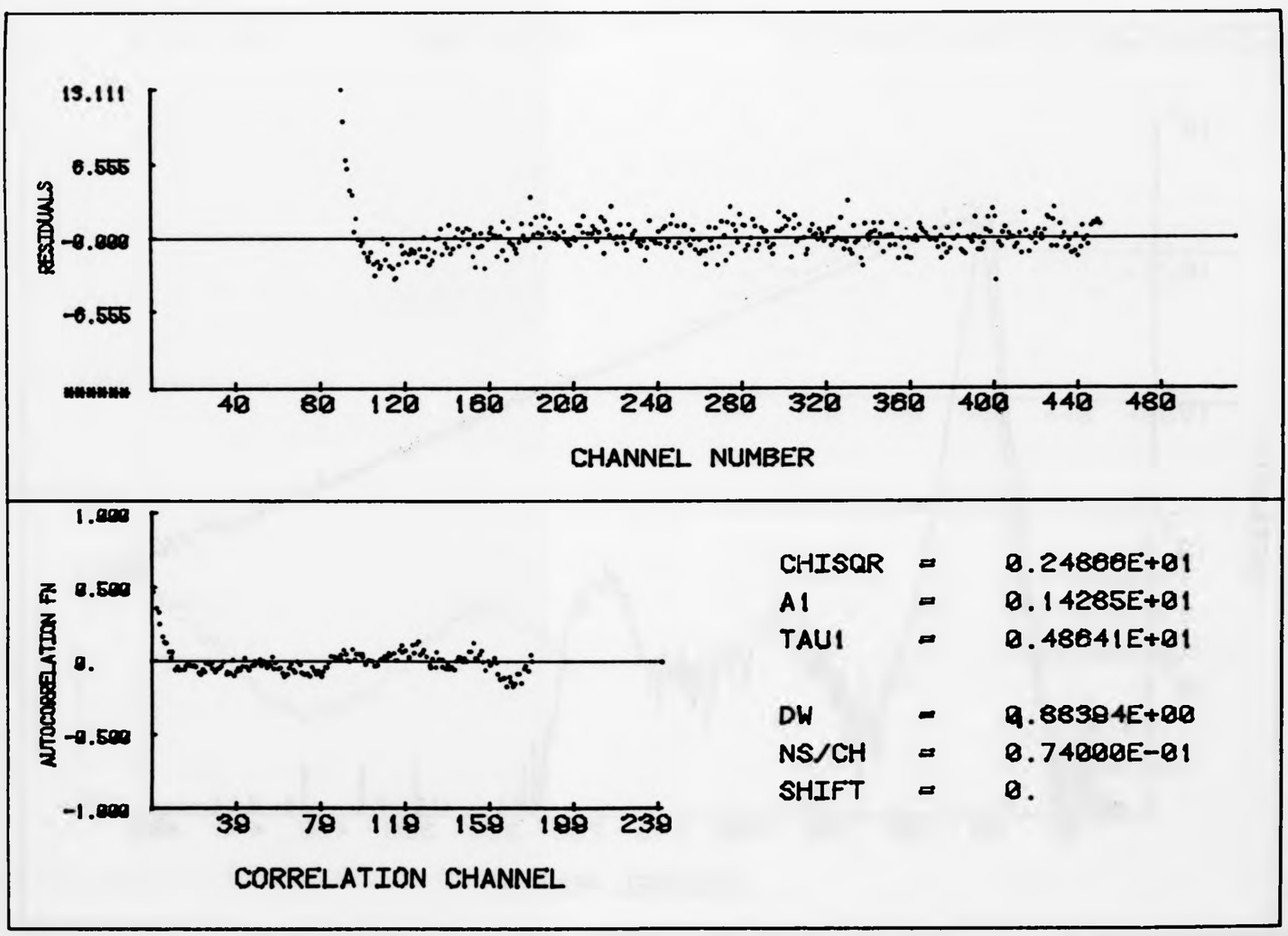
13.111
6.555
-0.000
-6.555
****
RESIDUALS
40
80
120
160
200
240
280
320
360
400
440
480
CHANNEL NUMBER
1.000
0.500
0.
-0.500
-1.000
AUTOCORRELATION FN
39
79
119
159
199
239
CORRELATION CHANNEL
CHISQR = 0.24666E+01
A1 = 0.14285E+01
TAU1 = 0.48641E+01
DW = 0.88394E+00
NS/CH = 0.74000E-01
SHIFT = 0.

1. M.D. Lumb in, "Luminescence Spectroscopy", Eds. M.D. Lumb, Academic Press, London, 1978, Chap. 2.

2. J.A. Barltrop and J.D. Coyle, "Principles of Photochemistry", Wiley, Chichester, 1978.

3. S.G. Schulman, "Fluorescence and Phosphorescence: Physicochemical Principles and Practice", Pergamon Press, New York, 1977, Chap. 2.

4. F. Wilkinson, "Chemical Kinetics and Reaction Mechanisms", Van Nostrand Reinhold Company Ltd., New York, 1980, Chap. 9.

5. R.B. Cundall and A. Gilbert, "Photochemistry", Thomas Nelson and Sons Ltd., London, 1970.

6. J.F. Rabek, "Experimental Methods in Photochemistry and Photophysics", Wiley, Chichester, 1982, Part 2, pp.727-745.

7. Th. Förster and K. Kasper, Z. Phys. Chem. (Frankfurt am Main), 1954, 1, 275; Ber. Bunsenges. Phys. Chem., 1955, 59, 977.

8. B. Stevens and E. Hutton, Nature (London), 1960, 186, 1045.

9. B. Stevens, Adv. Photochem., 1971, 8, 161.

10. N. Mataga and M. Ottolenghi in, "Molecular Association", Eds. R. Foster, Academic Press, London, 1978, Vol. 2, pp.1-78.

11. R.S. Davidson, Adv. Phys. Org. Chem., 1983, 19, 1.

12. N. Mataga, T. Okada and H. Oohari, Bull. Chem. Soc. Jpn., 1966, 39, 2563.

13. H. Leonhardt and Weller, Ber. Bunsenges. Phys. Chem., 1963, 67, 791.

14. D. Rehm and A. Weller, Z. Phys. Chem. (Frankfurt am Main), 1970, 69, 183.

15. D. Rehm and A. Weller, Isr. J. Chem., 1970, 8, 259.

16. D. Rehm and A. Weller, Ber. Bunsenges. Phys. Chem., 1969, 73, 834.

17. A. Weller, Z. Phys. Chem. (Frankfurt am Main), 1982, 130, 129.

18. A. Weller, Pure Appl. Chem., 1982, 54, 1885.

19. K.H. Grellmann, A.R. Watkins and A. Weller, J. Phys. Chem., 1972, 76, 469.

20. A.K. Chibisov, Prog. React. Kinet., 1984, 13, 1.

21. R.A. Caldwell, D. Creed, D.C. DeMarco, L.A. Melton, H. Ohta and P.H. Wine, J. Am. Chem. Soc., 1980, 102, 2369.

22. V. Balzani, F. Bolletta, M.T. Gandolfi and M. Maestri, Top. Curr. Chem., 1978, 75, 1.

23. M. Julliard and M. Chanon, Chem. Br., 1982, 18, 558.

24. M. Julliard and M. Chanon, Chem. Rev., 1983, 83, 425.

25. V. Balzani, F. Bolletta, M. Ciano and M. Maestri, J. Chem. Educt., 1983, 60, 447.

26. V. Balzani and F. Scandola in, "Photochemical Conversion and Storage of Solar Energy", Eds. J.S. Connolly, Academic Press, New York, 1981, Chap. 4.

27. L. Eberson, Adv. Phys. Org. Chem., 1982, 18, 79.

28. R.A. Marcus, J. Phys. Chem., 1963, 67, 853.

29. R.A. Marcus, J. Chem. Phys., 1965, 43, 679.

30. R.A. Marcus, Annu. Rev. Phys. Chem., 1964, 15, 155.

31. R.A. Marcus, Electrochim. Acta , 1968, 13, 995.

32. N. Sutin in "Inorganic Biochemistry", Eds. G. Eichhorn, Elsevier, Amsterdam, 1973, pp.611-653.

33. J. Ulstrup, "Charge Transfer Processes in Condensed Media, Lecture Notes in Chemistry, No. 10", Springer-Verlag, New York, 1979, p.162.

34. B.S. Brunschwing, J. Logan, M.D. Newton and N. Sutin, J. Am. Chem. Soc., 1980, 102, 5798.

35. N. Sutin and C. Creutz, J. Chem. Educt., 1983, 60, 809.

36. W.R. Reynolds and R.W. Lumry, "Mechanism of Electron Transfer", Ronald Press, New York, 1966.

37. R.D. Cannon, "Electron Transfer Reaction", Butterworths, London, 1980.

38. V. Balzani and F. Scandola in, "European Photochemistry Association", IV Summerschool on Photochemistry, West Germany, September 6-10, 1982, pp.345-446.

39. S. Fukuzumi and J.K. Kochi, J. Phys. Chem., 1980, 84, 2246; S. Fukuzumi and J.K. Kochi, J. Am. Chem. Soc., 1980, 102, 2141; S. Fukuzumi, C.L. Wong and J.K. Kochi, J. Am. Chem. Soc., 1980, 102, 2928.

40. M.A. Ratner and R.D. Levine, J. Am. Chem. Soc., 1980, 102, 4898.

41. N. Sutin, Prog. Inorg. Chem., 1983, 30, 441.

42. T.J. Meyer, Prog. Inorg. Chem., 1983, 30, 389.

43. B.E. Douglas, D.H. McDaniel and J.J. Alexander, "Concepts and Models of Inorganic Chemistry", Second Ed., Wiley, New York, 1983, p.381.

44. A. Weller in, "Fast Reactions and Primary Processes in Chemical Kinetics", Eds. S. Claesson, Almqvist and Wiksells Boktryckeri AB, Uppsala, 1967, pp.413-428.

45. A.A. Frost and R.G. Pearson, "Kinetics and Mechanism", Second Ed., Wiley, New York, 1961, Chaps. 5 and 7.

46. P. Debye, Trans. Electrochem. Soc., 1942, 82, 265.

47. M. Eigen, Z. Phys. Chem. (Frankfurt am Main), 1954, 1, 176.

48. R. Ballardini, G. Varani, M.T. Indelli, F. Scandola and V. Balzani, J. Am. Chem. Soc., 1978, 100, 7219.

49. C.R. Bock, T.J. Meyer and D.G. Whitten, J. Am. Chem. Soc. , 1975, 97, 2909.

50. J. Eriksen and C.S. Foote, J. Phys. Chem., 1978, 82, 2659.

51. W. Abraham, B. Dreher, K. Buck and D. Kreysig, J. Prakt. Chem., 1982, 324, 925.

52. K. Kikuchi, S-I. Tamura, C. Iwanaga, H. Kokubun and Y. Usui, Z. Phys. Chem. (Frankfurt am Main), 1977, 106, 17.

53. E. Vogelmann, S. Schreiner, W. Rauscher and H.E.A. Kramer, Z. Phys. Chem. (Frankfurt am Main), 1976, 101, 321.

54. E. Vogelmann, W. Rauscher, R. Traber and H.E.A. Kramer, Z. Phys. Chem. (Frankfurt am Main), 1981, 124, 13.

55. L.V. Natarajan and R.E. Blankenship, Photochem. Photobiol., 1983, 37, 329.

56. E. Amouyal, B. Zidler, P. Keller and A. Moradpour, Chem. Phys. Lett., 1980, 74, 314.

57. L.J.A. Martins, J. Chem. Soc., Faraday Trans.1, 1982, 78, 533.

58. L.J.A. Martins and T.J. Kemp, J. Chem. Soc., Faraday Trans. 1, 1984, 80, 2509.

59. M.G. Evans and M. Polanyi, Trans. Faraday Soc., 1938, 34, 11.

60. J. Horiuchi and M. Polanyi, Acta Physicochim. URSS, 1935, 2, 505.

61. F. Scandola and V. Balzani, J. Am. Chem. Soc., 1979, 101, 6140.

62. N. Sutin, Acc. Chem. Res., 1968, 1, 225.

63. F. Basolo and R. G. Pearson, "Mechanism of Inorganic Reactions", Second Ed., Wiley, New York, 1967, Chap. 6.

64. R.A. Marcus and P. Sider, J. Phys. Chem., 1982, 86, 622.

65. P. Siders and R.A. Marcus, J. Am. Chem. Soc., 1981, 103, 748.

66. R.A. Marcus, Int. J. Chem. Kinet., 1981, 13, 865.

67. R.A. Marcus and N. Sutin, Inorg. Chem., 1975, 14, 213.

68. S. Efrima and M. Bixon, Chem. Phys. Lett., 1974, 25, 34.

69. S. Efrima and M. Bixon, Chem. Phys., 1976, 13, 447.

70. F. Scandola, V. Balzani and G.B. Schuster, J. Am. Chem. Soc., 1981, 103, 2519.

71. F. Scandola and V. Balzani, J. Am. Chem. Soc., 1979, 101, 6140.

72. R.A. Marcus, J. Phys. Chem., 1968, 72, 891.

73. N. Agmon and R.D. Levine, Chem. Phys. Lett., 1977, 52, 197.

74. R.D. Levine, J. Phys. Chem., 1979, 83, 159.

75. F. Wilkinson and J. Schroeder, J. Chem. Soc., Faraday Trans. 2, 1979, 75, 441.

76. V.A. Kuzmin, I.V. Renge and Yu. E. Borisevich, Chem. Phys. Lett., 1980, 70, 257.

77. H. Shizuka, M. Nakamura and T. Morita, J. Phys. Chem., 1980, 84, 989.

78. H. Shizuka, T. Saito and T. Morita, Chem. Phys. Lett., 1978, 56, 519.

79. H. Shizuka and H. Obuchi, J. Phys. Chem., 1982, 86, 1297.

80. M.G. Kuzmin, N.A. Sadovskii and I.V. Soboleva, Chem. Phys. Lett., 1980, 71, 232.

81. I.V. Soboleva, N.A. Sadovskii and M.G. Kuzmin, Khim. Vys. Energ., 1980, 14, 26.

82. R.H. Kayser and R.H. Young, Photochem. Photobiol., 1976, 24, 395.

83. H.B. Ambroz, K.R. Butter and T.J. Kemp., Faraday Discuss. Chem. Soc., 1984, 78, Paper 78/4.

84. S-I. Tamura, K. Kikuchi, H. Kokubun and Y. Usui, Z. Phys. Chem. (Frankfurt am Main), 1978, 111, 7.

85. J.J. Dubien, R. Bonneau, P.F. Violet, R. Koussini and R. Lapouyade, Pure Appl. Chem., 1979, 51, 271.

86. E. Vogelmann, W. Rauscher and H.E.A. Kramer, Photochem. Photobiol., 1979, 29, 771.

87. R. Traber, E. Vogelmann, S. Schreiner, T. Werner and H.E.A. Kramer, Photochem. Photobiol., 1981, 33, 41.

88. N. Sabbatini, M.T. Indelli, M.T. Gandolfi and V. Balzani, J. Phys. Chem., 1982, 86, 3585.

89. P. Bortolus and S. Dellonte, J. Chem. Soc., Faraday Trans. 2, 1975, 71, 1338.

90. L. Eberson, Acta Chem. Scand., Ser. B, 1982, 36B, 533.

91. J. Eriksen, H. Lund and A.L. Nyvad, Acta Chem. Scand., Ser. B, 1983, 37B, 459.

92. J. Eriksen, K.A. Jorgensen, J. Linderberg and H. Lund, J. Am. Chem. Soc., 1984, 106, 5083.

93. C.N.R. Rao, S. Singh and V.P. Senthilnathan, Chem. Soc. Rev., 1976, 5, 297.

94. L. Bilot and A. Kawski, Z. Naturforsch., 1962, 17A, 621.

95. N.G. Bakhshiev, Opt. Spectrosc., 1965, 19, 196.

96. M.F. Nicol, Appl. Spectrosc. Rev., 1974, 8, 183.

97. W. Liptay in, "Excited States", Eds. E. Lim, Academic Press, New York, 1973, Vol. 1, P.129.

98. P. Suppan, J. Chem. Soc. A, 1968, 3125.

99. P. Suppan, J. Mol. Spectrosc., 1969, 30, 17.

100. A.T. Amos and B.L. Burrows, Adv. Quantum Chem., 1973, 7, 303.

101. B. Koutek, Collect. Czech. Chem. Commun., 1978, 43, 2368.

102. B. Koutek, Collect. Czech. Chem. Commun., 1984, 49, 1680.

103. J.R. Lakowicz, "Principles of Fluorescence Spectroscopy", Plenum Press, New York, 1983, Chap. 7.

104. L. Onsager, J. Am. Chem. Soc., 1936, 58, 1486.

105. J.R. Lombardi, J. Am. Chem. Soc., 1970, 92, 1831.

106. P. Suppan, Chem. Phys. Lett., 1983, 94, 272.

107. L.S. Prabhumirashi, Spectrochim. Acta, 1983, 39A, 91.

108. E.M. Kosower and K. Tanizawa, Chem. Phys. Lett., 1972, 16, 419.

109. E.M. Kosower, H. Dodiuk, K. Tanizawa, M. Ottolenghi and N. Orbach, J. Am. Chem. Soc., 1975, 97, 2167.

110. H. Dodiuk and E.M. Kosower, J. Am. Chem. Soc., 1977, 99, 859.

111. S.R. Meech, D.V. O'Connor, D. Phillips and A.G. Lee, J. Chem. Soc., Faraday Trans. 2, 1983, 79, 1563.

112. K.P. Ghiggino, A.G. Lee, S.R. Meech, D.V. O'Connor and D. Phillips, Biochemistry, 1981, 20, 5381.

113. A. Lablache-Combier, B. Planckaert and A. Pollet, J. Photochem., 1983, 21, 61.

114. C. Reichardt and K. Dimroth, Fortsch. Chem. Forsch., 1968, 11, 1.

115. C. Reichardt, Angew. Chem., Int. Ed. Engl., 1979, 18, 98.

116. E.M. Kosower, J. Am. Chem. Soc., 1958, 80, 3253.

117. E.M. Kosower, "An Introduction to Physical Organic Chemistry", J. Wiley and Sons, New York, 1968, pp.259-384.

118. M.J. Kamlet, J.L. Abboud and R.W. Taft, J. Am. Chem. Soc., 1977, 99, 6027.

119. M.J. Kamlet and R.W. Taft, J. Chem. Soc., Perkin Trans. 2, 1979, 349.

120. O.W. Kolling, Anal. Chem., 1981, 53, 54.

121. R.A. Loutfy and J.H. Sharp, J. Phys. Chem., 1979, 83, 1208.

122. T.C. Werner and D.B. Lyon, J. Phys. Chem., 1982, 86, 933.

123. L. Coosemans, F.C. De Schryver and A Van Dormael, Chem. Phys. Lett., 1979, 65, 95.

124. C. Capellos and G. Porter, J. Chem. Soc., Faraday Trans. 2, 1974, 70, 1159.

125. A. Garner and F. Wilkinson, J. Chem. Soc., Faraday Trans. 2, 1976, 72, 1010.

126. R.G.W. Norrish and G. Porter, Nature (London), 1949, 164, 658.

127. G. Porter and M.R. Topp, Nature (London), 1968, 220, 1228.

128. G. Porter and E.S. Reid in "Fast Processes in Radiation Chemistry and Biology", Eds. G.E. Adams, E.M. Fielden and B.D. Michael, The Institute of Physics, John Wiley, Chichester, 1975, p.33.

129. F. Kaplan and H. Conroy, J. Org. Chem., 1963, 28, 1593.

116. E.M. Kosower, J. Am. Chem. Soc., 1958, 80, 3253.

117. E.M. Kosower, "An Introduction to Physical Organic Chemistry", J. Wiley and Sons, New York, 1968, pp.259-384.

118. M.J. Kamlet, J.L. Abboud and R.W. Taft, J. Am. Chem. Soc., 1977, 99, 6027.

119. M.J. Kamlet and R.W. Taft, J. Chem. Soc., Perkin Trans. 2, 1979, 349.

120. O.W. Kolling, Anal. Chem., 1981, 53, 54.

121. R.A. Loutfy and J.H. Sharp, J. Phys. Chem., 1979, 83, 1208.

122. T.C. Werner and D.B. Lyon, J. Phys. Chem., 1982, 86, 933.

123. L. Coosemans, F.C. De Schryver and A Van Dormael, Chem. Phys. Lett., 1979, 65, 95.

124. C. Capellos and G. Porter, J. Chem. Soc., Faraday Trans. 2, 1974, 70, 1159.

125. A. Garner and F. Wilkinson, J. Chem. Soc., Faraday Trans. 2, 1976, 72, 1010.

126. R.G.W. Norrish and G. Porter, Nature (London), 1949, 164, 658.

127. G. Porter and M.R. Topp, Nature (London), 1968, 220, 1228.

128. G. Porter and E.S. Reid in "Fast Processes in Radiation Chemistry and Biology", Eds. G.E. Adams, E.M. Fielden and B.D. Michael, The Institute of Physics, John Wiley, Chichester, 1975, p.33.

129. F. Kaplan and H. Conroy, J. Org. Chem., 1963, 28, 1593.

130. R.K. Ingham, S.D. Rosenberg and H. Gilman, Chem. Rev., 1960, 60, 459.

131. M.E.R. Marcondes, V.G. Toscano and R.G. Weiss, J. Am. Chem. Soc., 1975, 97, 4485.

132. "Handbook of Chemistry and Physics", Eds. R.C. Weast, C.R.C. Press, Cleveland, 58th Edn., 1975-1976.

133. "Dictionary of Organic Compounds", Eds. J.R.A. Pollock and R. Stevens, Eyre and Spottiswoode Ltd., London, 1965.

134. R.S. Davidson and P.F. Lambeth, J. Chem. Soc., Chem. Commun., 1969, 1098.

135. M.E.R. Marcondes, V.G. Toscano and R.G. Weiss, J. Photochem., 1979, 10, 315.

136. E. Vander Donckt and J.P. Van Bellinghen, Chem. Phys. Lett., 1970, 7, 630.

137. S. Schoof, H. Gusten and C. Von Sonntag, Ber. Bunsenges. Phys. Chem., 1978, 82, 1068.

138. M.E.R. Marcondes, V.G. Toscano and R.G. Weiss, J. Photochem., 1979, 10, 425.

139. T.J. Kemp and L.J.A. Martins, J. Chem. Soc., Faraday Trans. 1, 1981, 77, 1425.

140. E.C.M. Chen and W.E. Wentworth, J. Chem. Phys., 1975, 63, 3183.

141. N. Barboy and J. Feitelson, J. Phys. Chem., 1984, 88, 1065.

142. V.M. Berdnikov and N.M. Bazhin, Russ. J. Phys. Chem., 1970, 44, 395.

143. D.M. Stanbury, W. K. Wilmarth, S. Khalaf, H.N. Po and J.E. Byrd, Inorg. Chem., 1980, 19, 2715.

144. W.K. Wilmarth, D.M. Stanbury, J.E. Byrd, H.N. Po and C-P. Chua, Coord. Chem. Rev., 1983, 51, 155.

145. W.M. Latimer, "Oxidation Potentials", Prentice Hall Inc., N.J. Englewood Cliffs, 1952.

146. L. Eberson, Acta Chem. Scand., 1963, 17, 2004.

147. M.A. Weiner, M. Lattman and S.O. Grim, J. Org. Chem., 1975, 40, 1292.

148. R.J. Klinger and J.K. Kochi, J. Am. Chem. Soc., 1980, 102, 4790.

149. T.P. Debies and J.W. Rabalais, Inorg. Chem., 1974, 13, 308.

150. H.C. Gradner and J.K. Kochi, J. Am. Chem. Soc., 1975, 97, 1855.

151. C.L. Wong, K. Mochida, A. Gin, M.A. Weiner and J.K. Kochi, J. Org. Chem., 1979, 44, 3979.

152. L. Meites and P. Zuman, "Handbook Series in Organic Electrochemistry", C.R.C. Press, Cleveland, 1977-1979, Vol. I-III.

153. P.L. Olive, Br. J. Cancer, 1979, 40, 89.

154. E.S. Pysh and N.C. Yang, J. Am. Chem. Soc., 1963, 85, 2124.

155. K. Rotkiewicz and Z.R. Grabowski, Trans. Faraday Soc., 1969, 65, 3263.

156. S.G. Schulman, P.J. Kovi, G. Torosian, H. Mcveigh and D. Carter, J. Pharm. Sci., 1973, 62, 1823.

157. J.E. Baggott and M.J. Pilling, J. Chem. Soc., Faraday Trans. 1, 1983, 79, 221.

158. N. Ikeda, T. Okada and N. Mataga, Chem. Phys. Lett., 1980, 69, 251.

159. K. Kaneta and M. Koizumi, Bull. Chem. Soc. Jpn., 1967, 40, 2254; M. Koizumi and H. Yamashita, Z. Phys. Chem. (Frankfurt am Main), 1968, 57, 103.

160. I.B. Berlman, "Handbook of Fluorescence Spectra of Aromatic Molecules", Second Ed., Academic Press, New York, 1971, p.360.

161. J.B. Birks, "Photophysics of Aromatic Molecules", Wiley, New York, 1970.

162. J.N. Demas and A.W. Adamson, J. Am. Chem. Soc., 1973, 95, 5159.

163. B.J. Tabner and J.R. Yandle, J. Chem. Soc.(A), 1968, 381.

164. H. Shizuka, K. Takada and T. Morita, J. Phys. Chem., 1980, 84, 994.

165. G. Winter, H. Shioyama and U. Steiner, Chem. Phys. Lett., 1981, 81, 547.

166. G. Winter and U. Steiner, Ber. Bunsenges. Phys. Chem., 1980, 84, 1203.

167. J.F. Ireland and P.A.H. Wyatt, J. Chem. Soc., Faraday Trans. 1, 1972, 68, 1053.

168. J.C. Scaiano and N. Kim-Thuan, Can. J. Chem., 1982, 60, 2286.

169. R.W. Yip, A.G. Szabo and P.K. Tolg, J. Am. Chem. Soc., 1973, 95, 4471.

170. S.F. Yates and G.B. Schuster, J. Org. Chem., 1984, 49, 3349.

171. J.C. Dalton and F.C. Montgomery, J. Am. Chem. Soc., 1974, 96, 6230.

172. T. Lai and E.C. Lim, Chem. Phys. Lett., 1980, 73, 244.

173. K. Suga and M. Kinoshita, Bull. Chem. Soc. Jpn., 1981, 54, 1651.

174. F. Wilkinson and A. Garner, J. Chem. Soc., Faraday Trans. 2, 1977, 73, 222.

175. R.O. Loutfy, S.K. Dogra and R.W. Yip, Can. J. Chem., 1979, 57, 342.

176. S.L. Murov, "Handbook of Photochemistry", M. Dekker, New York, 1973.

177. T. Aruga, O. Ito and M. Matsuda, J. Am. Chem. Soc., 1979, 101, 7585.

178. C.K. Mann and K.K. Barnes, "Electrochemical Reactions in Nonaqueous Systems", M. Dekker, New York, 1970, Chap. 6.

179. A. A. Gorman, C.T. Parekh, M.A.J. Rodgers and P.G. Smith, J. Photochem., 1978, 9, 11.

180. J.B. Guttenplan and S.G. Cohen, Tetrahedron Lett., 1972, 2163.

181. I.M. Kolthoff and W.J. Tomsicek, J. Phys. Chem., 1935, 39, 945.

182. D.W. Margerum, K.L. Chellappa, F.P. Bossu and G.L. Bruce, J. Am. Chem. Soc., 1975, 97, 6894.

183. M.J. Blandamer and M.F. Fox, Chem. Rev., 1970, 70, 59.

184. H.M. Rosenberg and E. Eimutis, Spectrochim. Acta, 1966, 22, 1751.

185. A.L. McClellan, "Tables of Experimental Dipole Moments", W.H. Freeman and Company, San Francisco and London, 1963.

186. H.J. Pownall and J.R. Huber, J. Am. Chem. Soc., 1971, 93, 6429.

187. R.E. Connors and W.R. Christian, J. Phys. Chem., 1982, 86, 1524.